

Zirconocenes as Models for Homogeneous Ziegler-Natta Olefin Polymerization Catalysts

Thesis by
Christopher G. Brandow

In Partial Fulfillment of the
Requirements for the Degree of
Doctor of Philosophy

Division of Chemistry
and Chemical Engineering

California Institute of Technology
Pasadena, California

2001

(Submitted April 13, 2001)

© 2001

Christopher G. Brandow

All Rights Reserved

For Dutch and George,

You made this possible

Acknowledgements

Acknowledging people for their contributions to me and my graduate career is at best a grossly incomplete endeavor. Simply thanking past and present Hogs, my wife, my parents, and my family covers the most significant contributors, but the culmination of 23 years of education and 28 years of life is not simply assisted by this short list of people. However, I can rest assured that barring bizarre coincidences, these are the only people with a chance of reading the following pages.

First to my God, everything that I do and have is from You. Without your saving grace and love, I would have nothing to celebrate.

Maggie. Your love has been endless and so often perfect. You give me so much. You have been my biggest fan, and your contributions to this accomplishment remain the largest (and I don't just mean your precise editing). I look forward to meeting the child that you have been happily carrying around with you for the last 5 months.

Of course, I wouldn't be here without my parents. Dad, you were a major cheerleader for me to come to Caltech in the first place. I am glad that I did for many reasons, not least of which was being near you. Mom, I could not have achieved many of the things that I have, were it not for how you raised me and so often held me to high standards academically and personally.

There are many others in my family that should be thanked. Specifically, Nini, I want to thank you for housing me during my first semester at Caltech and for giving to Maggie and me so generously throughout our time here.

To Pat and Dian, you are the real brains behind the whole operation, the Bercaw Group and Caltech.

Bill, thanks for giving me the many trillions of computer cycles to do research with you. Unfortunately, unlike Bierwagen before me, wet chemicals had the stronger pull.

John, you have been a great advisor. Thank you for letting this "Theoretician" into the group and for letting me get my experimental bearings. You are a great example of many things that I aspire to professionally. I think that despite much evidence to the contrary, I am more organized, better

prepared ahead of time, and somewhat clearer in my problem-solving, thanks to you. You have fostered a fantastic environment for chemistry in your group.

To 209 South Hogs past. Dr. Mike Abrams, you were my first lab mate. Thanks for teaching me high-vac techniques and a lot of air sensitive chemistry. Thanks also for your patience as I moved from theoretical to experimental status. You were always ready with your gentle words at various times, such as when I flooded the lab. Dr. Alex Muci, my longest lab mate. I enjoyed your stay tremendously. I learned an enormous amount of organic chemistry from you. We never lacked for conversation about many topics, "thanks for sharing!"

To my class of students in the Bercaw group. Dr. Jeff Yoder, I am really glad that you were in our class of Hogs. You also helped ease my transition into the Bercaw group. Without your fundamentally sound coaching of the Hogs, I don't think we would have been even as bad as we were. Dr. Deanna Zubris, Oh Yeah! I have continued on our proud tradition at least one messy desk in the nook. Dr. Paul Chirik, it seems strange that we ended up in the same group after rooming together on the MIT visit so many years ago, but I am glad to have learned a lot of chemistry from many discussions with you during our 5 years in the Bercaw group.

To all other Hogs past. Dr. Steve Miller I do not know how you could look at endless tables of polymer microstructure. Dr. John Scollard, my former nookmate, I don't know how much would have been accomplished on the computers without your constant, loving attention to all things Macintosh. Dr. Chris Levy, in addition to your excellent leadership on the whole Lobsterfest, you had tremendous cultural impact on the group with your encyclopedic repertoire of Simpsons references. To all of the above, thank you for football on the BI lawn (now BI lot), there were some epic and not-so-epic battles.

To Hogs present. The newest addition to the 209 contingent, Lily, you have been a great friend. I have really enjoyed the last couple of years with you being here. You were a welcome friend during crazy times. Just remember, if you work hard enough, someday you may be able to shovel chemicals in a room-sized buchner funnel.

Seva, the partial 209 member, I have enjoyed your entire stay in the Bercaw group. In particular, the last 6 months have been very enjoyable. Constant discussions of NY Times editorials or anything on the web that was minimally engaging were a welcome distraction. Thank you for introducing me

to "Gimme Shelter". The absence of your fat butt in its chair to my left will be a noticeable absence in my life. Oh, I also benefited on many occasions from discussing chemistry with you, due to your excellent insight.

Antek, I will miss your blunt assessments of everything. I will also miss your expertise in many areas of chemistry. Annita, you are a great example of tenacity in trying to solve problems. Reading your thesis chapters is quite an intellectual exercise. Collectively, I will miss the "discussions" that the two of you would have with each other.

Dr. Joseph Sadighi and Aloha Susan, I really enjoyed our trek partway up Mt. Darwin, when "we totally lived" and followed it up with an asphyxiatingly cold swim in some lake, whose name escapes me.

Man's pants Sarah, good luck with the inscrutable zirconocene cations.

Jonathan, WHAT ARE YOU DOING?? I will now concede that you are the chicken shooting king.

Cristoph, maybe when you leave the group you could have them chip in to help your parents buy a middle name. Anyway, keep up the group basketball outings.

Bekah and Dr. Cliff Baar (the third CB), I enjoyed getting to know you guys, good luck!

Finally.....

What's the good word? = Wow! Rats! The odd hog.

Abstract

Using density functional theory, we studied the fundamental steps of olefin polymerization for zwitterionic and cationic Group IV *ansa*-zirconocenes and a neutral *ansa*-ytrocene. Complexes $[\text{H}_2\text{E}(\text{C}_5\text{H}_4)_2\text{ZrMe}]^n$ ($n = 0$: E = BH_2 (1), BF_2 (2), AlH_2 (3); $n = +$: E = CH_2 (4), SiH_2 (5)) and $\text{H}_2\text{Si}(\text{C}_5\text{H}_4)_2\text{YMe}$ were used as computational models. The largest differences among these three classes of compounds were the strength of olefin binding and the stability of the β -agostic alkyl intermediate towards β -hydrogen elimination. We investigated the effect of solvent on the reaction energetics for 1 and 5. We found that in benzene the energetics became very similar except that a higher olefin insertion barrier was calculated for 1. The calculated anion affinity of $[\text{CH}_3\text{BF}_3]^-$ was weaker towards 1 than 5. The calculated olefin binding depended primarily on the charge of the *ansa* linker, and the olefin insertion barrier was found to decrease steadily in the following order: $[\text{H}_2\text{C}(\text{C}_5\text{H}_4)_2\text{ZrMe}]^+ > [\text{F}_2\text{B}(\text{C}_5\text{H}_4)_2\text{ZrMe}] \approx [\text{H}_2\text{B}(\text{C}_5\text{H}_4)_2\text{ZrMe}] > [\text{H}_2\text{Si}(\text{C}_5\text{H}_4)_2\text{ZrMe}]^+ > [\text{H}_2\text{Al}(\text{C}_5\text{H}_4)_2\text{ZrMe}]$.

We prepared *ansa*-zirconocene dicarbonyl complexes $\text{Me}_2\text{ECp}_2\text{Zr}(\text{CO})_2$ (E = Si, C), and *t*-butyl substituted complexes $(t\text{-BuCp})_2\text{Zr}(\text{CO})_2$, $\text{Me}_2\text{E}(t\text{-BuCp})_2\text{Zr}(\text{CO})_2$ (E = Si, C), $(\text{Me}_2\text{Si})_2(t\text{-BuCp})_2\text{Zr}(\text{CO})_2$ as well as analogous zirconocene complexes. Both the reduction potentials and carbonyl stretching frequencies follow the same order: $\text{Me}_2\text{SiCp}_2\text{ZrCl}_2 > \text{Me}_2\text{CCp}_2\text{ZrCl}_2 > \text{Cp}_2\text{ZrCl}_2 > (\text{Me}_2\text{Si})_2\text{Cp}_2\text{ZrCl}_2$. This ordering is a result of both the donating abilities of the cyclopentadienyl substituents and the orientation of the cyclopentadiene rings. Additionally, we prepared a series of analogous cationic zirconocene complexes $[\text{LZrOCMe}_3][\text{MeB}(\text{C}_6\text{F}_5)_3]$ (L = Cp_2 , Me_2SiCp_2 , Me_2CCp_2 , $(\text{Me}_2\text{Si})_2\text{Cp}_2$) and studied the kinetics of anion dissociation. We found that the enthalpy of anion dissociation increased from $10.3 \text{ kcal}\cdot\text{mol}^{-1}$ to $17.6 \text{ kcal}\cdot\text{mol}^{-1}$ as exposure of the zirconium center increased.

We also prepared series of zirconocene complexes bearing 2,2-dimethyl-2-sila-4-pentenyl substituents (and methyl-substituted olefin variants). Methide abstraction with $\text{B}(\text{C}_6\text{F}_5)$ results in reversible coordination of the tethered olefin to the cationic zirconium center. The kinetics of olefin dissociation have been examined using NMR methods, and the effects of ligand variation for unlinked, singly $[\text{SiMe}_2]$ -linked and doubly $[\text{SiMe}_2]$ -linked bis(cyclopentadienyl) arrangements has been compared (ΔG^\ddagger for olefin dissociation varies from 12.8 to 15.6 $\text{ kcal}\cdot\text{mol}^{-1}$). Methide abstraction from 1,2- $(\text{SiMe}_2)_2(\eta^5\text{-C}_5\text{H}_3)_2\text{Zr}(\text{CH}_3)$ - $(\text{CH}_2\text{CMe}_2\text{CH}_2\text{CH}=\text{CH}_2)$ results in rapid β -allyl elimination with loss of isobutene yielding the allyl cation $[\{1,2-(\text{SiMe}_2)_2(\eta^5\text{-C}_5\text{H}_3)_2\text{Zr}(\eta^3\text{-CH}_2\text{CH}=\text{CH}_2)\}^+]$.

Table of Contents

Dedication	iii
Acknowledgements	iv
Abstract	vii
Table of Contents	viii
List of Figures	ix
List of Tables	xiii
Chapter 1:	1
History and Mechanism of Homogeneous Ziegler-Natta Catalysis	
Chapter 2:	8
The Group IV Zwitterion <i>Ansa</i> -Metallocene Ziegler-Natta Catalyst	
Appendix A: Calculated Energies	35
Chapter 3:	36
<i>Ansa</i> Effects in Zirconocene Dicarboxyls and Zirconocene Dichlorides	
Appendix B: Carbonyl Stretching Frequencies	70
Appendix C: X-Ray Crystallographic Information	72

Chapter 4:		94
	Ancillary Ligand and Olefin Substituent Effects on Olefin Dissociation for Cationic Zirconocene Complexes Bearing a Coordinated Pendant Olefin	
Appendix D:	Selected ^1H NMR Spectra	129
Appendix E:	Selected Eyring Plot	133
Appendix F:	X-Ray Crystallographic Information	134

List of Figures

Chapter 1:

Figure 1. Zirconocene-MAO catalyzed α -olefin polymerization.....	3
Figure 2. Catalysts used in the stereoselective polymerization of α -olefins.....	4
Figure 3. Mechanism of α -olefin polymerization by cationic group IV metallocene catalysts.	5

Chapter 2:

Figure 1. Initial identification of cationic alkyl titanocenes as active olefin polymerization catalysts.	11
Figure 2. Cationic olefin polymerization catalysts.....	12
Figure 3. Isolobal analogy of neutral Group III metallocenes and cationic Group IV metallocenes.....	12
Figure 4. Neutral d^0 zirconocene complexes.	13

Figure 5. Zwitterionic zirconocenes.	14
Figure 6. Preparation of borate <i>ansa</i> -zirconocene complexes.....	15
Figure 7. Geometric parameters for intermediates of 5 in ethylene polymerization.....	18
Figure 8. Geometry of hydride complexes 5 , 1 , and 7	19
Figure 9. Comparison of coordinated methyl borate geometries.	20
Figure 10. Energy profile of ethylene insertion and subsequent β -H elimination.....	21
Figure 11. Energy profile of olefin polymerization and termination for complexes 5 and 7	22
Figure 12. More accurate polymer propagation model.....	23
Figure 13. Energy profile of olefin polymerization and termination for complexes 1 and 5	24
Figure 14. Reaction profiles of 1 and 5 in benzene solvent.....	26
Figure 15. Effect of different <i>ansa</i> bridges on olefin binding and insertion.....	28
Figure 16. Cp _{cent} -Zr-Cp _{cent} versus olefin insertion barrier.....	29

Chapter 3:

Figure 1. Stereoselective polymerization of propylene.	38
Figure 2. Selected examples of <i>ansa</i> -bridges.	39
Figure 3. Molecular orbital description of ferrocene (eclipsed).....	40
Figure 4. Bending of the zirconocene fragment to accommodate bonding.....	41

Figure 5. Derivation of frontier molecular orbitals of bent metallocenes.....	41
Figure 6. Molecular Orbitals in Cp_2ZrX_2 complexes.....	42
Figure 7. Backbonding from Zr(II) HOMO into CO π^*	42
Figure 8. Walsh diagram for bending $\text{Cp}_{\text{cent}}\text{-Zr-Cp}_{\text{cent}}$ angle of Cp_2ZrCl_2	43
Figure 9. Geometries of metallocene dichlorides examined in this study.....	44
Figure 10. Steric interactions of the 1,2-(Me_2Si) $_2\text{Cp}_2$ ligand with "1a $_1$ " orbital.....	45
Figure 11. Attempted syntheses of unsubstituted <i>ansa</i> -zirconocenes.....	46
Figure 12. Synthesis of unsubstituted <i>ansa</i> -zirconocenes.....	46
Figure 13. Synthesis of <i>t</i> -Bu substituted zirconocenes.....	47
Figure 14. Racemic and meso <i>ansa</i> -zirconocenes.	48
Figure 15. Vibrational modes of carbonyl ligands in zirconocene complexes.....	48
Figure 16. Plot of A $_1$ stretching frequencies versus B $_2$ stretching frequencies for zirconocene dichlorides.	49
Figure 17. Proposed π -bonding stabilization of planar cation.	51
Figure 18. Preparation of <i>t</i> -butoxy zirconocene cations.	52
Figure 19. Attempted syntheses 1,2-(Me_2Si) $_2(\text{C}_5\text{H}_3)_2\text{ZrMe}(\text{OCMe}_3)$	52
Figure 20. Preparation of doubly bridged <i>ansa t</i> -butoxy cation.	53
Figure 21. Proposed mechanism of alcoholysis of Zr-CH $_3$ bond.....	53
Figure 22. Site epimerization via anion dissociation/recoordination.	54
Figure 23. X-Ray crystal structure of $[\text{Me}_2\text{SiCp}_2\text{ZrOCMe}_3][\text{MeB}(\text{C}_6\text{F}_5)_3]$	55

Figure 24. Symmetric carbonyl stretching frequency of Zr(II) dicarbonyl complexes vs. reduction potentials of Zr(IV) dichloride complexes.....	56
Figure 25. Reduction potentials vs. σ^+ para for various zirconocenes.....	59
Figure 26. Selected potentials vs. σ^+ para.....	59
Figure 27. Molecular mechanics structure of meso-Me ₂ Si(<i>t</i> -BuCp) ₂ ZrCl ₂ and (Me ₃ SiCp) ₂ ZrCl ₂	61
Figure 28. Electron affinity of Cp ₂ ZrCl ₂ with different rotamers.	62
Figure 29. Plot of zirconocene geometric parameter β versus binding energy.....	63

Chapter 4:

Figure 1. Molecular orbital diagram of transition-metal olefin complex.....	97
Figure 2. Bonding descriptions of d^0 transition-metal olefin complexes.	98
Figure 3. d^0 Complexes that bind free olefin.	99
Figure 4. Cationic zirconocene alkoxy-olefin complex.....	99
Figure 5. d^0 Yttrocene alkyl-olefin complex.....	100
Figure 6. Cationic zirconocene alkyl-olefin complexes.	101
Figure 7. Cationic zirconocene olefin complexes studied in this chapter.	102
Figure 8. Synthesis of <i>cis</i> and <i>trans</i> 2-butenyl halomethyl(dialkyl)silanes.	103
Figure 9. Preparation of methyl(4-pentenyl)zirconocene.....	103
Figure 10. Preparation of Me ₂ Si(η^5 -C ₅ H ₄) ₂]Zr(CH ₃)(CH ₂ SiMe ₂ -CH ₂ CH=CH ₂).....	104

Figure 11. Activation of methyl(4-pentenyl)zirconocene complexes.....	104
Figure 12. Static ^1H NMR spectra of 8	105
Figure 13. 8-d₂ is a 1:1 mixture of 3,3-d ₂ -2-sila-4-pentene and 5,5-d ₂ -2-sila-4-pentene.....	107
Figure 14. No alkyl-olefin insertion is observed in the ^1H NMR of 8-d₂	107
Figure 15. Methyl substituent stabilizes positive charge on olefinic carbon.....	109
Figure 16. Site epimerization occurs simultaneously with olefin dissociation.....	110
Figure 17. Olefin dissociation is faster than site epimerization for 11	111
Figure 18. Equilibrium between olefin binding and anion binding.....	112
Figure 19. Preparation of allyl complex and resulting fluxional behavior.....	113

List of Tables

Chapter 2:

Table 1. Anion dissociation energy in benzene and chlorobenzene.....	27
--	----

Chapter 3:

Table 1. Carbonyl stretching frequencies of unsubstituted zirconocene dicarbonyl complexes.....	50
Table 2. Carbonyl stretching frequencies of <i>t</i> -Bu substituted zirconocenes.....	50
Table 3. Activation parameters for anion dissociation/recoordination.....	54
Table 4. Reduction potentials of unsubstituted zirconocenes.....	56
Table 5. Reduction potentials of zirconocene dichlorides.....	58

Chapter 4:

Table 1. Free energies of activation for zirconocene complexes.....	128
---	-----

Chapter 1

History and Mechanism of Homogeneous Ziegler-Natta Catalysis

Introduction

Polyethylene and polypropylene are produced on an enormous scale from ethylene or propylene primarily by a process known as Ziegler-Natta polymerization. 100 billion pounds of polyethylene are produced annually worldwide using this process. This production is expected to grow annually by approximately 10%. The tremendous scale of this reaction and the usefulness of the polymer are responsible for motivating a large research effort into understanding and improving catalysts. In the last 45 years there have been tremendous advances made.

Transition metal catalyzed polymerization of olefins was first observed by Karl Ziegler in 1955.¹ In the course of studying olefin oligomerization by trialkyl aluminum species, he discovered that mixtures of transition metals with trialkyl aluminum were very active ethylene polymerization catalysts. Natta discovered that such catalysts could be used to polymerize propylene and do so stereoselectively. These discoveries provide the foundation for the enormous production of poly- α -olefins that exists today. Significant improvements have been made in the catalysts since then, though heterogeneous catalyst discovery remains highly empirical. Improvements are made haphazardly rather than designed rationally. While this may not be as satisfying intellectually, it must be recognized that tremendously active and selective catalysts have been made this way.

However, while the heterogeneous catalysts have been continuously improved over the last 45 years, a useful homogeneous catalyst for olefin polymerization was discovered 25 years ago when Sinn and Kaminsky showed

that mixtures of Group IV metallocene dichloride complexes with methylalumoxane could polymerize ethylene and α -olefins at significant rates (Figure 1).²

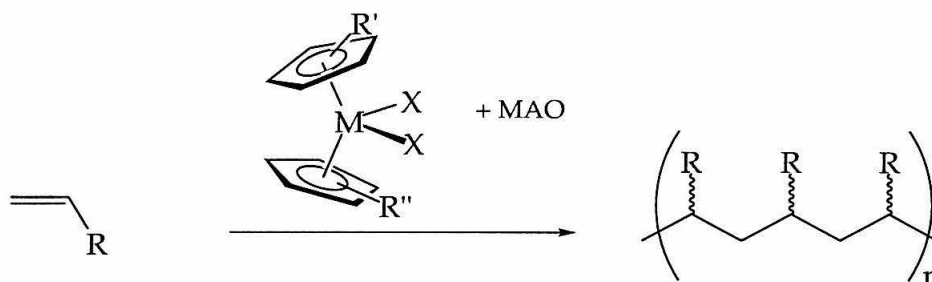


Figure 1. Zirconocene-MAO catalyzed α -olefin polymerization.

While this discovery held great promise, it was not very useful for α -olefins until advances made by Brintzinger and Ewen.³ They separately showed that substituted zirconocene dichlorides with tethered Cp ligands, so called *ansa* zirconocenes,⁴ could polymerize propylene stereoselectively, and that the stereoselectivity was controlled by the structure of the metallocene. These discoveries touched off a torrent of research that continues to the present. While these catalysts were initially viewed as models for heterogeneous catalysts, they are becoming useful industrial catalysts in their own right. As of this writing, metallocene polymerization accounts for the production of approximately 8% of the U.S. market of polyethylene and this fraction is expected to grow extremely rapidly.⁵

As previously mentioned, *ansa* metallocenes can polymerize α -olefins in a stereoselective fashion. The most common type of stereoregular poly- α -olefin is

isotactic polymer, which results from repeated iso-facial insertions. The second type is syndiotactic polymer, which results from α -olefin insertions of perfectly alternating stereochemistry. These stereoregular polymers are shown below with examples of catalysts that produce each type.

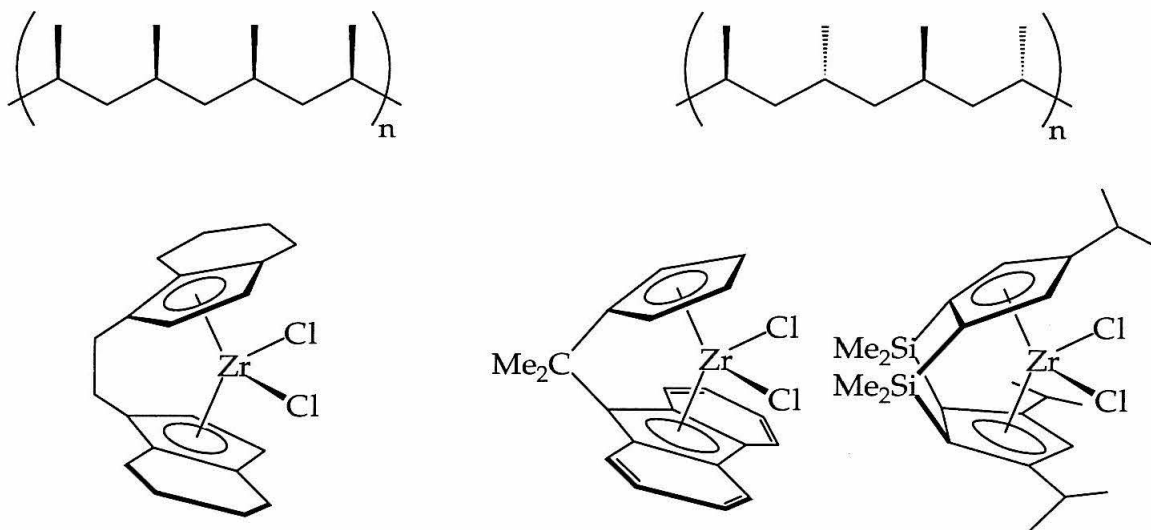


Figure 2. Catalysts used in the stereoselective polymerization of α -olefins.

Highly stereoregular isotactic polypropylene is commonly prepared by heterogeneous catalysts,⁶ but there are very few examples of syndiotactic polymer produced from heterogeneous catalysts. There have been other novel variations of polymer microstructure from metallocene catalysts that have continued to spur further research into understanding the basic mechanism of polymerization so that better catalysts can be designed in the future.

In addition to the industrial utility that metallocene catalysts are beginning to have, they are useful as models for studying the mechanism of olefin polymerization.⁷ The generally accepted mechanism is shown below and has a

few notable features. The active species is a cationic Group IV metallocene alkyl species.⁸ The resting state of this catalyst has a coordinated anion which occupies a potentially vacant orbital.⁹ This anion is displaced by an olefin, yielding a coordinated olefin complex.¹⁰ The subsequent olefin insertion into the zirconium-alkyl bond is assisted by an α -agostic interaction from the alkyl chain into the LUMO of the complex.¹¹ The resulting γ -agostic species then rearranges quickly to a β -agostic species, which can either undergo further insertion or can associate with the anion.

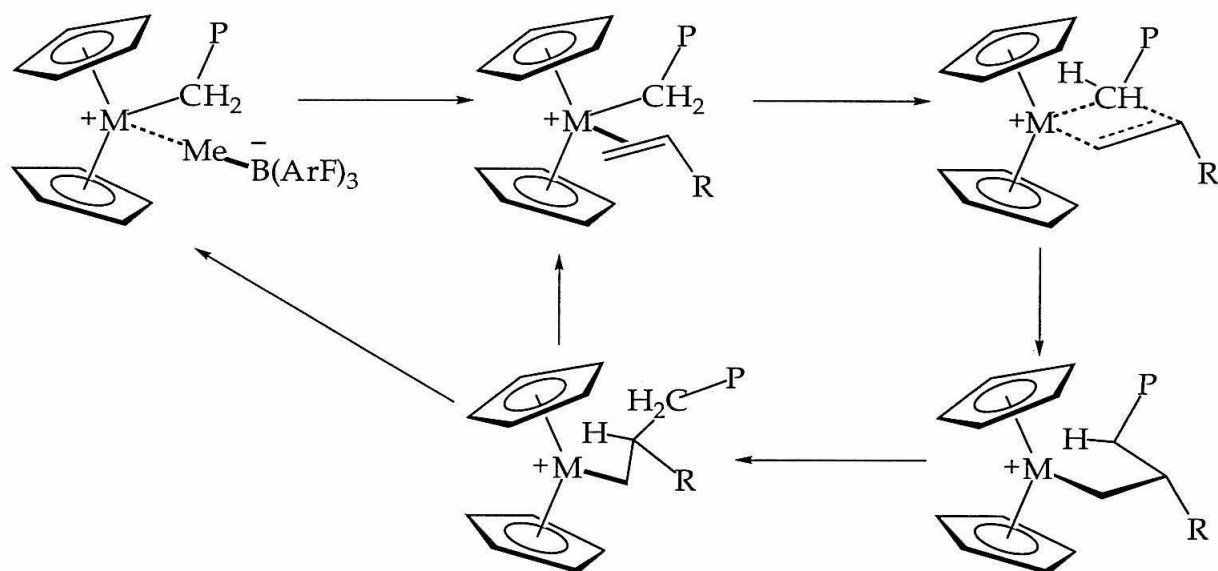


Figure 3. Mechanism of α -olefin Polymerization by Cationic Group IV Metallocene Catalysts.

Some aspects of the polymerization mechanism are still not entirely understood. This thesis will address some of these issues. The first chapter is a computational study of the effect of replacing a neutral *ansa* metallocene linker

with an anionic *ansa* borate linker. This is an attempt to improve catalyst design by eliminating the need for excess catalyst activator. The effects of solvent, anion, and size of the *ansa* linker are also addressed. The second chapter addresses how variation in *ansa* metallocenes affects the electronic structure and reactivity of these metallocenes. Specifically, the reduction potentials of zirconocene dichlorides, carbonyl stretching frequencies of zirconocene dicarbonyls, and anion dissociation barriers are compared to geometric parameters for different complexes. Finally, the third chapter examines the d^0 olefin complex. By preparing cationic complexes with a 2-sila-4-pentenyl substituent, olefin coordination is favored over anion coordination and various elimination pathways. Dynamic behavior consistent with olefin dissociation and subsequent recoordination is observed. Additional observations concerning the site epimerization mechanism, which has relevance for syndiotactic polymerization catalysts, are also made.

-
1. Ziegler, K.; Holzcamp, E.; Breil, H.; Martin, H. *Angew. Chem.* **1955**, *67*, 541.
 2. Andresen, A.; Cordes, H.-G.; Herwig, J.; Kaminsky, W.; Merck, A.; Mottweiler, R.; Pein, J.; Sinn, H.; Vollmer, H.-J. *Angew. Chem. Int. Ed. Engl.* **1976**, *15*, 630.
 3. a) Ewen, J. A. *J. Am. Chem. Soc.* **1984**, *106*, 6355.
(b) Kaminsky, W.; Kulper, K.; Brintzinger, H. H.; Wild, F. R. W. P. *Angew. Chem. Int. Ed. Engl.* **1985**, *24*, 507.
 4. (b) Kaminsky, W.; Kulper, K.; Brintzinger, H. H.; Wild, F. R. W. P. *Angew. Chem. Int. Ed. Engl.* **1985**, *24*, 507.
 5. a) Tulio, A. H. *Chemical & Engineering News* **2000**, *78*, 35.

-
- b) Morse, P. M. *Chemical & Engineering News* **1999**, 77, 11.
6. Natta, G.; Corradini, P. *Atti. Accad. naz. Lincei Mem. Cl. Sci. Fis. Mat. Nat. Sez. II* **1955**, 5, 73.
7. Brintzinger, H.-H.; Fischer, D.; Müllhaupt, R.; Rieger, B.; Waymouth, R. M. *Angew. Chem. Int. Ed. Engl.* **1995**, 34, 1143.
8. a) Eisch, J. J.; Piotrowski, A. M.; Brownstein, S. K.; Gabe, E. J.; Lee, F. L. J. *Am. Chem. Soc.* **1985**, 107, 7219.
- b) Jordan, R. R.; Bajgur, C. S.; Dasher, W. E.; Rheingold, A. L. *J. Am. Chem. Soc.* **1986**, 108, 7410.
9. Wendt, O.; Bercaw J. E. *Manuscript in Preparation*.
10. (a) Wu, Z.; Jordan, R. F.; Petersen, J. L. *J. Am. Chem. Soc.* **1995**, 117, 5867.
- (b) Casey, C. P.; Hallenbeck, S. L.; Pollock, D. W.; Landis, C. R. *J. Am. Chem. Soc.* **1995**, 117, 9770.
- (d) Casey, C. P.; Fagan, M. A.; Hallenbeck, S. L. *Organometallics* **1998**, 17, 287.
- (e) Galakhov, M. V.; Heinz, G.; Royo, P. J. *Chem. Soc., Chem. Commun.* **1998**, 17.
- (f) Casey, C. P.; Carpenetti, D. W.; Sakuri, H. *J. Am. Chem. Soc.* **1999**, 121, 9483.
11. Grubbs, R. H.; Coates G. W. *Acc. Chem. Res.* **1996**, 29, 85.

Chapter 2

The Group IV Zwitterion *Ansa*-Metallocene Ziegler-Natta Catalyst

Abstract

Using density functional theory we studied the fundamental steps of olefin polymerization for both zwitterionic *ansa* metallocenes and cationic *ansa* metallocenes. Complexes $[\text{H}_2\text{E}(\text{C}_5\text{H}_4)_2\text{ZrMe}]^n$ ($n = 0$: E = BH_2 (**1**), BF_2 (**2**), AlH_2 (**3**); $n = +$: E = CH_2 (**4**), SiH_2 (**5**)) were used as computational models. We also studied the neutral complexes $((\text{CH}_2)_3\text{C})(\text{C}_5\text{H}_5)\text{ZrMe}$ (**6**) and $\text{H}_2\text{Si}(\text{C}_5\text{H}_5)_2\text{YMe}$ (**7**) as examples of poor olefin polymerization catalysts. For three representative examples (**1**, **5**, **7**) the calculated olefin binding energy decreased in the following order: $[\text{H}_2\text{Si}(\text{C}_5\text{H}_4)_2\text{ZrMe}]^+ > [\text{H}_2\text{B}(\text{C}_5\text{H}_4)_2\text{ZrMe}] > \text{H}_2\text{Si}(\text{C}_5\text{H}_5)_2\text{YMe}$. The olefin insertion barrier into a Zr- CH_3 bond was similar in these three cases. Including a dielectric field on the energy calculations decreased the olefin binding energy for **5**, leaving the insertion barrier unchanged, but it increased the insertion barrier for **1**, leaving the olefin binding energy unchanged. The overall difference in insertion barrier between **1** and **5** remained the same. $[\text{CH}_3\text{BF}_3]^-$ was used to model anion dissociation from the metal center. The anion was bound more weakly to **1** than to **5**. Finally, while the calculated olefin binding depended primarily on the charge of the *ansa* linker, the olefin insertion barrier was found to decrease steadily in the following order: $[\text{H}_2\text{C}(\text{C}_5\text{H}_4)_2\text{ZrMe}]^+ > [\text{H}_2\text{B}(\text{C}_5\text{H}_4)_2\text{ZrMe}] \approx [\text{F}_2\text{B}(\text{C}_5\text{H}_4)_2\text{ZrMe}] > [\text{H}_2\text{Si}(\text{C}_5\text{H}_4)_2\text{ZrMe}]^+ > [\text{H}_2\text{Al}(\text{C}_5\text{H}_4)_2\text{ZrMe}]$. The insertion barrier correlates linearly with the $\text{Cp}_{\text{cent}}\text{-Zr-Cp}_{\text{cent}}$ angle.

Introduction

The development of current transition-metal catalyzed olefin polymerization of olefins can be traced to the discovery that a small amount of nickel in the presence of trialkyl aluminum rapidly catalyzes the polymerization of ethylene.¹ Since this discovery, heterogeneous catalysts have matured to complicated mixtures of early transition metals, alkyl aluminum chlorides, Lewis acid activators, and a number of chemical additives. Despite tremendous improvement in activities and selectivities, heterogeneous catalyst development remains largely a black box process.

The discovery of heterogeneous Ziegler-Natta polymerization occurred just as the field of organometallic chemistry was taking shape. The discovery of the surprisingly stable ferrocene led to the preparation of a wide variety of transition-metal cyclopentadienyl complexes.² Because heterogeneous titanium catalysts show high activity, it was logical to examine whether homogeneous cyclopentadienyl titanium complexes activated with alkyl aluminum would be active towards olefin polymerization. They indeed were, and some of these original complexes produced polyethylene with properties superior to that produced by heterogeneous catalysts, albeit at lower rates and yields. Although it was known early on that the active catalyst in these systems was a Ti(IV) species,³ further understanding was achieved slowly. Indeed, the most important advancement in the practical application of metallocene polymerization catalysts was the discovery that addition of methylalumoxane (MAO) to dimethyl titanocene resulted in a dramatic increase in olefin polymerization rates.⁴ MAO also activates zirconocenes, which had previously been inactive towards olefin polymerization when activated with trialkyl aluminum. Twenty years after the initial titanocene dichloride catalyzed polymerization of ethylene, this discovery marked the beginning of a major shift in Ziegler-Natta polymerization research towards metallocene based catalysts.

While many proposals for the identity of the active species in homogeneous olefin polymerizations were made, direct evidence remained elusive.⁵ In 1984, Eisch and co-workers published the first convincing evidence that the active species was an alkyl metallocene cation.⁶ They demonstrated that, upon the activation of titanocene dichloride with methyl aluminum dichloride,

the bulky trimethyl(phenylethynyl)silane inserted irreversibly into a Ti-CH₃ bond, yielding an alkenyl cation (Figure 1).

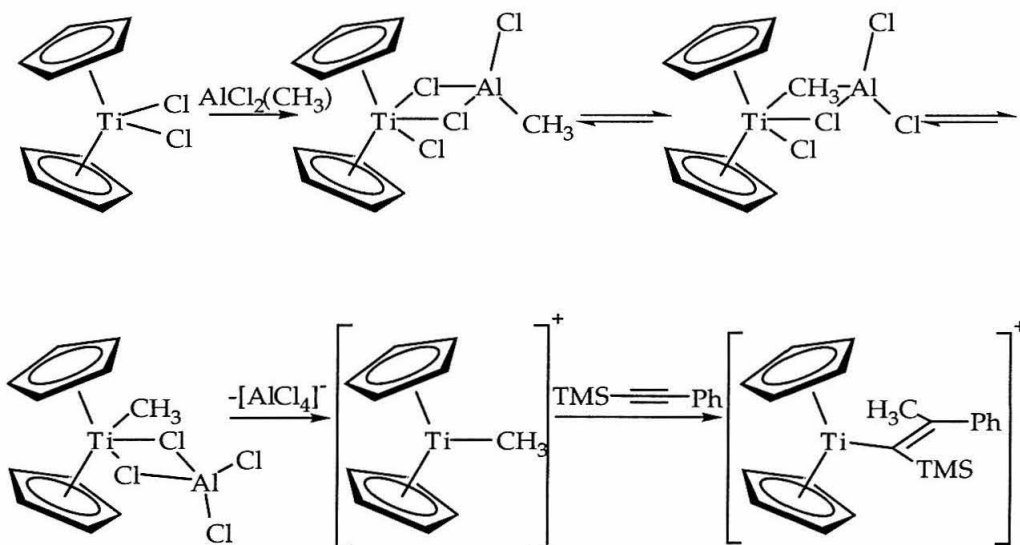


Figure 1. Initial identification of cationic alkyl titanocenes as active olefin polymerization catalysts.

Later studies have continued to support this assignment.⁷ In particular, Jordan and co-workers prepared a discrete zirconocene methyl cation with coordinated THF ligand that oligomerized ethylene slowly in the absence of any co-catalyst, emphasizing that the transition-metal alkyl cation was the active catalyst.⁸ In an attempt to prepare a well-defined, base-free zirconocene methyl cation, Turner and Hlatky prepared zwitterionic zirconocenes containing a zirconium-bound tetraphenyl borate anion (Figure 2).⁹ They were also able to prepare a discrete zirconocene methyl cation with a coordinated carborane anion. Both the zwitterion and the discrete cation polymerized olefins at much higher rates than Jordan's cationic zirconocenes with coordinated Lewis bases. Later, Marks and co-workers prepared a zirconocene cation by abstracting a methyl group from a dimethyl zirconocene complex with B(C₆F₅)₃ (Figure 2).¹⁰ This complex catalyzed olefin polymerization at very high rates. Cationic zirconocene alkyl complexes with perfluoroaryl borate anions often have polymerization activities that rival methylalumoxane activated metallocenes.¹¹

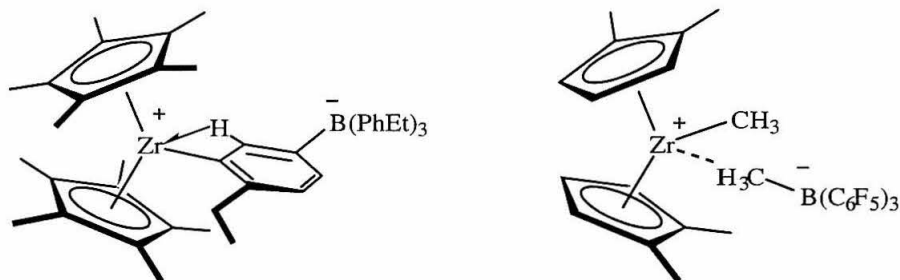


Figure 2. Cationic olefin polymerization catalysts.

Many methods for the preparation of cationic metallocenes with a weakly coordinating anion have been developed.¹² However, even the most weakly coordinating anions bind to the metal, inhibiting polymerization and interacting with the catalyst in unknown ways.¹³ This interaction complicates mechanistic studies and catalyst design.

Because cationic, 14-electron, three-coordinate, alkyl zirconocenes were such active polymerization catalysts, individual steps of polymerization occurred too quickly to be observed by standard spectroscopic methods. There were numerous efforts to make catalyst models that were *neutral*, 14-electron, three coordinate complexes. Neutral Group III and trivalent f-block alkyl metallocene complexes are isoelectronic and isolobal to cationic Group IV alkyl metallocene complexes. These complexes are useful for mechanistic studies since they do not have the complicating influence of a coordinating anion.¹⁴

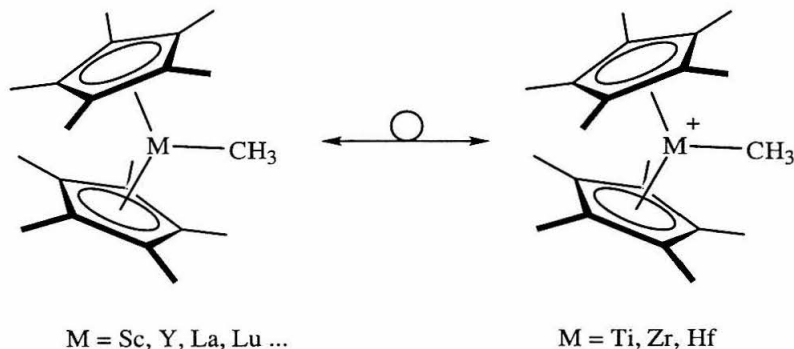


Figure 3. Isolobal analogy of neutral Group III metallocenes and cationic Group IV metallocenes.

This relationship was utilized by Watson and Parshall to study olefin polymerization in analogy to the proposed cationic titanocene-based catalysts.^{14b} In these systems, olefin polymerization occurs slowly enough that discrete olefin insertions were observed. Bercaw and co-workers used these model systems extensively in several investigations of three coordinate metallocene alkyl complexes, which improved the understanding of many fundamental transformations related to olefin polymerization.¹⁵ However, the complexes are useless as practical catalysts because their primary virtue is their modest activity.

Several researchers have attempted to make neutral Zr(IV) alkyl complexes that could polymerize olefin without activation. Along these lines, Group IV complexes with a cyclopentadienyl ligand replaced by a dianionic ligand have been prepared. Jordan and co-workers prepared a number of complexes with a dicarbolyde ligand.¹⁶ The zirconium methyl complex polymerized ethylene with moderate rates. Similarly, Bercaw and co-workers used amine derivatives of the borollide ligand popularized by Herberich to prepare neutral complexes.¹⁷ The $\text{Cp}^*(\text{C}_4\text{Me}_4\text{BNiPr}_2)\text{Zr}(\text{C}_3\text{H}_5)$ complex (Figure 4) polymerized ethylene without activation at unremarkable rates. Bazan and co-workers sought to improve the polymerization activities of these types of complexes.¹⁸ However, complexes with the dianionic trimethylenemethane ligand had low rates of ethylene polymerization.

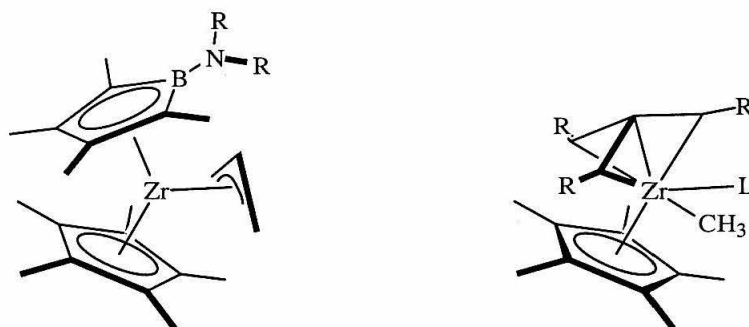


Figure 4. Neutral d^0 zirconocene complexes.

While these neutral metallocene catalysts were attractive because they required no activator, they had very little practical application due to their low polymerization activities. The source of this low activity is not entirely clear, but it seems possible that the dianionic ligands render these complexes less electrophilic.

Thus, in order to retain high polymerization activity, it appeared that retention of a cationic metal center was necessary. With this in mind, researchers have attempted to prepare zwitterionic metallocenes with an anion that was attached to the ligand.¹⁹ (Figure 5) This would result in a catalyst that requires no activator yet retains high activity. Also, because the anion would be attached rigidly to the ligand, it could not interact with the metal center, whereas the rigid binding of a metal-bound anion that separates the charges is lost upon olefin insertion into the metal-carbon bond. Along these lines, Bochmann and co-workers prepared a zirconocene catalyst with a tris(pentafluorophenyl)borate anion attached to one of the cyclopentadienyl ligands. (Figure 5) Unfortunately, an active catalyst could not be made from this complex without activation by MAO.

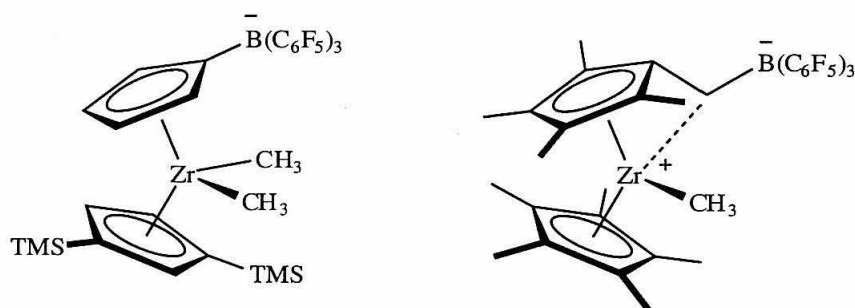


Figure 5. Zwitterionic zirconocenes.

Piers has successfully employed this strategy with zwitterion complexes that polymerize ethylene at high rates without any added activator.²⁰ This complex has a ligand with a pendant $\text{CH}_2\text{B}(\text{C}_6\text{F}_5)_3^-$ that weakly coordinates one of the vacant orbitals on the metal *via* the methylene carbon (Figure 5) and is readily displaced by olefin.

Another particularly attractive approach is to replace the neutral linking atom in *ansa* metallocenes with an anionic moiety, such as a tetracoordinate boron or aluminum. This design prevents the anion from blocking the active site of the catalyst, yet its proximity should still stabilize the cation. Unlike complexes with a dianionic ligand, which render the metal neutral and have poor polymerization activity, complexes with this ligand would retain a cationic metal center. While the design is aesthetically elegant, Shapiro²¹ as well as others have

shown that the synthesis of such complexes is not trivial. A representative example of these complexes and its synthesis are shown in Figure 6.

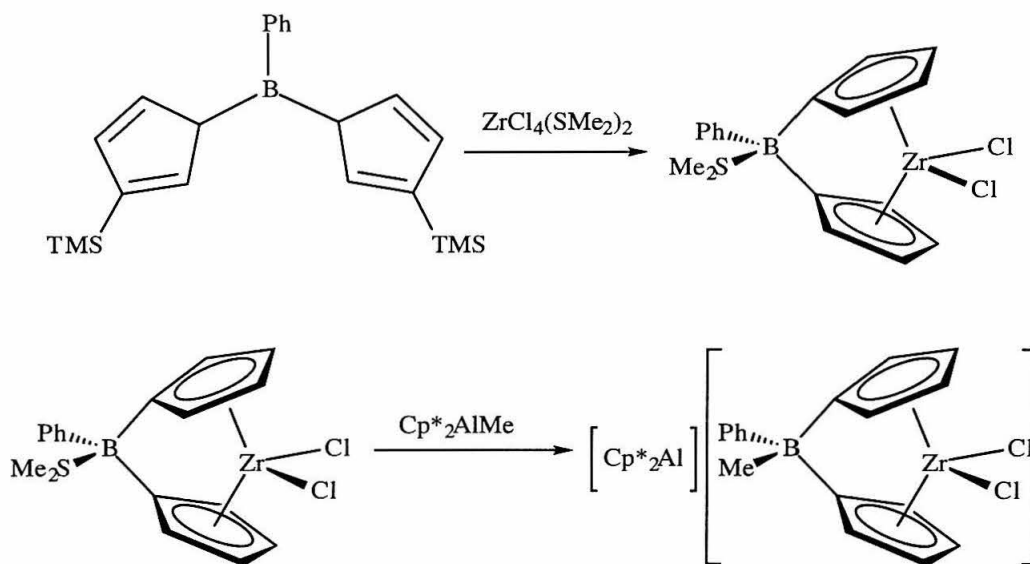
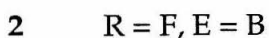
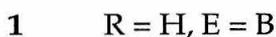
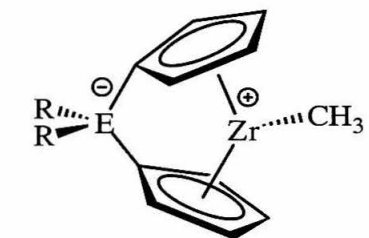


Figure 6. Preparation of borate *ansa* zirconocene complexes.

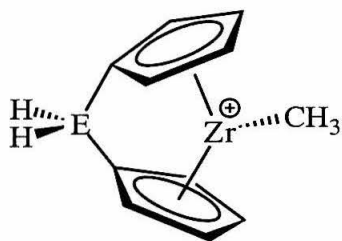
However, no complexes with an anionic borate *ansa* linker have been prepared as alkyl derivatives. While some neutral borane *ansa*-metallocenes activated with MAO are moderately active catalysts,²² no anionic borate *ansa*-metallocene catalyzed polymerizations have been reported.

In order to determine if this approach to catalyst design could lead to improved catalytic performance, we investigated the viability of such zwitterionic *ansa*-metallocenes using first principle quantum mechanics (B3LYP density functional theory), with metallocenes **1-3** as models.



3. R = H, E = Al

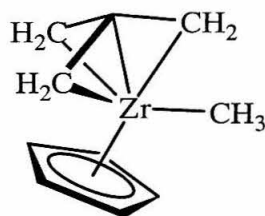
For comparison, we also examined two models of standard cationic Group IV Ziegler-Natta catalysts (4, 5)



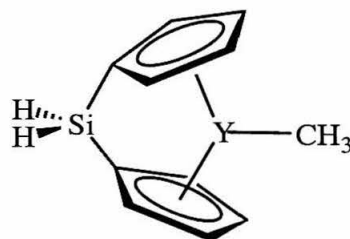
4 E = C

5 E = Si

In order to understand the differences in reactivity between Group IV cationic metallocenes and neutral Group IV and Group III metallocenes, we also studied complexes 6 and 7.

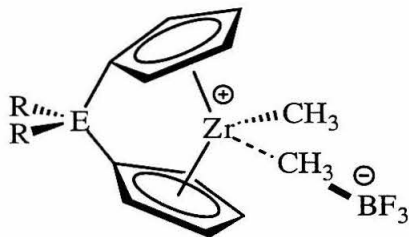


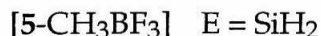
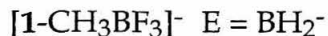
6



7

Lastly, in order to study how the anionic *ansa* linker might affect the dissociation of the ion pair, we studied the binding of $[\text{CH}_3\text{BF}_3]^-$ to metallocenes 1 and 5. The anion $[\text{CH}_3\text{BF}_3]^-$ that is used as a simple model of $[\text{CH}_3\text{B}(\text{C}_6\text{F}_5)]^-$





Calculation Methods

We carried out density functional theory (DFT) calculations using the Jaguar program.^{23,24,25,26} The Zr was described using the LACVP Hay and Wadt effective core potential (ECP) to replace the core electrons {leaving the $(4s)^2(4p)^6[(4d)(5s)(5p)]^4$ electrons to be described explicitly} and using the standard double zeta contraction. In addition, all other atoms (B, C, H) were described using the 6-31G** basis.²⁷ Collectively, this ECP basis is referred to as LACVP**. We used the generalized gradient approximate (GGA) but included exact exchange in the hybrid 3 parameter Becke scheme. The correlation density function was LYP. All structures in this study were optimized using this hybrid B3LYP method.

All geometries of stable intermediates and transition states were fully optimized with the above basis and methods. Geometries of all intermediates of **6** were optimized with no symmetry restraints. The geometries of the intermediates of all other metallocenes (except for the methyl complexes, bound ethylene complexes and hydride complexes, which were optimized under C_s symmetry) were optimized with no symmetry constraints.

Solution phase energies were obtained by optimizing the structures in the gas phase and determining the single point solvation energy without further optimization.

The metallocene catalysts are generally referred to by a number that primarily serves to distinguish among different ligand frameworks. Specific intermediates of a particular complex will be identified by the number followed by two initials, which are abbreviations of the intermediate's name.

Results and Discussion

Geometries.

In general, the geometries of the intermediates of the cationic metallocenes are unexceptional and consistent with previous studies. Selected

bond lengths and bond angles of the intermediates of olefin polymerization are shown in Figure 7.

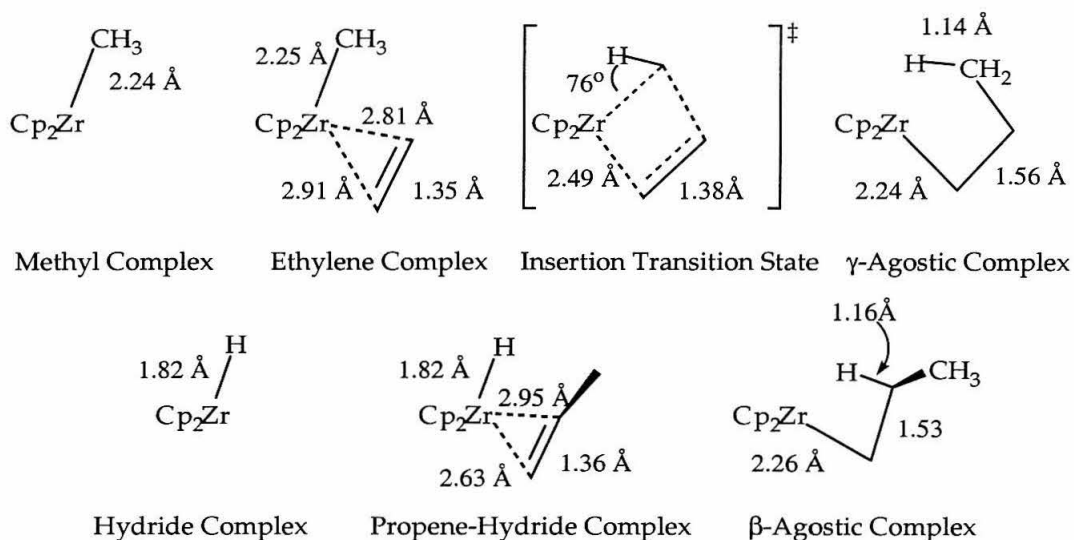


Figure 7. Geometric parameters for intermediates of **5** in ethylene polymerization.

Only the most notable features are summarized here. Upon binding ethylene to zirconium, the C=C bond length is almost unchanged, as expected for d^0 complexes of olefins, because there is no backbonding to populate the π^* orbital of the olefin. The insertion transition state structure exhibits evidence of α -agostic assistance, interpreted as the extremely small H-C-Zr angle (72°) and a lengthened α -C-H bond distance (1.2 Å). Additionally, stable γ -agostic and β -agostic intermediates were found along the reaction pathway with a small transition state between the two. The evidence for these agostic structures is the lengthening of coordinated C-H bonds in those intermediates to 1.17 Å. The β -agostic structure is interesting because the Zr-C-C angle is 86° , indicating a rehybridization of the α -carbon in contrast to the γ -agostic structure in which all of the carbon atoms are roughly tetrahedral. This structural feature has been observed previously in experimental and computational studies and has been shown to result from delocalization of the electrons in the M-C bond into a pseudo- π bond on the C-C axis in the Zr-C-C plane.²⁸ The methyl complexes have pyramidal structures with the methyl group approximately 52° out of the $\text{Cp}_{\text{cent}}\text{-Zr-Cp}_{\text{cent}}$ plane. The cationic hydrides were similar in this respect with the H atom 78° out of the plane.

The zwitterionic complexes were geometrically similar in all respects to the cationic complexes. The Zr-C bond lengths of these complexes were consistently lengthened by ~ 0.03 Å. The methyl group is also 52° out of the plane and the hydride is only 66° out of the plane. One explanation for the decreased pyramidal distortion might be a larger contribution of *s* orbital character in the Zr-H bond, although the source of this hybridization change is unclear. All of the other intermediates and transition states were stationary points on the potential energy curve and shared nearly identical structures with **5**.

While metallocene **6** is a zirconium (IV) complex, this methyl complex (**6-Me**) is quite distinct geometrically from complexes **1** and **5**. The methyl group sits in the Cp-Zr-TMM plane instead of in a pyramidal arrangement with respect to the other ligands. This is due to a change of the frontier molecular orbitals for the Cp-Zr-TMM fragment with respect to the Cp-Zr-Cp fragment. The sigma bonding orbital of the Cp(TMM)Zr fragment has significant *s* orbital character and lies in the Cp-Zr-TMM plane. The bond lengths are consistently longer than those in **5** by ~ 0.06 Å. In all other respects, the bound ethylene and insertion transition structures that were calculated for this metallocene were similar to **5**.

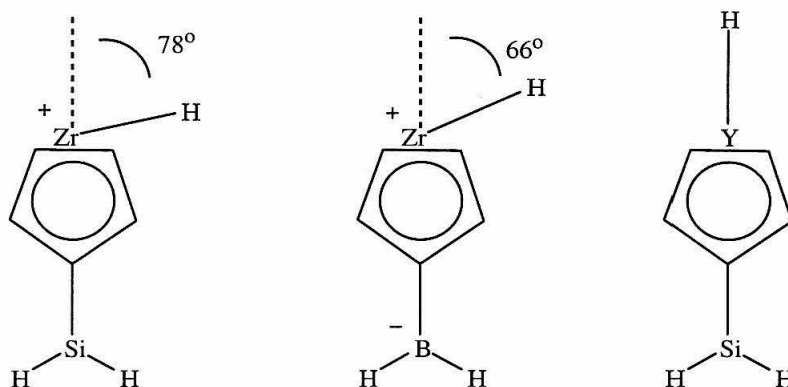


Figure 8. Geometry of hydride complexes **5**, **1**, and **7**.

The bond lengths in complex **7** are very different from the other complexes due to the substitution of Zr by Y, but the bond lengths are consistent with geometric parameters found in analogous crystal structures.²⁹ The structures of the intermediates are otherwise similar to **5** with one exception. As in previous predictions, we found that the metal center in $\text{H}_2\text{SiCp}_2\text{Y-Me}$ (**7-Me**)

structure is planar, not pyramidal. In this case, Y(III) prefers a hybridization with more *s* orbital character, whereas Zr(IV) prefers more *d* orbital contribution.³⁰

Lastly, we calculated the geometry of the methyl cation of metallocenes **1-Me** and **5-Me** with a coordinated methyl borate anion, $[\text{MeBF}_3]^-$. To determine whether $[\text{MeBF}_3]^-$ serves as a reasonable model of $[\text{MeB}(\text{C}_6\text{F}_5)_3]^-$, we compared the structure of this complex with crystal structures of analogous complexes. We found that the Zr-C bond distances are similar, although this model underestimates the Zr-- $\text{H}_3\text{CB}(\text{C}_6\text{F}_5)_3$ bond distance by ~ 0.1 Å.³¹ The geometries of the methyl group in anions bound to **1** and **5** are different, and this difference provides insight into the electronic nature of the two metal centers.

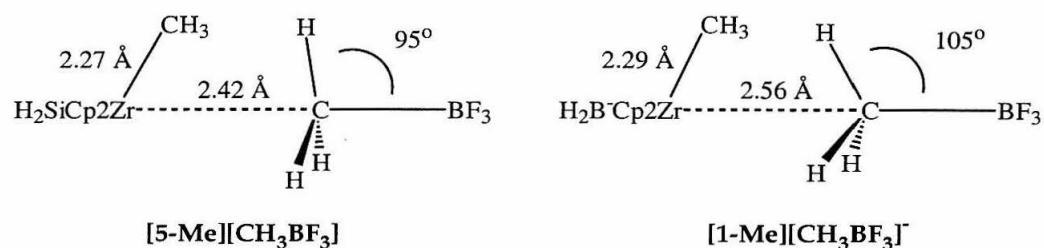


Figure 9. Comparison of coordinated methyl borate geometries.

The abstracted methyl group is nearly planar in the case of **5**, but in the case of **1**, the methyl group is pyramidal and its hydrogen atoms are directed towards zirconium, indicating less Zr-C bonding. Although the calculated electrostatic potentials for the Zr atom are approximately the same in both metallocenes (**1** = 1.3 Å, **5** = 1.25 Å), the structural evidence indicates that the bonding between the Zr and $[\text{H}_3\text{CBF}_3]^-$ is weakened by adding an anionic backbone.

Reaction Energetics.

The results for **5** are similar to those in previous studies of cationic metallocene catalysts³² and can be summarized here briefly. The results are graphed in Figure 10 and are summarized in Appendix 1. Ethylene binding to the **5-Me** is exothermic by 22 kcal·mol⁻¹. The insertion of ethylene into the Zr-CH₃ bond of the resulting methyl ethylene complex occurs with a low barrier (7 kcal·mol⁻¹). The resulting propyl species with a coordinated γ -hydrogen (**5- γ ag**) is 8 kcal·mol⁻¹ more stable than the ethylene complex. The **5- γ ag** overcomes a 4 kcal·mol⁻¹ barrier to adopt the β -agostic structure (**5- β ag**), which is the more

stable by 2 kcal·mol⁻¹ and is the most stable structure on the potential energy surface that we studied. These four steps constitute the catalytic polymerization cycle.

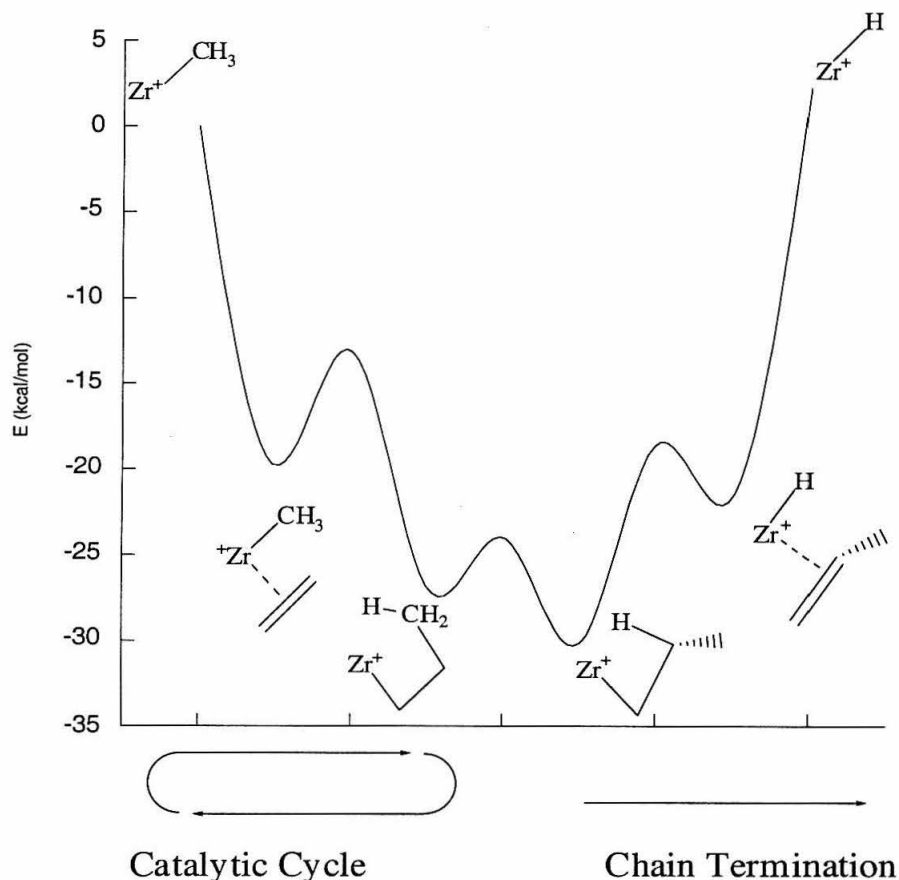


Figure 10. Energy profile of ethylene insertion and subsequent β -H elimination.

Termination of polymerization can occur by β -H or β -CH₃ elimination. β -hydrogen elimination from the 5- β ag has a barrier of 12 kcal·mol⁻¹, and the loss of propene from the resulting olefin hydride complex is endothermic by 24 kcal·mol⁻¹. The total energy required to lose propylene from the β -agostic species is 32 kcal·mol⁻¹. However, the resulting hydride complex and free propylene are only 0.7 kcal·mol⁻¹ higher in energy than the methyl complex and free ethylene. In the model that we have chosen to study, β -CH₃ methyl elimination is the microscopic reverse of the olefin insertion into the Zr-CH₃ bond. While loss of propylene is almost isoenergetic with loss of ethylene, the barrier for β -hydrogen elimination is 5.5 kcal·mol⁻¹ lower than that for β -methyl

elimination, thus partially explaining the experimentally observed preference for chain termination *via* β -hydrogen elimination.

We then turned our attention to understanding why neutral metallocene catalysts perform so poorly compared to cationic metallocene catalysts. We studied the same reaction pathway for the yttrium metallocene **7** that we studied for **5**.

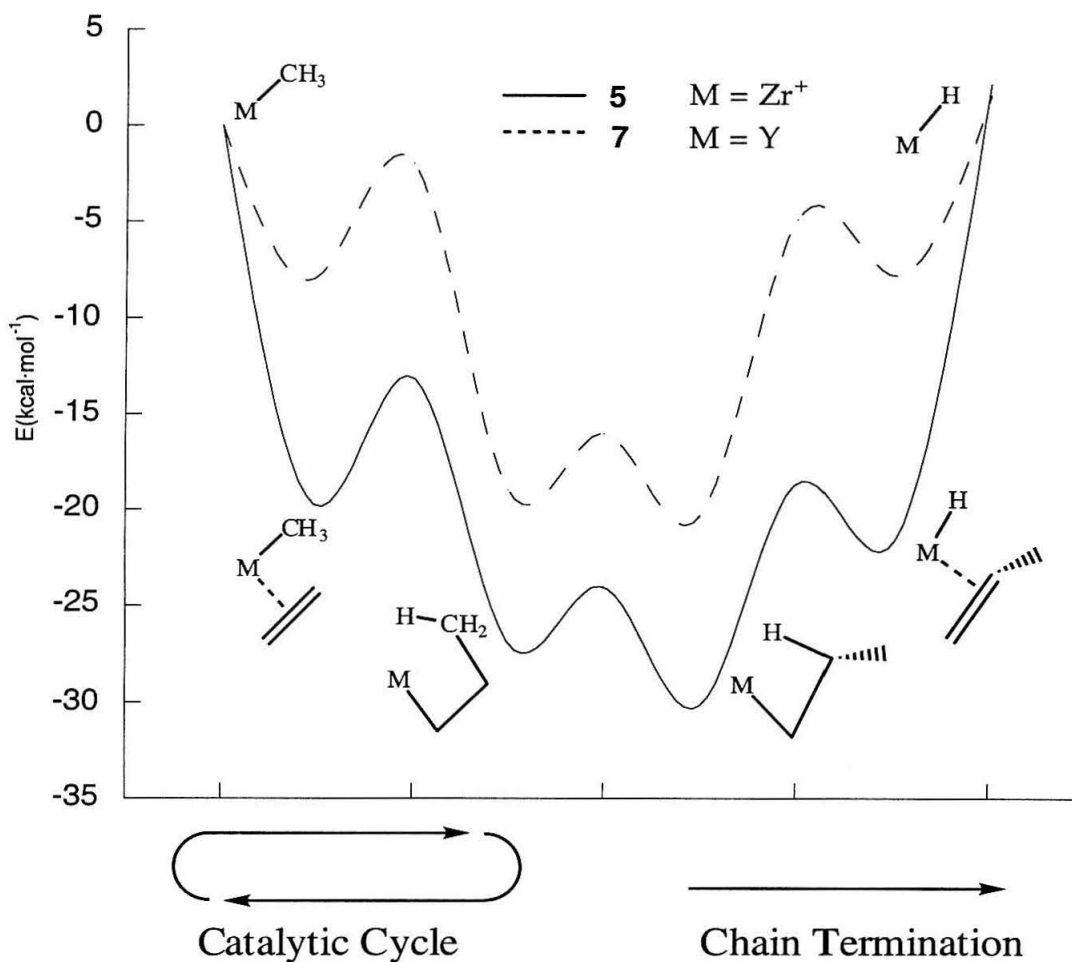


Figure 11. Energy profile of olefin polymerization and termination for complexes **5** and **7**.

The energy profile is shown in Figure 11 and the energies are listed in appendix 1. The most significant difference between **7** and **5** is the ethylene binding energy. The binding energy to **7-Me** is 8 kcal·mol⁻¹, less than half of the binding

energy to **5-Me**. The insertion barrier is $6 \text{ kcal}\cdot\text{mol}^{-1}$, which is comparable to **5**. However, since the binding energy is similar to the olefin insertion barrier, the ethylene is more likely to dissociate from **7-Me** than from **5-Me**. β -hydrogen elimination from **7- β ag** is endothermic by $22 \text{ kcal}\cdot\text{mol}^{-1}$, compared to $30.5 \text{ kcal}\cdot\text{mol}^{-1}$ from **5- β ag**. These results are consistent with the experimentally observed low polymerization activity and low molecular weight polymers observed for Group III metallocenes. The small olefin binding energy has been observed previously by both computational and experimental studies.^{33,34} The formation of inactive metal-hydride dimers, which all known Group III metallocene hydrides form, also inhibits catalyst activity.^{15b}

If the energy profile of ethylene insertion in Figure 11 is extrapolated to the energy profile of chain propagation, it implies that olefin polymerization of ethylene by Group III metallocene catalysts is less exothermic than the same reaction catalyzed by cationic Group IV metallocene catalysts. This is impossible since the net reaction is exactly the same and catalysts cannot change the overall energy of a reaction, only the rate of the reaction. The apparent discrepancy can be explained by the fact that the initial M-CH_3 complex has no β -agostic interactions whereas the product does. The cationic **5** forms a stronger β -agostic interaction than the neutral **7**. If, however, ethylene is inserted into a $\text{M-CH}_2\text{CH}_2\text{CH}_3$ bond (Figure 12), the reaction is equally exothermic for **5** and **7**. This point was confirmed with a model reaction for **5** and **7**.³⁵ However, the β -H and β -methyl elimination energies can still be taken directly from the energy diagrams.

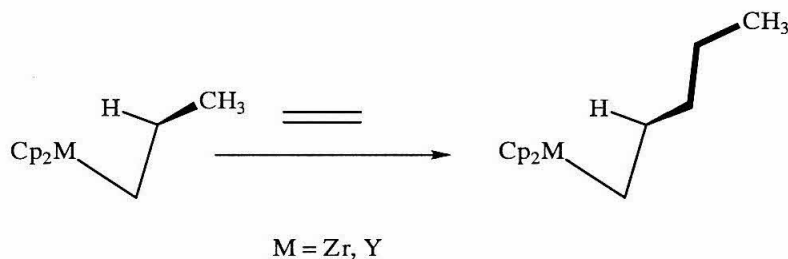


Figure 12. More accurate polymer propagation model.

We did not study the complete reaction pathway for the trimethylenemethane complex **6**. Binding ethylene to this complex is only exothermic by $5 \text{ kcal}\cdot\text{mol}^{-1}$, and the barrier is $18 \text{ kcal}\cdot\text{mol}^{-1}$. Obviously, this is

consistent with the poor catalysis activity exhibited by these complexes. They were not studied further.

The results from the three previous metallocenes thus indicate that an active Ziegler-Natta polymerization catalyst capable of producing a high molecular weight polymer requires strong olefin binding, a low olefin insertion barrier, and a high barrier to β -hydrogen elimination. The results of the complete reaction profile for **1** and **5** are shown in Figure 13.

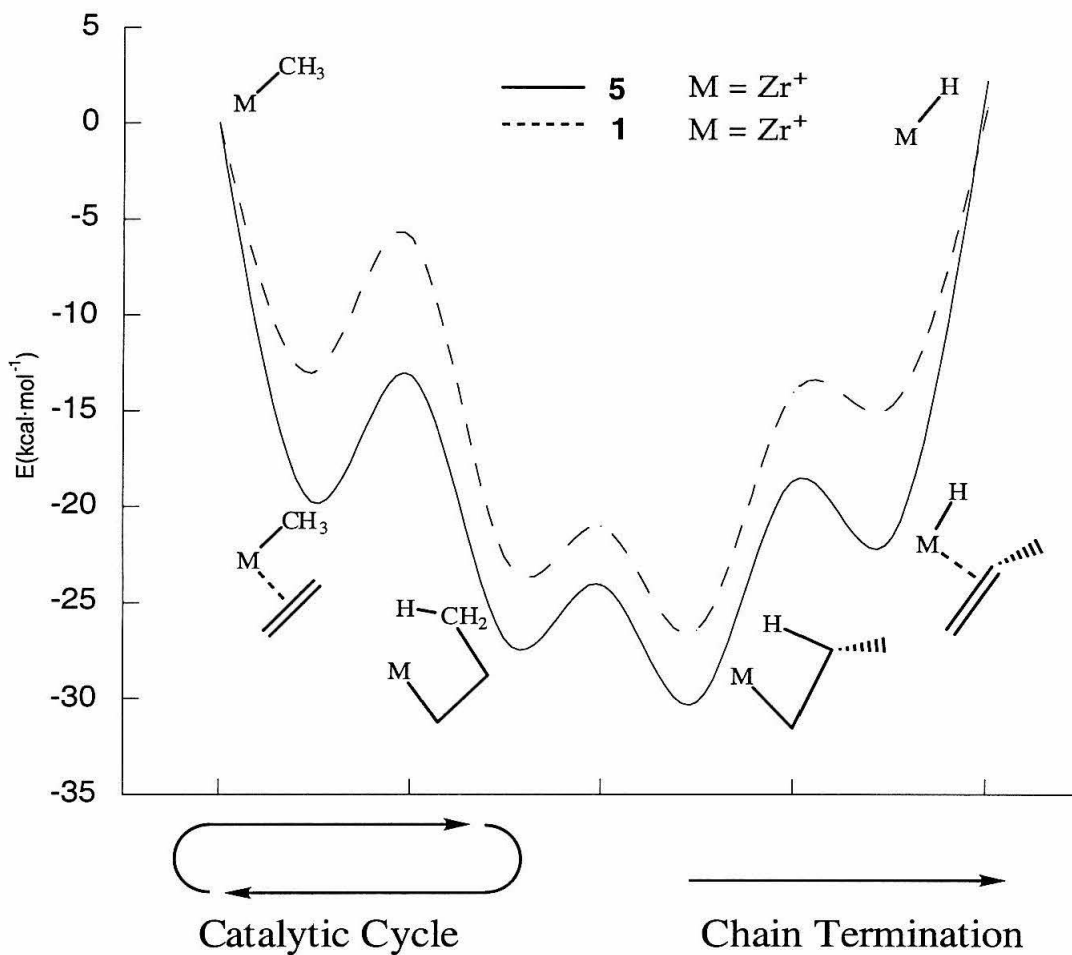


Figure 13. Energy profile of olefin polymerization and termination for complexes **1** and **5**.

The binding of ethylene ($13 \text{ kcal}\cdot\text{mol}^{-1}$) is stronger to **1-Me** than to neutral metallocenes, although it is not quite as strong as it is to **5-Me**. The larger olefin

binding energy of **1-Me** compared to **7-Me** indicates that separation of the negative charge from the metal center allows the zirconium to act as though it were cationic. The ethylene insertion barrier in complex **1** is only 7 kcal·mol⁻¹, similar to this barrier for complex **5**. We found that the total energy for the loss of propylene from **1-βag** is between the values found for metallocenes **5-βag** and **7-βag**. This represents a larger barrier than was found for **7**, so we expect zwitterionic catalysts to produce higher molecular weight polymers rather than oligomers.

While olefin binding to **1-Me** is not as favorable as it is to **5-Me**, it should be noted that the relative effect of the anionic linker is exaggerated in comparison to **5-Me**, since no anion is included in our model cationic metallocenes. Additionally, the role of solvent is not included in these calculations and should influence the energetics. In order to represent the conditions of actual polymerization more accurately, we examined both solvent and anion effects computationally.

Solvent Effects.

The magnitude of the effect solvent would have on the reaction profile was unknown. To simulate the solvent effect, a constant dielectric was added to single point energy calculations on geometries that were optimized in the gas phase. Specifically, we examined catalysts **1** and **5** in benzene solution. The results in Figure 14 show that the solvent does change the energetics of isolated steps in the reaction, but the absolute difference in insertion barriers remains approximately the same.

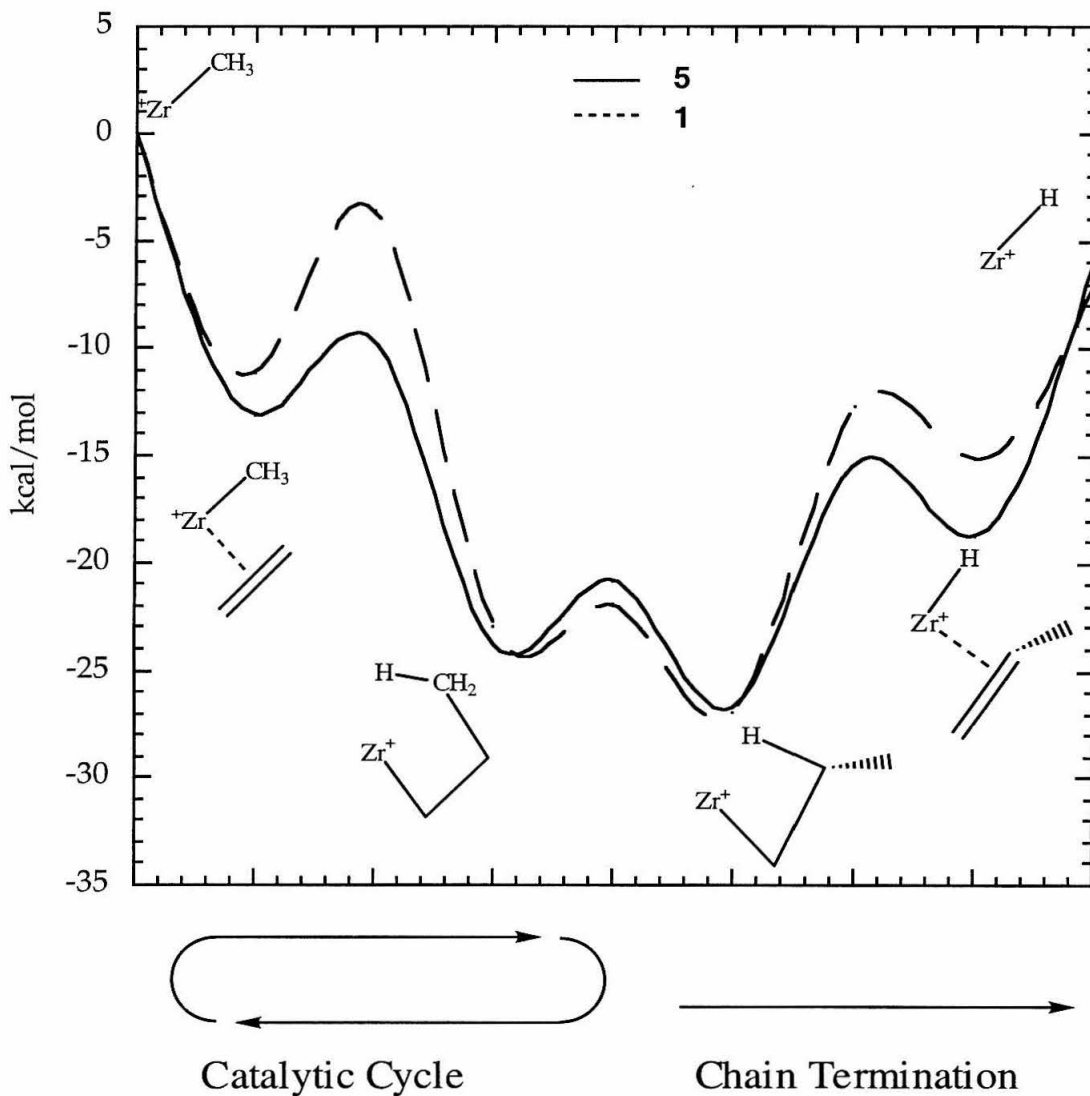
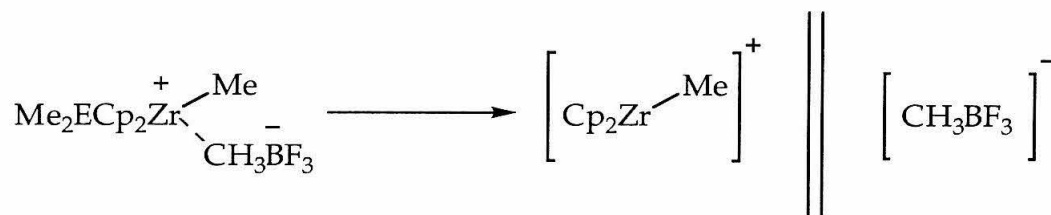


Figure 14. Reaction profiles of **1** and **5** in benzene solvent.

This results from opposing changes in the two catalysts. The addition of solvent decreases the binding energy to **5-Me**, but likewise lowers the ethylene insertion barrier. The binding energy to **1-Me** is only slightly decreased, but the insertion barrier actually increases. The absolute difference between the transition state

energies decreases by ~ 1 kcal in the presence of benzene. For both **1** and **5** the insertion barrier remains the highest barrier for this reaction. Interestingly, the β -agostic structures have the same energy relative to the methyl complexes.

Because complexes **5** and **6** differ in their overall charge, their interaction with solvent and ions in solution was expected to be quite different. For example, it is known that in cationic metallocene catalysts activated with $B(C_6F_5)_3$, only a tiny fraction of the catalyst is active in the polymerization.³⁶ One explanation for this is that complexes exist predominantly as a tight ion pair.^{13a} **1-Me** was expected to have a much lower affinity towards an anion than **5-Me**, because **1-Me** is already stabilized by an anion. We tested this conjecture computationally by comparing the affinities of complexes **5** and **6** towards $[CH_3BF_3]^-$ in both a benzene dielectric ($\epsilon=2.28$ D) and a chlorobenzene dielectric ($\epsilon = 11.2$ D) in order to see how anion affinity varied with solvent polarity. The geometries were optimized in the gas phase and then single point energies were calculated in varying dielectrics.



	Binding Energy (Benzene)	Binding Energy (Chlorobenzene)
5-Me	49.9 kcal·mol ⁻¹	14.6 kcal·mol ⁻¹
1-Me	23.8 kcal·mol ⁻¹	11.8 kcal·mol ⁻¹

Table 1. Anion dissociation energy in benzene and chlorobenzene.

The anion dissociation energies appear to be overestimated in the case of benzene compared to experimental results with toluene.³⁷ Ziegler *et al.* studied anion dissociation with a complete $[CH_3B(C_6F_5)_3]^-$ anion model using an MO-MM treatment³⁸ and found that the dissociation energies are overestimated if a discrete coordinated benzene is not included. Even accounting for this correction they did not find dissociation energies that were quite as large in nonpolar solvents as we did. We have already shown based on geometric considerations,

that anion model $[\text{CH}_3\text{BF}_3]^-$ overestimates the bonding to zirconium. However, these errors are consistently applied to both metallocenes, so the relative trends can still be analyzed. As shown in Table 1, the anion affinities differ greatly in non-polar solvents, whereas in the polar chlorobenzene the difference in anion affinity is much smaller. In either case, the anion would be displaced more easily by olefin from complex **1** than from complex **5**. Since complex **1** is neutral overall, it is not strictly necessary that an anion be present, but such a catalyst might be activated *in situ*, resulting in the presence of an anion.

Ansa Effects.

Because altering the *ansa* linker introduces geometric variations in the metallocenes, we wanted to confirm that the differences that we calculated were indeed due to the charge of the *ansa* linker and not to geometric perturbations. Therefore, we studied the binding and insertion of ethylene for [1-5]-Me. Figure 15 summarizes the results, which are also contained in Appendix 1.

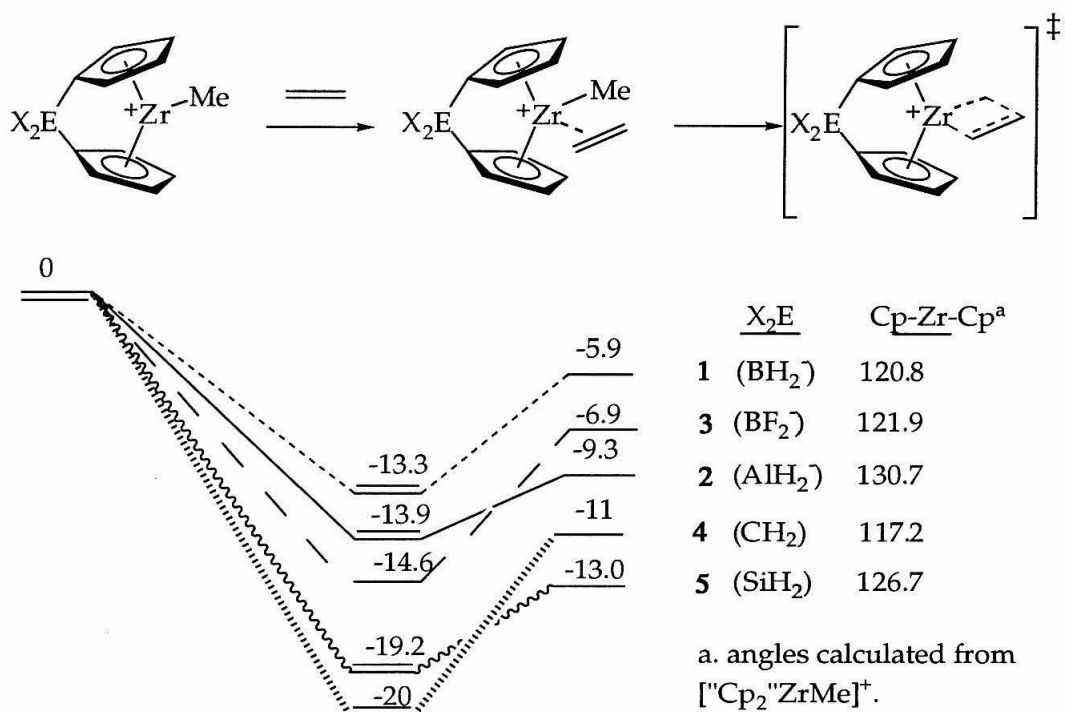


Figure 15. Effect of different *ansa* bridges on olefin binding and insertion. a) $Cp_{cent}-Zr-Cp_{cent}$ angles were calculated from $["Cp'_2ZrMe]^+$ structures.

The olefin binding energies are primarily dependent on the charge of the *ansa* linker. The only significant deviation from this trend is the addition of F substitution on the boron linker, which increases the binding energy by 1.3 kcal·mol⁻¹. However, the insertion barrier seems to be more sensitive to the size of the *ansa* linker. In fact, there is a linear relationship between the Cp_{cent}-Zr-Cp_{cent} angle and the olefin insertion barrier, illustrated graphically in Figure 16.

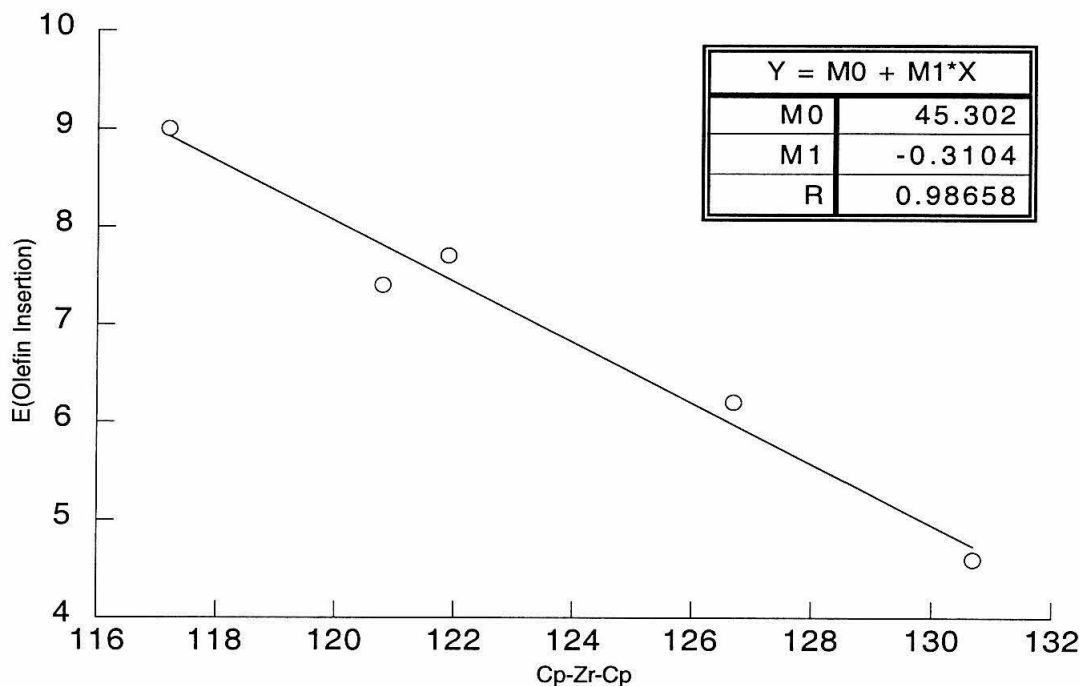


Figure 16. Cp_{cent}-Zr-Cp_{cent} versus olefin insertion barrier.

Based on these calculations, the most effective zwitterionic catalyst should be one with an aluminate linker. While such a linker has never been synthesized, there are recent reports on the preparation of tetracoordinate aluminates, which can be used as co-catalysts in Ziegler-Natta polymerization.³⁹ This observed *ansa* effect is primarily an electronic effect, since the geometric perturbations of the metallocenes are small, and close contacts between the ligand and the olefin (in the cases that we have studied) are few. Changing the substitution on boron from hydrogen to fluorine has a small effect.

Conclusions

We have studied selected examples of neutral Group III and Group IV metallocenes as polymerization catalysts and have shown that their failure as polymerization catalysts seems to stem from two primary factors. First, the olefin binding is rather weak compared to cationic metallocenes, which is probably responsible for the typically sluggish reactivity of these complexes. Second, for neutral Group III metallocenes, such as **7**, the overall loss of propylene *via* β -hydrogen elimination is less endothermic than it is for cationic metallocenes.

Initial examination of zwitterionic *ansa* metallocene catalysts in the gas phase shows that these catalysts could be expected to be more active than neutral metallocenes, but not as active as cationic metallocenes. The binding of ethylene is not as strong, and the overall loss of propylene is slightly more favorable. However, upon inclusion of solvent and an anion model, the prospects of this catalyst improve. The inclusion of solvent equalizes the olefin binding energy for both cationic metallocenes and zwitterionic metallocenes. It also equalizes the overall barrier for loss of propylene. But the insertion barrier for the zwitterionic metallocene remains meaningfully higher than that of the cationic metallocene. In a nonpolar solvent, we have shown that an anion binds quite tightly to the cationic metallocenes whereas the binding energy to zwitterionic metallocenes is only half as strong. This tight binding of anions certainly inhibits the propagation rates of olefin polymerization catalysts. In this regard, the zwitterionic metallocenes may in fact be more productive catalysts since olefins will more easily displace anions.

On the other hand, based on the calculations presented, it seems likely that zwitterionic metallocenes will likely be moderately active catalysts that may produce lower molecular weight polymers compared to similar cationic metallocenes. This conclusion is based on predictions of a slower propagation rate and an equivalent β -hydrogen elimination rate. In addition, synthesis of these zwitterionic catalysts will be nontrivial. While they might be prepared as single-component catalysts requiring no activator, their advantage over dimethyl zirconocene complexes activated with perfluoroboranes is semantic. However, due to their lower anion affinity, they do in fact bear closer experimental scrutiny.

-
1. Ziegler, K.; Holzcamp, E.; Breil, H.; Martin, H. *Angew. Chem.* **1955**, *67*, 541.
 2. Elschenbroich, C.; Salzer, *Organometallics*; VCH: New York, 1992; 317.
 3. (a) Breslow, D. S.; Newburg, N. R. *J. Am. Chem. Soc.* **1957**, *79*, 5072.
(b) Breslow, D. S.; Newburg, N. R. *J. Am. Chem. Soc.* **1959**, *81*, 81.
(c) Henrici-Olivé, G.; Olivé, S. *Angew. Chem.* **1967**, *79*, 764.
 4. Andresen, A.; Cordes, H.-G.; Herwig, J.; Kaminsky, W.; Merck, A.; Mottweiler, R.; Pein, J.; Sinn, H.; Vollmer, H.-J. *Angew. Chem. Int. Ed. Engl.* **1976**, *15*, 630.
 5. (a) Ewen, J. A. *J. Am. Chem. Soc.* **1984**, *106*, 6365.
(b) Kaminsky, W.; Kulper, K.; Brintzinger, H. H.; Wild, F. R. W. P. *Angew. Chem. Int. Ed. Engl.* **1985**, *24*, 507.
 6. Eisch, J. J.; Piotrowski, A. M.; Brownstein, S. K.; Gabe, E. J.; Lee, F. L. *J. Am. Chem. Soc.* **1985**, *107*, 7219.
 7. Gassman, P. G.; Callstrom, M. R. *J. Am. Chem. Soc.* **1987**, *109*, 7875.
 8. Jordan, R. R.; Bajgur, C. S.; Dasher, W. E.; Rheingold, A. L. *J. Am. Chem. Soc.* **1986**, *108*, 7410.
 9. Hlatky, G. G.; Turner, H. W.; Eckman, R. R. *J. Am. Chem. Soc.* **1989**, *111*, 2728.
 10. Yang, X.; Stern, C. L.; Marks, T. J. *J. Am. Chem. Soc.* **1991**, *113*, 3623.
 11. Jia, L.; Yang, X.; Ishihara, A.; Marks, T. J. *J. Am. Chem. Soc.* **1995**, *117*, 3135.
 12. (a) Karl, J.; Dahlmann, M.; Erker, G.; Bergander, K. *J. Am. Chem. Soc.* **1998**, *120*, 5643.
(b) Chen, Y.-X.; Stern, C. L.; Yang, S.; Marks, T. J. *J. Am. Chem. Soc.* **1996**, *118*, 12451.

-
- (c) Li L. T., Stern C. L.; Marks T. J. *Organometallics* **2000** , 19, 3332.
- (d) Li L. T.; Marks T. J. *Organometallics* **1998** , 17, 3996.
13. (a) Liu, Z.; Somsook, E.; Landis, C. R. *J. Am. Chem. Soc.* **2001**, 123, 2916.
- (b) Beck, S.; Lieber, S.; Schaper, F.; Geyer, A.; Brintzinger, H.-H. *J. Am. Chem. Soc.* **2001**, 123, 1483.
14. (a) Thompson, M. E.; Bercaw, J. E. *Pure Appl. Chem.* **1984**, 56, 1.
- (b) Watson, P. L.; Parshall, G. W. *Acc. Chem. Res.* **1985**, 18, 51.
15. (a) Hajela S.; Bercaw, J. E. *Organometallics* **1994** , 13, 1154.
- (b) Shapiro, P. J.; Cotter, W. D.; Schaeffer, W. P.; Labinger, J. A.; Bercaw, J. E. *J. Am. Chem. Soc.* **1994** , 116, 4623.
- (c) Mitchell J. P.; Hajela S.; Brookhart S. K.; Hardcastle, K. I.; Brookhart, S. K.; Bercaw, J. E. *J. Am. Chem. Soc.* **1996** , 118, 1045.
16. Crowther, D. J.; Baezinger, N. C.; Jordan, R. F. *J. Am. Chem. Soc.* **1991**, 113, 1455.
17. Pastor, A.; Kiely, A. F.; Henling, L. M.; Day, M. W.; Bercaw, J. E. *J. Organomet. Chem.* **1997**, 528, 65.
18. Rodriguez, G; Bazan, G. C. *J. Am. Chem. Soc.* **1997**, 119, 343.
19. Piers, W. E. *Chem. Eur. J.* **1998**, 4, 13.
20. Sun, Y.; Spence, R. E. v. H.; Piers, W. E.; Parvez, M.; Yap, G. P. A. *J. Am. Chem. Soc.* **1997**, 119, 5132.
21. Burns, C. T.; Stelk, D. S.; Shapiro, P. J.; Vij, A.; Kunz, K.; Kehr, G.; Concolino, T.; Rheingold, A. L. *Organometallics* **1999**, 18, 5432.
22. (a) Ashe, A. J.; Fang, X.; Kampf, J. W. *Organometallics* **1999**, 18, 2288.

-
- (b) Stelk, D. S.; Shapiro, P. J.; Basicckes, N. *Organometallics* **1999**, *18*, 4546.
- (c) Reetz, M. T.; Willuhn, M.; Psiorz, C.; Goddard, R. *Chem. Comm.* **1999**, 1105.
23. Ringnalda, M. N.; Langlois, J.; Murphy, R. B.; Greeley, B. H.; Cortis, C.; Russo, T. V.; Marten, B.; Donnely, R. E.; Pollard, W. T.; Cao, Y.; Muller, R. P.; Mainz, D. T.; Wright, J. R.; Miller, G. H.; Goddard, W. A. III; Friesner, R. A.; PS-GVB, 2.3 Schrodinger, Inc. 1996.
24. Hay, P. J.; Wadt, W. R. *J. Phys. Chem.* **1985**, *82*, 270.
25. Frisch, M. J.; Pople, J. A.; Binkley, J. S. *J. Chem. Phys.* **1984**, *80*, 3265.
26. a) Slater, J. C. *Quantum Theory of Molecules and Solids, vol. 4: The Self-Consistent Field for Molecules and Solids* (McGraw-Hill, New York, 1974).
- b) Perdew, J. P. *Electronic Structure Theory of Solids*, Ziesche, P.; Eschrig, H. eds. (Akademie Verlag, Berlin, 1991).
27. Kaupp, M; Schleyer P. von R.; Dolg, M; Stoll, H. *J. Am. Chem. Soc.* **1992**, *114*, 8202.
28. (a) Scherer, W.; Priermeier, T.; Haaland, A.; Volden, H. V.; McGrady, G. S.; Downs, A. J.; Boese, R.; Bläser *Organometallics* **1998**, *17*, 4406. (and references therein)
29. Coughlin E. B.; Henling L. M.; Bercaw J. E. *Inorg. Chim. Acta.* **1996**, *242*, 205-210.
30. Bierwagen, E. P.; Bercaw, J. E.; Goddard III, W. A. *J. Am. Chem. Soc.* **1994**, *116*, 1481.
31. (a) Yang, X.; Stern, C. L.; Marks, T. J. *J. Am. Chem. Soc.* **1994**, *116*, 10015.
- (b) Yang, X.; Stern, C. L.; Marks, T. J. *J. Am. Chem. Soc.* **1991**, *113*, 3623.

-
- (c) Beck, S.; Lieber, S.; Schaper, F.; Geyer, A.; Brintzinger, H.-H. *J. Am. Chem. Soc.* **2001**, *123*, 1483.
32. (a) Margl, P.; Deng, L.; Ziegler, T. *J. Am. Chem. Soc.* **1998**, *120*, 5517.
(b) Margl, P.; Deng, L.; Ziegler, T. *Organometallics* **1998**, *17*, 933.
(c) Yoshida, T; Nobuaki, K; Morokuma, K. *Organometallics* **1995**, *14*, 746.
33. (a) Margl, P.; Deng, L.; Ziegler, T. *J. Am. Chem. Soc.* **1998**, *120*, 5517.
(b) Margl, P.; Deng, L.; Ziegler, T. *Organometallics* **1998**, *17*, 933.
34. (a) Casey, C. P.; Hallenbeck, S. L.; Pollock, D. W.; Landis, C. R. *J. Am. Chem. Soc.* **1995**, *117*, 9770.
(b) Casey, C. P.; Carpenetti, D. W. *Organometallics* **2000**, *19*, 3970.
35. $\Delta H(5\text{-Pr} + \text{C}_2\text{H}_4 \rightarrow 5\text{-pent}) = -24.9 \text{ kcal}\cdot\text{mol}^{-1}$; $\Delta H(7\text{-Pr} + \text{C}_2\text{H}_4 \rightarrow 7\text{-pent}) = -23.7 \text{ kcal}\cdot\text{mol}^{-1}$. The difference between the two catalysts is much closer than it was in the original calculation. There may be a remaining small steric contribution that is not captured adequately by our model reaction to simulate the propagation step.
36. Brintzinger, H.-H.; Fischer, D.; Müllhaupt, R.; Rieger, B.; Waymouth, R. M. *Angew. Chem. Int. Ed. Engl.* **1995**, *34*, 1143.
37. Deck, P; Marks, T. J. *J. Am. Chem. Soc.* **1995**, *117*, 6128.
38. Vanka, K.; Chan, M. S. W.; Pye, C. C.; Ziegler, T. *Organometallics* **2000**, *19*, 1841.
39. Chen Y. X.; Metz M. V; Li L. T.; Stern, C. L.; Marks, T. J. *J. Am. Chem. Soc.* **1998**, *20*, 6287.

Appendix A. Energies of Intermediates

	5	7	1	4	2	3	6
Me							
BE	-19.8	-7.9	-13.0	-20.1	-14.3	-13.2	
TS	-13.1	-2.0	-5.9	-11.1	-6.9	-7.9	
GA	-26.9	-18.9	-22.6				
BG	-24.0	n/a	-21.0				
BA	-30.2	-20.3	-26.4				
BH	-18.6	-4.9	-14.0				
BP	-21.7	-7.8	-14.8				
H	+2.2	+1.6	+0.8				

Chapter 3

Ansa Effects in Zirconocene Dicarbonyls and Zirconocene Dichlorides

Abstract

We have prepared a series of zirconocene dicarbonyl complexes and zirconocene dichloride complexes. We prepared *ansa*-zirconocene dicarbonyl complexes $\text{Me}_2\text{ECp}_2\text{Zr}(\text{CO})_2$ ($\text{E} = \text{Si}, \text{C}$), as well as *t*-butyl substituted complexes $(\text{tBuCp})_2\text{Zr}(\text{CO})_2$, $\text{Me}_2\text{E}(\text{t-BuCp})_2\text{Zr}(\text{CO})_2$ ($\text{E} = \text{Si}, \text{C}$), $(\text{Me}_2\text{Si})_2(\text{t-BuCp})_2\text{Zr}(\text{CO})_2$. We studied the electrochemistry of the corresponding zirconocene dichlorides in addition to other zirconocene dichlorides. The reduction potentials increase in the following order: $\text{Me}_2\text{SiCp}_2\text{ZrCl}_2 > \text{Me}_2\text{CCp}_2\text{ZrCl}_2 > \text{Cp}_2\text{ZrCl}_2 > (\text{Me}_2\text{Si})_2\text{Cp}_2\text{ZrCl}_2$, and the corresponding *t*-Butyl substituted zirconocene carbonyl stretching frequencies follow the same ordering. This ordering is a result of the donating abilities of the cyclopentadienyl substituents and the orientation of the cyclopentadiene rings. Additionally, we prepared a series of cationic zirconocene complexes $[(\text{MeCp})_2\text{ZrOCMe}_3][\text{MeB}(\text{C}_6\text{F}_5)_3]$, $[\text{Me}_2\text{SiCp}_2\text{ZrOCMe}_3][\text{MeB}(\text{C}_6\text{F}_5)_3]$, $[\text{Me}_2\text{CCp}_2\text{ZrOCMe}_3][\text{MeB}(\text{C}_6\text{F}_5)_3]$, $[(\text{Me}_2\text{Si})_2\text{Cp}_2\text{ZrOCMe}_3][\text{MeB}(\text{C}_6\text{F}_5)_3]$, and studied the kinetics of anion dissociation from these complexes in CD_2Cl_2 or $\text{C}_6\text{D}_5\text{Cl}$. We found that the enthalpy of anion dissociation increased in the listed order from $10.3 \text{ kcal}\cdot\text{mol}^{-1}$ to $17.6 \text{ kcal}\cdot\text{mol}^{-1}$, while the entropy of activation remained close to 0 for all of these complexes.

Introduction

Not long after the discovery of Ziegler-Natta olefin polymerization catalysts,¹ it was found that mixtures of titanocene dichloride with trialkyl aluminum or dialkyl aluminum chloride were also capable of catalyzing ethylene polymerization, albeit at a slower rate.² The nature of the catalyst was not fully understood; in fact, it was not entirely clear that the cyclopentadienyl rings remained attached to the metal.² With the subsequent discovery that the activation of dimethyl zirconocene with methylalumoxane (MAO) produced very active olefin polymerization catalysts, research into the role of the metallocene in olefin polymerization flourished. It was found that by tethering the cyclopentadienyl rings with an ethylene bridge and adding substituents to the cyclopentadienyl rings, a chiral metal center could be formed that produces poly- α -olefins in a stereoselective fashion as shown in Figure 1.³

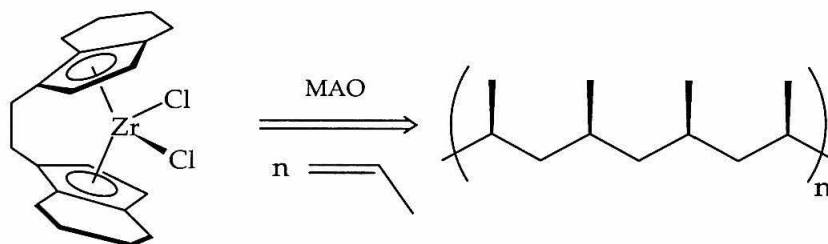


Figure 1. Stereoselective polymerization of propylene.

This discovery confirmed that the cyclopentadienyl rings were indeed bound to the metal center during polymerizations. This discovery has allowed a degree of rational catalyst that is impossible with current heterogeneous polymerization catalysts.⁴

Metallocenes in which the cyclopentadienyl rings are linked by one or more atoms (Figure 2) have been designated *ansa* metallocenes by Brintzinger.⁵ Countless examples of such metallocenes have been studied in an effort to improve olefin polymerization.⁶ It would be desirable to know exactly how geometric variations introduced by *ansa* bridges affect the polymerization behavior (i.e., rates of monomer insertion, rates of chain transfer, rates of chain termination, *etc.*).



Figure 2. Selected examples of *ansa* bridges.

Unfortunately, simply measuring the overall rate of polymerization cannot adequately describe these fundamental rates. One major obstacle is that under catalytic conditions the number of active species often varies from metallocene to metallocene in ways that are not fully understood.⁶ In fact, the number of active sites most likely changes throughout the course of the reaction. This ambiguity precludes a careful measurement of the rate of chain propagation by olefin insertion.⁷ Thus, it was thought that by assessing the electronic effect of changing ligand geometry with *ansa* bridges, a better understanding of the effects of *ansa* ligands on fundamental catalyst behavior could be achieved. In order to understand the changes that might be expected, a brief description of the molecular orbitals of bent metallocene complexes follows.

The first known metallocene was ferrocene, and it remains the most thoroughly studied metallocene complex.⁸ Its discovery and subsequent analysis by Wilkinson and Woodward is a foundational event in the history of organometallic chemistry.⁹ The molecular orbital diagram for a metallocene with D_{5h} symmetry is shown below with the metal-based d orbitals set off in the box (Figure 3).

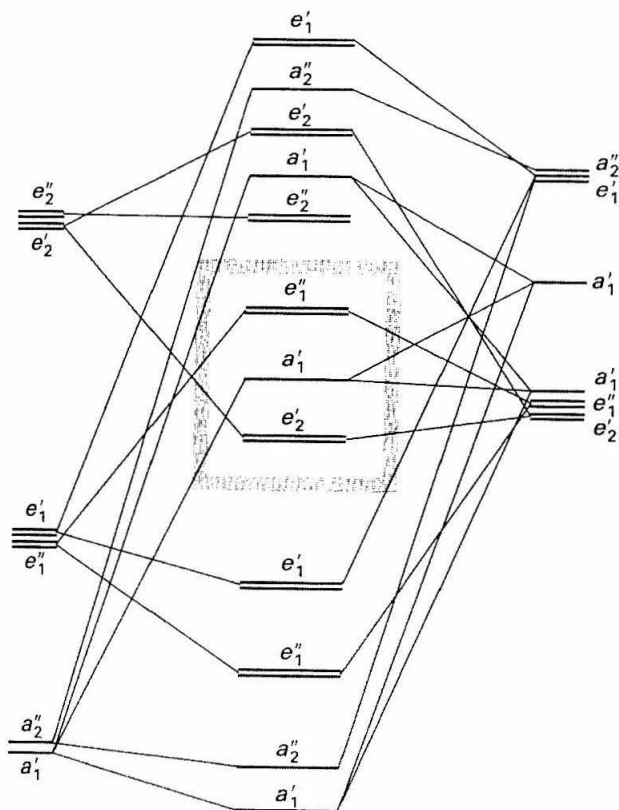


Figure 3. Molecular orbital description of ferrocene (eclipsed).

The three non-bonding d orbitals are the d_{z^2} , d_{xy} , and $d_{x^2-y^2}$ orbitals. In ferrocene, these non-bonding orbitals are filled as expected for an 18-electron complex; in the 14-electron Cp_2Zr fragment, there are only 2 electrons in these non-bonding orbitals. These two unpaired electrons allow zirconium to increase its valence by two. The additional ligands force the Cp rings to bend back in order to provide room for and improve the bonding with the ligands by rehybridizing the orbitals. Indeed, the cyclopentadienyl rings in Cp^*_2Ti are parallel, indicating that the additional ligands are the source of the bent structure.¹⁰

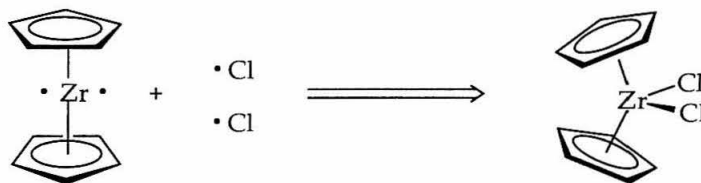


Figure 4. Bending of the zirconocene fragment to accommodate bonding.

The orbitals at various geometries can be visualized using electronic structure methods, such as Hückel theory¹¹ or density functional theory.¹² We compare in Figure 5 the shape of the frontier orbitals for metallocenes having parallel Cp rings (D_{5h} symmetry) versus metallocenes with bent Cp rings (C_{2v} geometry). Instead of showing computer generated molecular orbitals, a cartoon representation of the orbitals is used in order to highlight the shape of the metal based orbital.

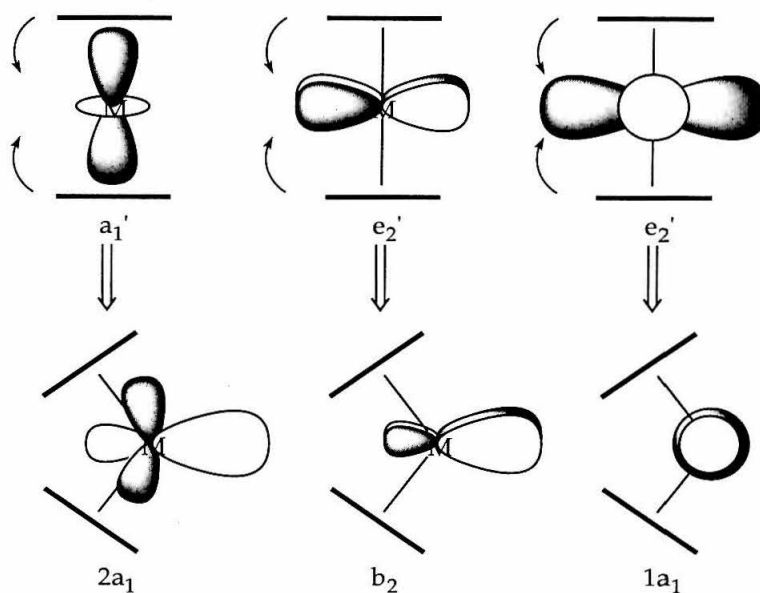


Figure 5. Derivation of frontier molecular orbitals of bent metallocenes.

These orbitals are the frontier molecular orbitals for bonding to ligands in the metallocene wedge (i.e., the open site of the bent metallocene). According to symmetry considerations, two ligands bonding to a metal in the metallocene wedge must use one orbital of a_1 symmetry and one of b_2 symmetry. Despite being higher in energy than the $1a_1$ orbital, the $2a_1$ orbital is used for bonding because it has better overlap with ligands in the metallocene wedge (Figure 6).¹¹

The LUMO in the resulting molecular orbital picture for a 16-electron complex has two large lobes pointing to the sides of the metallocene wedge.¹¹

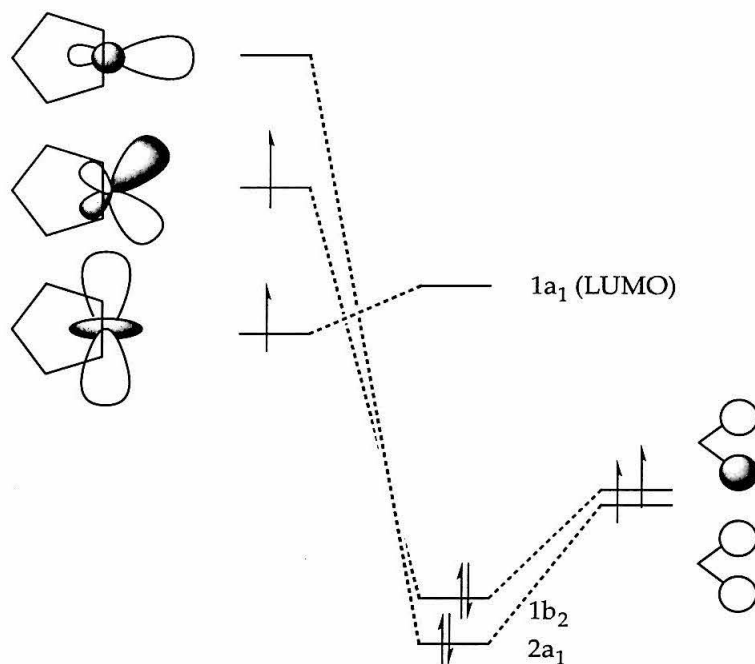


Figure 6. Molecular Orbitals in Cp_2ZrX_2 complexes.

This a_1 orbital is the LUMO in Zr(IV) complexes, but it is the HOMO in Zr(II) complexes. In Zr(II) dicarbonyl complexes, this orbital backbonds with the π^* orbital of CO as shown below (Figure 7).

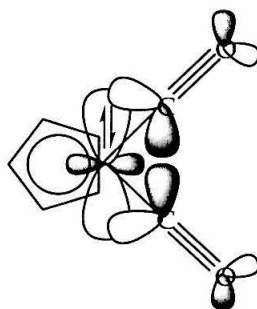


Figure 7. Backbonding from Zr(II) HOMO into CO π^* .

In the context of this investigation, it is informative to understand how the stability of this orbital is affected as the $\text{Cp}_{\text{cent}}\text{-Zr-Cp}_{\text{cent}}$ angle is varied. This was calculated by Green and coworkers.¹²

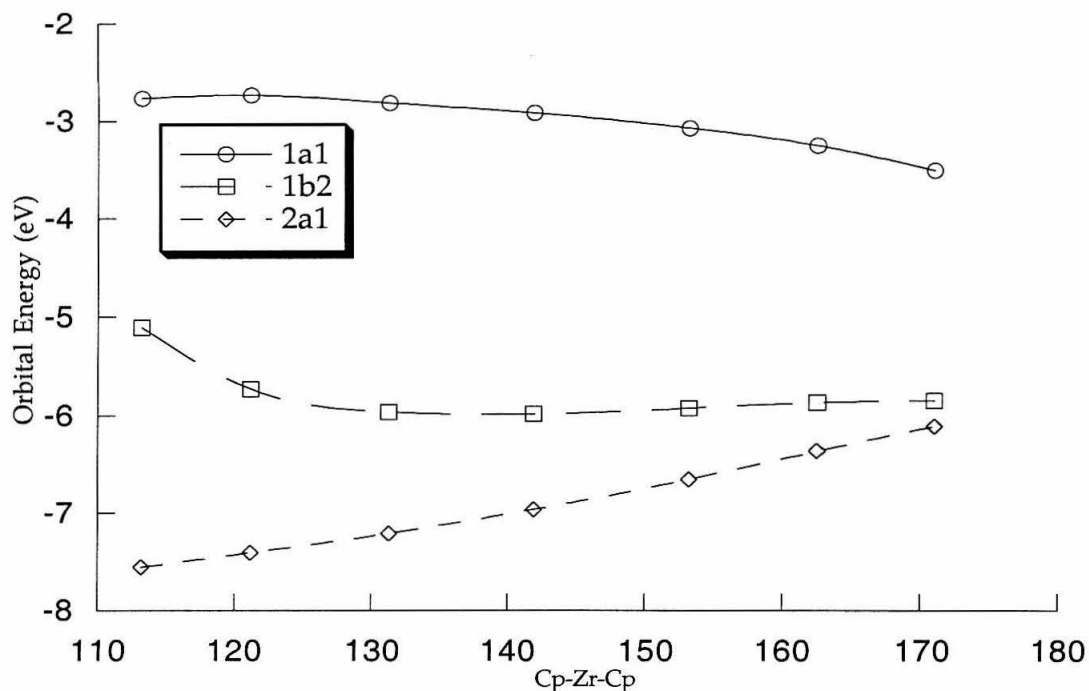


Figure 8. Walsh diagram for bending $\text{Cp}_{\text{cent}}\text{-Zr-Cp}_{\text{cent}}$ angle of Cp_2ZrCl_2 .

Changes in the *ansa* linker can vary the geometry in a number of ways. While the previous molecular orbital analysis examined the effect of the changing $\text{Cp}_{\text{cent}}\text{-Zr-Cp}_{\text{cent}}$ angle, this variation does not stand alone. Other geometric parameters are used to describe the bent metallocene geometry. Figure 9 shows three such parameters as well as their values for the types of metallocenes that are examined in this chapter.¹³ The parameter α is the $\text{Cp}_{\text{cent}}\text{-Zr-Cp}_{\text{cent}}$ angle. The parameter β is the angle between the $\text{Cp}_{\text{cent}}\text{-Zr}$ axis and the cyclopentadienyl plane. Parameters α and β can vary independently, but γ is dependent on both of these parameters according to: $\gamma = 360^\circ - 2\beta - \alpha$.

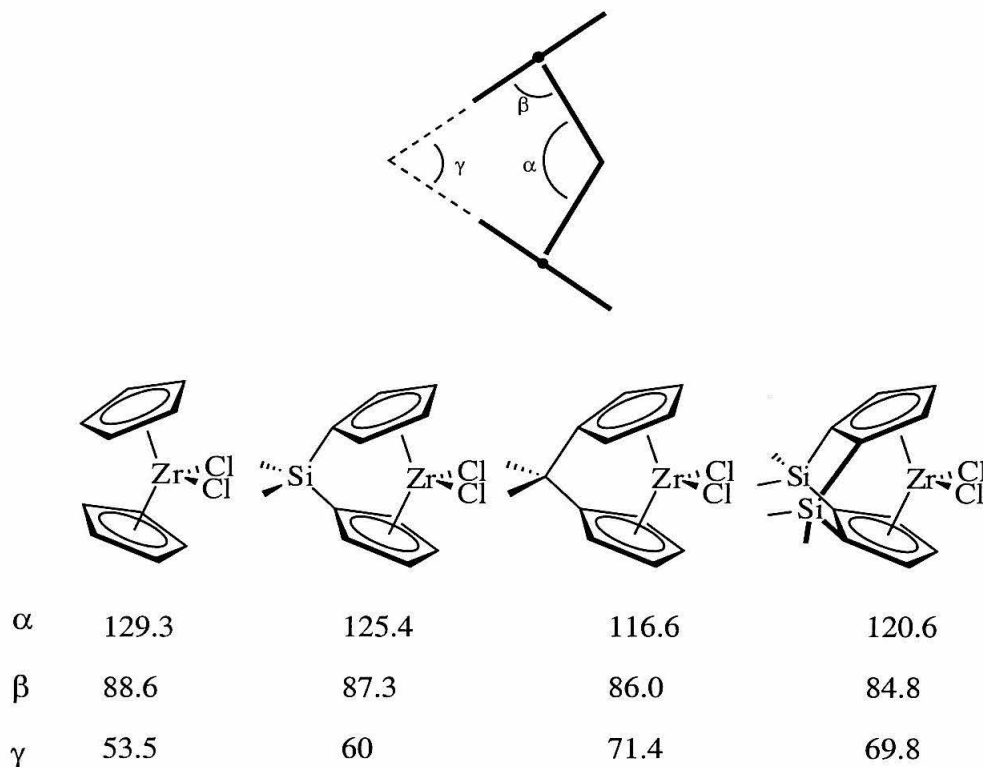


Figure 9. Geometries of metallocene dichlorides examined in this study.

The geometric parameters for the unlinked and singly linked compounds vary in a similar fashion: As α and β decrease, γ increases. The doubly bridged metallocene does not follow this trend. Angle α is intermediate between the values for silicon-linked and carbon-linked metallocenes, yet β is less and γ is nearly the same as it is in carbon bridged metallocenes. This indicates that doubly linking the cyclopentadiene rings puts tremendous strain on the bound ligand, but the zirconium remains tightly bound.

A difference between singly bridged and doubly-bridged *ansa*-metallocenes that is not described by the parameters α , β , γ is the conformation of the cyclopentadienyl rings. As shown above in Figure 9, the singly bridged metallocene has two cyclopentadienyl carbons towards the metallocene wedge, whereas the doubly bridged metallocene has only one. In unlinked metallocenes, for example, there is believed to be free rotation around the metal- Cp_{cent} axis with little difference in the relative energy or molecular orbital description. In ferrocene, the rotational barrier is approximately 1 kcal·mol⁻¹.⁸

However, in *ansa* metallocenes, Green and co-workers have proposed that the orientation of the Cp rings may have consequences for the electronic structure of the zirconocenes due to differing orbital overlap in each rotamer.¹² This conjecture will be explored further in the Discussion section.

The description of metallocenes by the parameters α , β , and γ is adequate for metallocenes whose ancillary substitution is similar, but in some cases the reactivity patterns can be a result of different steric environments. For example, the vacant orbital of 16-electron doubly silyl-bridged zirconocenes is generally unavailable to nucleophiles as opposed that of unlinked or singly bridged *ansa* metallocenes.

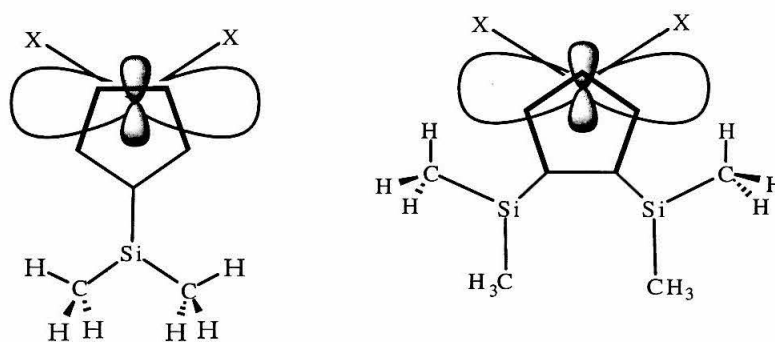


Figure 10. Steric interactions of the 1,2-(Me₂Si)₂Cp₂ ligand with "1a₁" orbital.

Bercaw and Wendt found, for example, that phosphine exchange in [Cp(Cp*)ZrCH₃(PMe₃)]⁺ is associative, whereas the mechanism of exchange is dissociative for the doubly linked *ansa* zirconocene [1,2-(Me₂Si)₂(C₅H₂CHMe₂)(3,5-(CHMe₂)-C₅H)ZrCH₃(PMe₃)]⁺.

To understand the electronic effects of *ansa* metallocenes, we prepared zirconocene dichloride complexes, zirconocenes dicarbonyl complexes, and zirconocene alkoxy cations. We studied the effect of *ansa* linker variation on the zirconocene properties.

Results

Zirconocene Dicarbonyl Complexes.

We initially turned our attention to a series of unsubstituted metallocenes in order to minimize complication by ancillary substitution of the cyclopentadienyl ligands. However, the synthesis of the dicarbonyl complexes was quite difficult. Standard methods of reduction did not yield any isolable Zr(II) dicarbonyl complexes. Reductions with Na/Hg, Mg, and BuLi met with no success. Surprisingly, while Mg reductions of Cp₂ZrCl₂ have been successful in the literature, in our hands they did not yield any desired dicarbonyl product for the *ansa* metallocenes that we attempted.

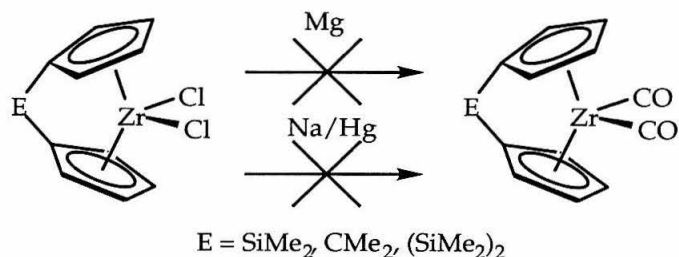


Figure 11. Attempted syntheses of unsubstituted *ansa* zirconocenes.

It appears that the unprotected, open face of the metallocene does not adequately protect the intermediate generated by 1 e⁻ reduction of the metal long enough to prevent unidentified side reactions. The product in most of these reactions was a red solid that was insoluble in every solvent that we tried. However, using sodium naphthalenide as a reductant, trace amounts of LZr(CO)₂ were isolated.¹⁴ (Figure 12) Unfortunately, the unsubstituted doubly bridged *ansa* zirconocene could not be prepared.

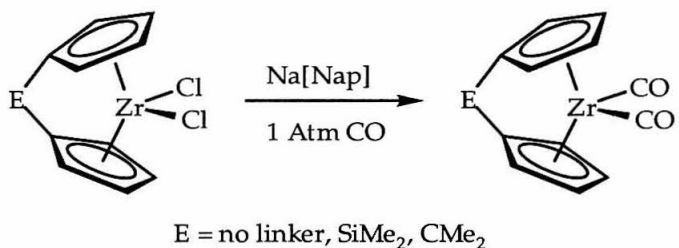


Figure 12. Synthesis of unsubstituted *ansa* zirconocenes.

The dicarbonyl was extracted with hexane, and an IR spectrum was taken of this solution. Two bands were recorded for each complex, a finding which is consistent with an LZr(II)(CO)₂ complex having C_{2v} symmetry.

When it became clear that synthesis of Zr(II) dicarbonyl complexes was hampered by their lack of steric protection, we turned our attention to *t*-butyl substituted zirconocenes. This approach was validated when yields of >50% were obtained by reducing the Zr(IV) dichloride complexes using Na/Hg amalgam. In all cases, the dicarbonyl complexes were purified by vacuum sublimation. Infrared spectroscopy was carried out on these complexes, and two bands were observed in each case, consistent with the symmetry of each complex.

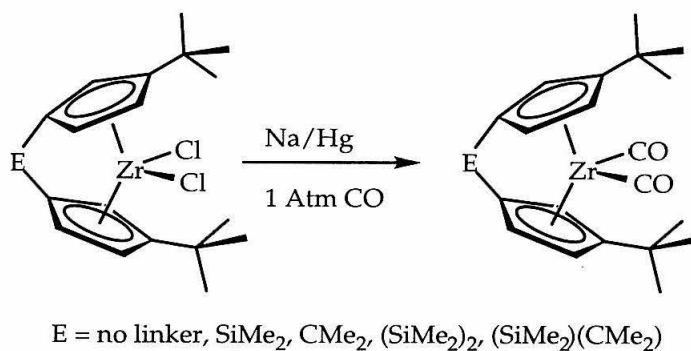


Figure 13. Synthesis of *t*-Bu substituted zirconocenes.

Singly-bridged *ansa* metallocenes with a single substitution on each of the cyclopentadienyl rings can result in two isomeric forms: racemic and meso. (Figure 14)

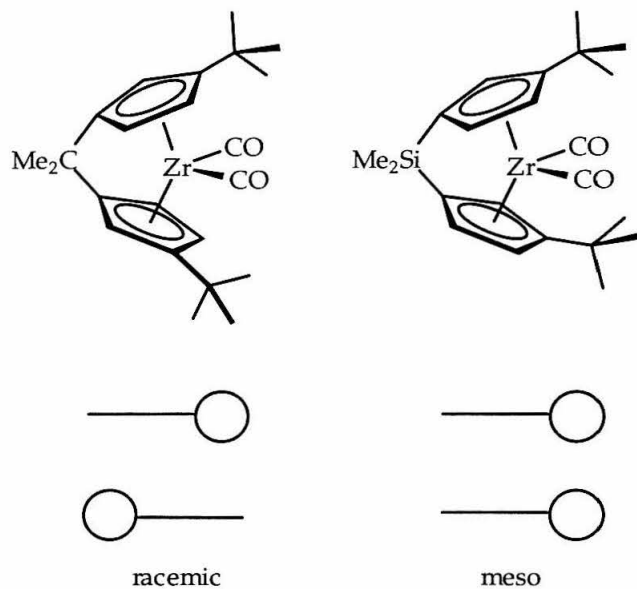


Figure 14. Racemic and meso *ansa* zirconocenes.

The preference for *rac* or *meso* metallocenes is difficult to predict and even more difficult to control. In the preparation of *ansa* [SiMe₂] and *ansa* [CMe₂] linked zirconocene dichloride, which was carried out by Jordan's amine elimination,¹⁵ both *ansa* zirconocenes were prepared as a mixture of *rac* and *meso* isomers. However, for the [CMe₂] linked zirconocene, only the *rac* form was isolated, but for the [SiMe₂] zirconocene, only the *meso* form was isolated.

There are two bands in the infrared spectrum corresponding to the symmetric and anti symmetric stretching modes of the CO ligands (in C_{2v} symmetry: a₁ and b₂).

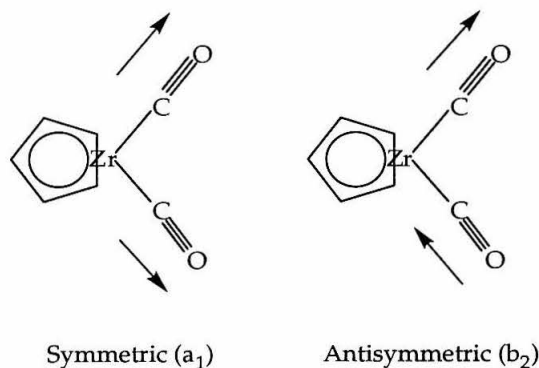


Figure 15. Vibrational modes of carbonyl ligands in zirconocene complexes.

The symmetric vibrational mode is observed approximately 90 cm^{-1} higher than the anti symmetric mode. In complexes from our study, the two modes vary linearly with each other with only one exception.¹⁶ We chose, therefore, to use the A_1 stretching frequency as our standard of comparison.

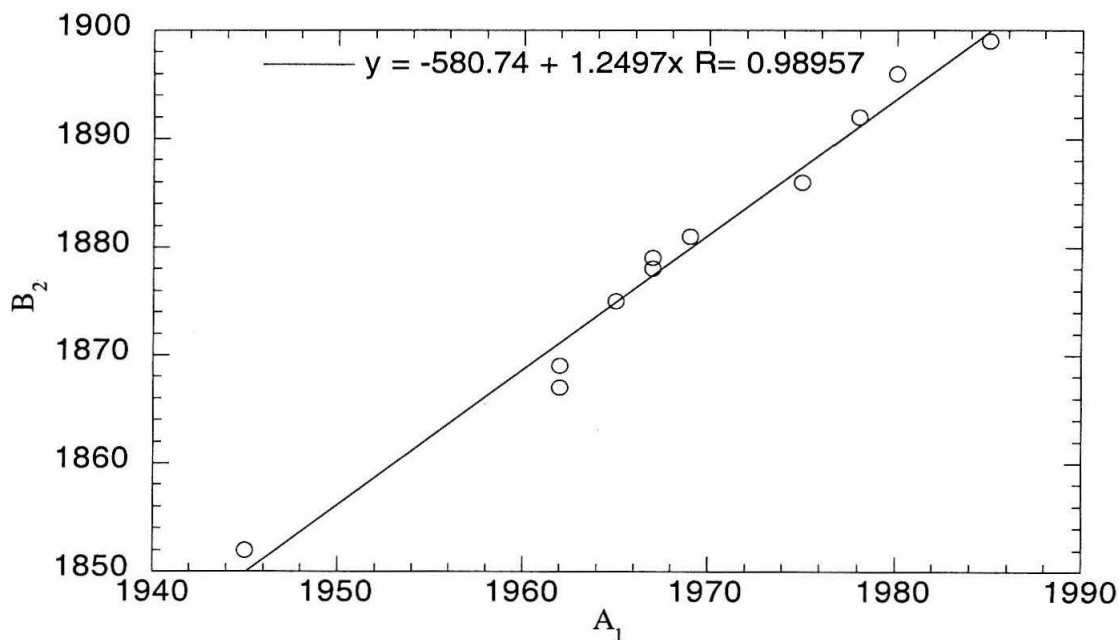


Figure 16. Plot of A_1 stretching frequencies vs. B_2 stretching frequencies for zirconocene dichlorides.

The most striking feature of the data obtained from the infrared spectroscopy is how small an effect the geometry changes have on the stretching frequencies. Table 1 lists the values obtained in our study for the unsubstituted zirconocenes. A more complete table is found in Appendix 1 of this chapter.

Complex	A ₁ Stretching Mode (cm ⁻¹)	B ₂ Stretching Mode (cm ⁻¹)
Cp ₂ Zr(CO) ₂	1975	1886
Me ₂ SiCp ₂ Zr(CO) ₂	1980	1896
Me ₂ CCp ₂ Zr(CO) ₂	1978	1892

Table 1. Carbonyl stretching frequencies of unsubstituted zirconocene dicarbonyl complexes.

What is also striking about this data is that despite our initial conjecture that the smallest *ansa* linker, CMe₂, would make the zirconocene most electrophilic, SiMe₂ actually rendered the complex most electrophilic. This indicated that not only should the Cp-Zr-Cp angle be considered when predicting the electrophilicity, but also the inductive effects of the *ansa* bridge should be considered.

Since the carbonyl derivatives of the *t*-Bu substituted zirconocenes were easier to prepare, a wider range of compounds was prepared. In Table 2, the relevant compounds are listed along with their carbonyl stretching frequencies.

Complex	Sym. CO Stretch (cm ⁻¹)	Asym. CO Stretch (cm ⁻¹)
(<i>t</i> -BuCp) ₂ Zr(CO) ₂	1967	1879
Me ₂ Si(<i>t</i> -BuCp) ₂ Zr(CO) ₂	1969	1881
Me ₂ C(<i>t</i> -BuCp) ₂ Zr(CO) ₂	1967	1878
(Me ₂ Si) ₂ (<i>t</i> -BuCp) ₂ Zr(CO) ₂	1962	1867

Table 2. Carbonyl stretching frequencies of *t*-Bu substituted zirconocenes.

The changes in carbonyl stretching frequencies for the singly bridged *ansa* zirconocenes are even smaller than they were in the unsubstituted metallocenes. Again, as with the electrochemistry for the unsubstituted metallocenes, the data

implies that the doubly bridged *ansa* zirconocene is less electrophilic than the unlinked metallocene.

t-Butoxy Metallocene Cations.

We sought a simple reaction that could assess the electrophilicity of *ansa* zirconocene complexes. Ideally, such a complex would be a 14- or 16-electron Zr(IV) complex similar that would have relevance to proposed intermediates in olefin polymerization catalyst mixtures. We chose to study the dissociation of coordinated anion complexes from zirconocene alkoxy cation complexes by measuring the coalescence of protons on one side of the metallocene with those on the other. This system was selected for a number of reasons.

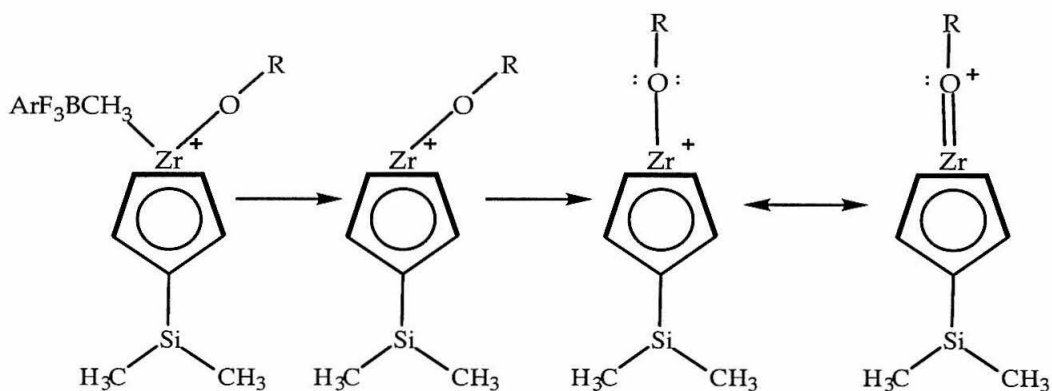


Figure 17. Proposed π -bonding stabilization of planar cation.

First, it was believed that in the absence of donor solvents, the anion dissociation might occur through a dissociative pathway since the electrons in the oxygen *p* orbitals could form a donor bond with the vacant equatorial orbital. Second, by similar reasoning, we believed that site epimerization would be much faster than anion recoordination since the proposed π -bonding from the ligand should cause the oxygen to seek the center of the metallocene wedge after every dissociation.¹⁷ While the nature of the anion dissociation was not proven rigorously, it appears to be the case that ligand dissociation occurs from alkoxy zirconocene cations without any associative assistance.¹⁸

Additionally, these complexes can be prepared from the readily synthesized zirconocene dimethyl complexes whose syntheses have been described in the literature.¹⁹ (Figure 18)

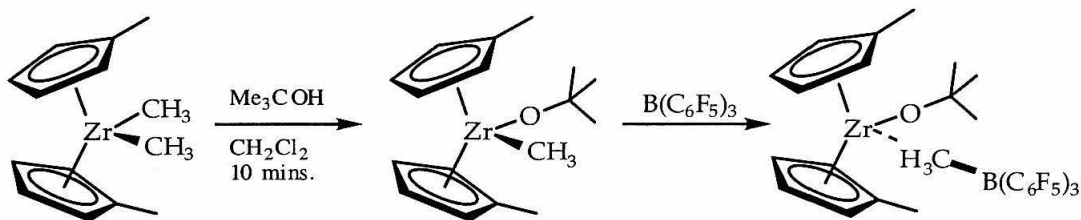


Figure 18. Preparation of *t*-butoxy zirconocene cations.

The preparation was facile for both the unlinked and singly-bridged *ansa* zirconocenes and was achieved by the addition of 1.05 equivalents of Me_3COH to 1 equivalent of zirconocene dimethyl in CH_2Cl_2 . The reaction was complete in less than 10 minutes and was quantitative. This product was then activated with $\text{B}(\text{C}_6\text{F}_5)_3$ to quantitatively produce *t*-butoxy zirconocene cation.

On the other hand, there was no reaction between Me_3COH and 1,2- $(\text{Me}_2\text{Si})_2(\text{C}_5\text{H}_3)_2\text{ZrMe}_2$ under the same conditions. Even under prolonged reaction times, there was no evidence for the formation of desired product, though an unidentified decomposition reaction had begun occurring.

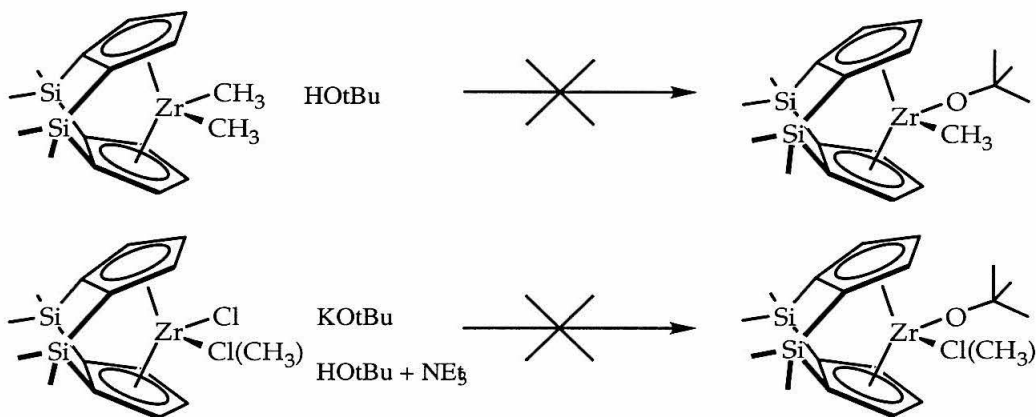


Figure 19. Attempted syntheses 1,2- $(\text{Me}_2\text{Si})_2(\text{C}_5\text{H}_3)_2\text{ZrMe}(\text{OCMe}_3)$.

Several reactions were attempted without success to directly add a *t*-butoxide ligand to the metal. Finally, however, we activated a small amount of the dimethyl complex with 1 equivalent of $\text{B}(\text{C}_6\text{F}_5)_3$ and then added 1 equivalent of acetone which inserts into the metal-carbon bond to yield the *t*-butoxy cation.²⁰

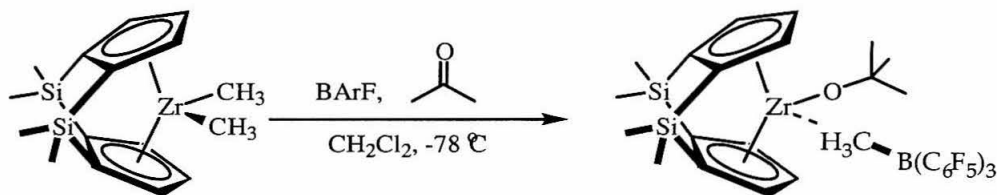


Figure 20. Preparation of doubly bridged *ansa* *t*-butoxy cation.

While the lack of reactivity of the dimethyl complex towards *t*-butanol was surprising, can be rationalized. The doubly dimethyl silyl-bridged metallocenes are unique in their reactivity. As mentioned in the Introduction, the methyl groups add steric protection, which effectively blocks the vacant orbital in 16-electron metallocene complexes. The implication of the unreactivity towards *t*-butanol is that precoordination of the alcohol is required to increase its acidity before it can protonate the methyl group selectively.

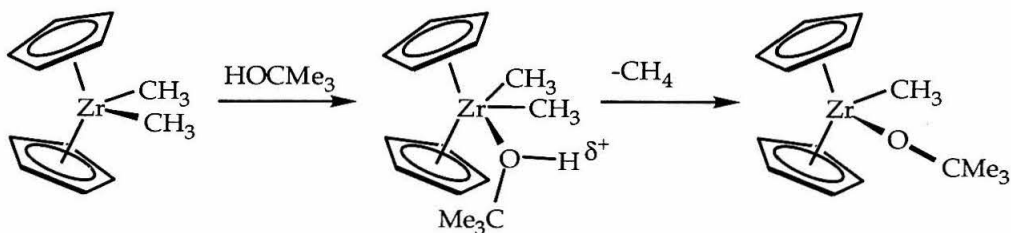


Figure 21. Proposed mechanism of alcoholysis of Zr-CH₃ bond.

The anion dissociation from the zirconocene was measured by studying the rate of site epimerization. Site epimerization is the process in which a substituent of the zirconocene moves from one side of the metallocene wedge to the other. If the rate of site epimerization is much faster than the rate of anion dissociation and recoordination, then the rate of anion recoordination to either metallocene face will be equal and the rate of site epimerization will be half the rate of anion dissociation. The cationic alkoxy complexes have a preference for the ligand to reside in the center of the metallocene wedge, so the rate of site epimerization must be greater than that of anion dissociation/recoordination.

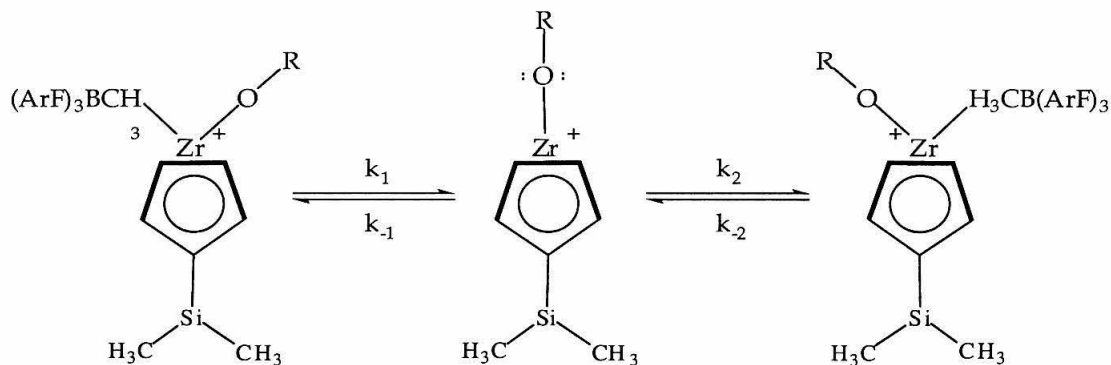


Figure 22. Site epimerization *via* anion dissociation/recoordination.

Site epimerization was measured by lineshape analysis of dynamic NMR spectra obtained in CD_2Cl_2 for each complex. Due to higher temperatures required for $[(\text{Me}_2\text{Si})_2(\text{Cp})_2\text{ZrOCMe}_3][\text{MeB}(\text{C}_6\text{F}_5)_3]$, this spectrum was determined in $\text{C}_6\text{D}_5\text{Br}$. The temperature range in which coalescence of Cp peaks occurred in the ^1H spectra varied greatly for each complex. For $[(\text{MeCp})_2\text{ZrOCMe}_3][\text{MeB}(\text{C}_6\text{F}_5)_3]$, coalescence begins at $-90\text{ }^\circ\text{C}$; however, for $[(\text{Me}_2\text{Si})_2(\text{Cp})_2\text{ZrOCMe}_3][\text{MeB}(\text{C}_6\text{F}_5)_3]$, coalescence does not begin until $320\text{ }^\circ\text{C}$. An Eyring plot was constructed using the kinetic data determined from line shape simulations, and the activation parameters are summarized in Table 3.

Complex	ΔH^\ddagger (kcal \cdot mol $^{-1}$)	ΔS^\ddagger e.u.
$[(\text{MeCp})_2\text{ZrOCMe}_3][\text{MeB}(\text{C}_6\text{F}_5)_3]$	10.3	-6
$[\text{Me}_2\text{SiCp}_2\text{ZrOCMe}_3][\text{MeB}(\text{C}_6\text{F}_5)_3]$	11.3	8
$[\text{Me}_2\text{CCp}_2\text{ZrOCMe}_3][\text{MeB}(\text{C}_6\text{F}_5)_3]$	15.4	-2
$[(\text{Me}_2\text{Si})_2\text{Cp}_2\text{ZrOCMe}_3][\text{MeB}(\text{C}_6\text{F}_5)_3]$	17.6	-2

Table 3. Activation parameters for anion dissociation/recoordination.

The entropies of activation are all close to zero, which is encouraging because at the very least it indicates that the mechanism does not change as the ligand array is changed. A steady increase in the binding energy is observed as the ligands

are further distorted from the unlinked zirconocene geometry. Since the entropy of activation for three of the four complexes is consistently negative, the entropy calculated for $[\text{Me}_2\text{SiCp}_2\text{ZrOCMe}_3][\text{MeB}(\text{C}_6\text{F}_5)_3]$ may be too positive. This would lead to a slightly underestimated enthalpy.

Lastly, crystals of the $[\text{Me}_2\text{SiCp}_2\text{ZrOCMe}_3][\text{MeB}(\text{C}_6\text{F}_5)_3]$ complex that were suitable for X-ray diffraction were grown from a concentrated CD_2Cl_2 solution at room temperature. These cations are extremely stable in halogenated solvent, as opposed to zirconocene alkyl cations which have very limited stability in halo-alkane solvents.²¹ The $[\text{MeB}(\text{C}_6\text{F}_5)_3]^-$ anion was coordinated to the metal center and the methyl protons were located. This structure is unexceptional. The Zr-C distance (2.615 Å) is longer than that in comparable $[\text{Cp}_2\text{ZrR}][\text{MeB}(\text{C}_6\text{F}_5)_3]$ structures, which range from 2.5-2.55 Å.²² The Zr-O bond distance is very short (1.90 Å) and the Zr-O-C bond angle is 172°; these structural features are consistent with Zr-O multiple bonding

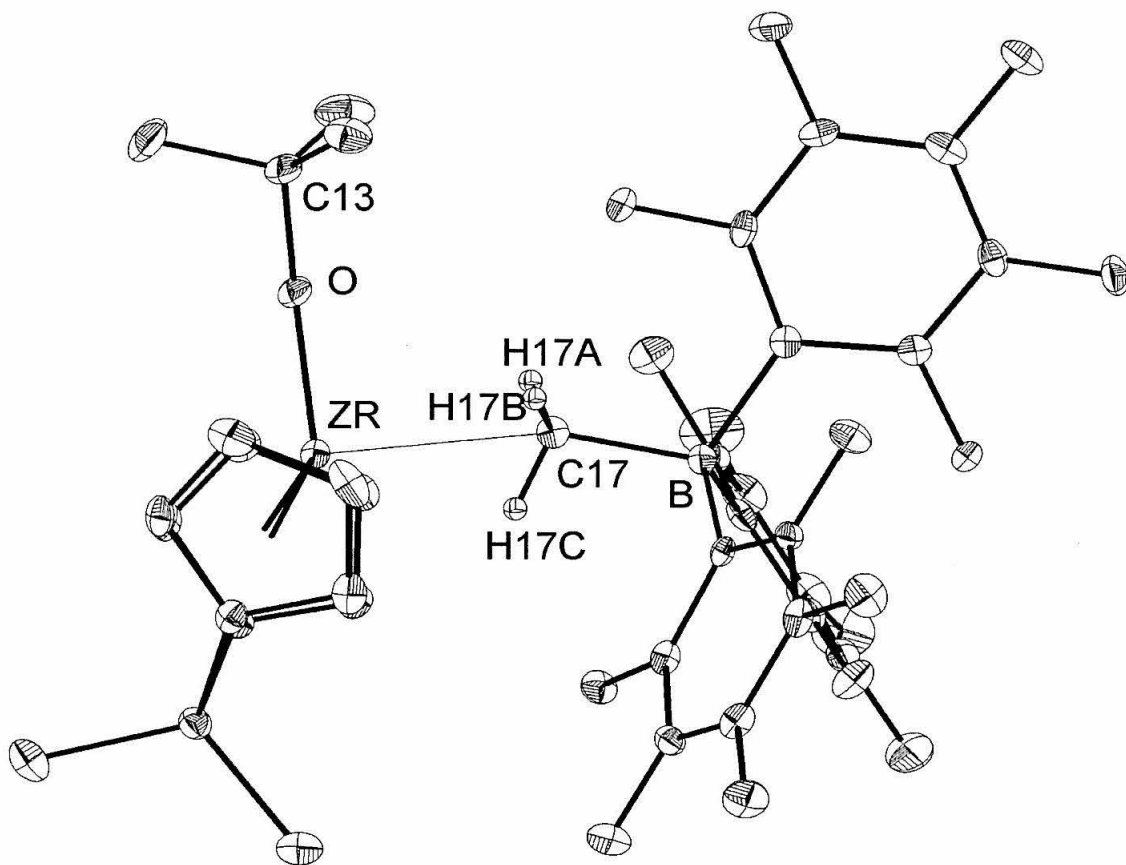


Figure 23. X-Ray crystal structure of $[\text{Me}_2\text{SiCp}_2\text{ZrOCMe}_3][\text{MeB}(\text{C}_6\text{F}_5)_3]$.

Reduction Potentials of Zirconocene Dichlorides Complexes.

The reduction potentials of the zirconocene(IV) dichloride complexes were also examined using cyclic voltammetry. The results shown in Table 4 are consistent with the trends observed in the zirconocene(II)dicarbonyl stretching frequencies.

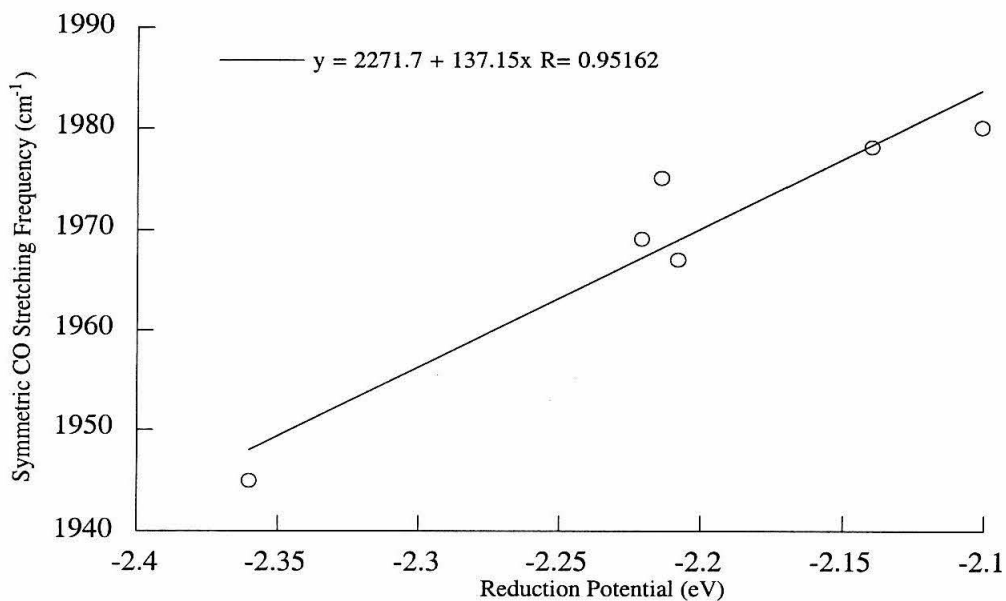


Figure 24. Symmetric carbonyl stretching frequency of Zr(II) dicarbonyl complexes vs. reduction potentials of Zr(IV) dichloride complexes.

The zirconocene dichlorides with lower reduction potentials correspond to zirconocene dicarbonyl complexes with lower carbonyl stretching frequencies.

Zirconocene Complex	Reduction Potential (eV)
Cp_2ZrCl_2	-2.214
$\text{Me}_2\text{SiCp}_2\text{ZrCl}_2$	-2.101
$\text{Me}_2\text{CCp}_2\text{ZrCl}_2$	-2.146
$(\text{Me}_2\text{Si})_2\text{Cp}_2\text{ZrCl}_2$	-2.241

Table 4. Reduction potentials of unsubstituted zirconocenes.

Unfortunately, the electrochemistry was not very informative for the *t*-Bu substituted metallocenes, because the reduction waves were irreversible in some cases. The reversible reduction potentials are included in Table 5.

Discussion

Carbonyl Stretching Frequencies and Zirconocene Dichloride Reduction Potentials.

The variation of carbonyl stretching frequencies was smaller than had been anticipated. For example, addition of a *t*-Bu substituent to each Cp ring of zirconocene lowers the $\nu(\text{CO})$ by 9 cm^{-1} , whereas addition of a CMe_2 bridge, which donates into both Cp rings, increases the $\nu(\text{CO})$ by 3 cm^{-1} . In fact, the largest difference evident for zirconocenes that differ only by *ansa* linkers is 5 cm^{-1} .

The change in reduction potentials is also small. The maximum change that is observed within the series of unsubstituted metallocenes is 140 mV. The trend showing that the single silyl *ansa* zirconocene is the easiest to reduce and the doubly silyl-linked *ansa* zirconocene is the hardest to reduce is consistent with the results from the carbonyl stretching frequencies.

In an attempt to understand the electronic effect of the *ansa* bridges on the metallocene, the reduction potentials of the zirconocene dichlorides were plotted against the sum of the Hammett parameters of each substituent. *Ansa* linkers were counted twice, as either Me_3C or Me_3Si . If no geometric variations were introduced, then a single linear correlation of the data would be expected. This data is included in Table 5. Looking at the graph in Figure 25, no clear trends are apparent. However, if we remove two data points (compounds **9** and **12**), then the data can be classified into three different series. The justification for removal of these two points is clarified below. The revised graph (Figure 26) indicates that there are three separate linear correlations of this data. The top line corresponds to singly *ansa*-bridged complexes, whether they are $[\text{CMe}_2]$ -linked or $[\text{SiMe}_2]$ -linked, despite the Cp-M-Cp angle being different by $\sim 10^\circ$. The line running through the middle corresponds to the reduction potentials of the unlinked zirconocenes. The lowest line corresponds to the doubly-bridged *ansa*-zirconocenes, though the line is at a somewhat different angle than the lines for the other two series. This may be due to a lack of data points for this line.

Key	Compound	Red. Potential (eV)	σ_p^+
1	$[(C_5H_5)_2ZrCl_2]$	-2.214	0
2	$[(C_5H_4Me)_2ZrCl_2]$	-2.24	-0.62
3	$[(C_5H_4Et)_2ZrCl_2]$	-2.25	-0.60
4	$[(C_5H_3i-Pr)_2ZrCl_2]$	-2.31	-1.12
5	$[(C_5Me_5)(C_5Me_4Et)ZrCl_2]$	-2.49	-3.09
6	$[(C_5Me_5)(C_5H_3t-Bu)_2ZrCl_2]$	-2.364	-2.07
7	$[(C_5Me_5)(C_5H_4t-Bu)ZrCl_2]$	-2.380	-1.81
8	$[(C_5Me_5)_2ZrCl_2]$	-2.493	-3.10
9	$[(Me_3SiC_5H_4)_2ZrCl_2]$	-2.10	0.04
10	$[Me_2C(C_5H_4)_2ZrCl_2]$	-2.146	-0.52
11	$[Me_2C(C_5H_3t-Bu)_2ZrCl_2]$	-2.208	-1.04
12	$[Me_2Si(C_5H_4)_2ZrCl_2]$	-2.101	0.04
13	$[Me_2Si(C_5H_3t-Bu)_2ZrCl_2]$	-2.221	-0.48
14	$[(Me_2Si)_2(C_5H_3)_2ZrCl_2]$	-2.241	0.08
15	$[(Me_2Si)_2(C_5Hi-Pr_2)(C_5H_2SiMe_3)ZrCl_2]$	-2.387	-0.48
16	$[(Me_2Si)_2(C_5Hi-Pr_2)(C_5H_2i-Pr)ZrCl_2]$	-2.383	-0.76

Table 5. Reduction potentials of zirconocene dichlorides.

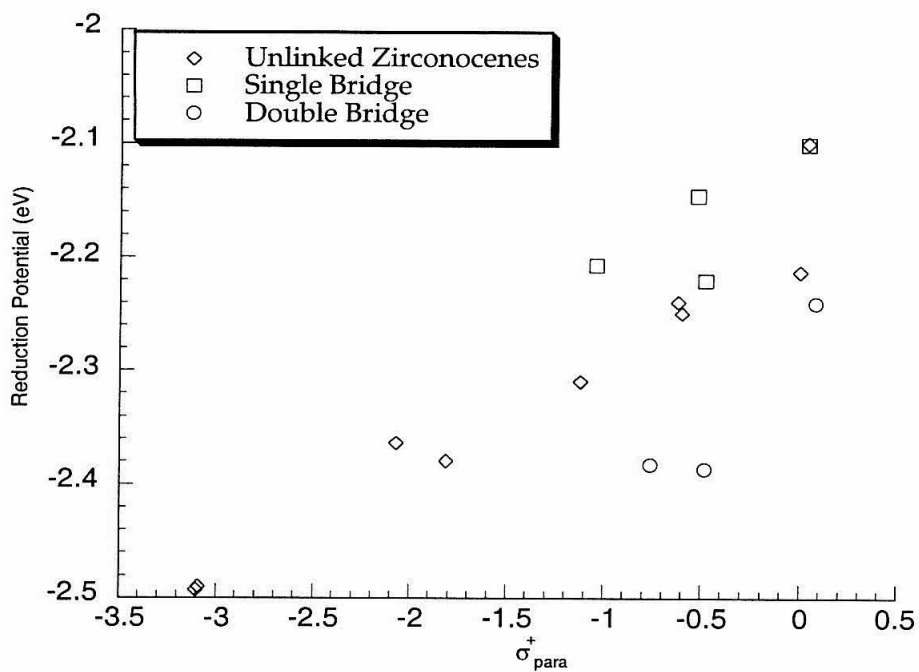


Figure 25. Reduction potentials vs. σ^+_{para} for various zirconocenes.

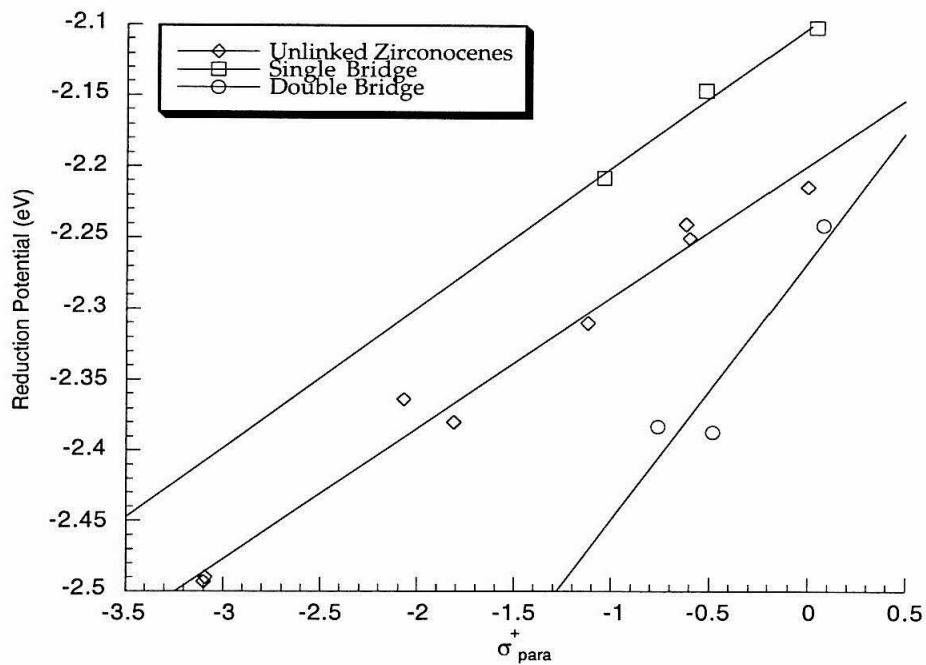


Figure 26. Selected potentials vs. σ^+_{para} .

The carbonyl stretching frequencies and the dichloride reduction potentials ultimately reflect the variation in the stability of the $1a_1$ orbital on zirconium. This is the orbital that contains the Zr lone pair in the carbonyl complexes, and it is the orbital into which an electron is added when the Zr(IV) dichloride complexes are reduced. In this respect, a Walsh diagram that describes the variation of this orbital from complex to complex would clearly predict the trends of either reduction potentials or carbonyl stretching frequencies of zirconocene complexes with differing $Cp_{cent}-Zr-Cp_{cent}$ angles. Based upon the linear correlation between singly-bridged *ansa* zirconocenes and Hammett parameters, regardless of linker size, it appears that the variation of $1a_1$ orbital energy due to $\Delta(Cp_{cent}-Zr-Cp_{cent})$ is very small. In fact, the predicted change is indeed quite small. In the Walsh diagram in Figure 8, between $Cp-Zr-Cp$ angles of $113-131^\circ$, there is very little change in the energy of the $1a_1$ orbital. The predicted difference in reduction potentials based on the $Cp_{cent}-Zr-Cp_{cent}$ angles in $[Me_2C]$ and $[Me_2Si]$ -*ansa* metallocene is only 7 mV. The $Cp_{cent}-Zr-Cp_{cent}$ angle of doubly linked zirconocenes is between the two extremes of $[Me_2C]$ and $[Me_2Si]$.

Therefore, because there is no dependence of the reduction potentials on the $Cp_{cent}-Zr-Cp_{cent}$ angle, the cause of three separate linear correlations must originate elsewhere. The largest difference in reduction potentials is between the singly linked and doubly linked zirconocenes, which is surprising because a cursory analysis would suggest that these two classes of metallocenes are the most similar. The only significant difference between these two classes of compounds is the orientation of their Cp ring. The singly bridged metallocenes have *two* carbons of each Cp ring facing the front of the metallocene, whereas each Cp ring of the doubly bridged metallocenes has only *one* carbon facing the front of the metallocene. The unlinked metallocenes typically have staggered Cp rings, which makes the Cp ring orientation intermediate between the singly bridged and doubly bridged metallocenes. Thus, according to this rationale, it is not surprising that the reduction potentials of the unlinked zirconocenes falls in between the two types of *ansa* metallocenes. It is also possible to explain, then, the two data points that were removed from the plot in Figure 25. The data points refer to the metallocenes $(Me_3SiCp)_2ZrCl_2$, **9**, and *meso*- $Me_2Si(t-BuCp)_2ZrCl_2$, **12**. Molecular modeling indicates that the lowest energy conformation $(Me_3SiCp)_2ZrCl_2$ has the same ring orientation as singly linked

metallocenes. A molecular model of *meso*-Me₂Si(*t*-BuCp)₂ZrCl₂ indicates that due to steric repulsion of the *t*-Bu substituents by the chloride ligands, the orientation of the Cp rings is intermediate between singly linked and doubly linked metallocenes.

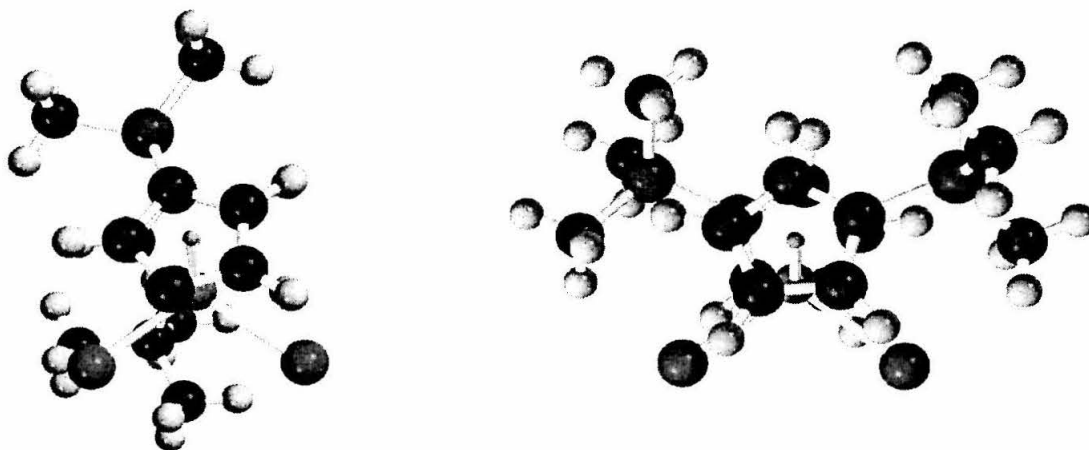


Figure 27. Molecular mechanics structure of *meso*-Me₂Si(*t*-BuCp)₂ZrCl₂ (Note: one *t*-butyl substituent was removed for clarity) and (Me₃SiCp)₂ZrCl₂.

Green and co-workers have investigated this ring conformation effect on reduction potentials of zirconocene dichloride.¹² Their study employed density functional theory to calculate the electron affinity of zirconocene dichlorides, which correlates linearly with reduction potential. They were able to reproduce the same trends for a number of *ansa* and unlinked metallocenes. They found that the ring conformation changes reduction potentials enough to account for the difference in reduction potentials among the three classes of metallocenes that were studied.

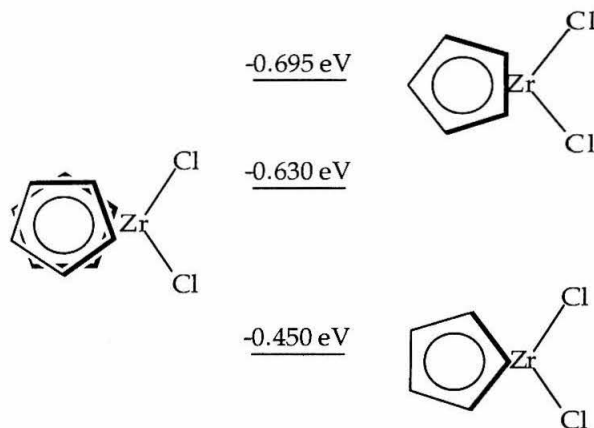


Figure 28. Electron affinity of Cp_2ZrCl_2 with different rotamers.

Experimental and theoretical evidence thus suggest that the primary electronic effect of *ansa* metallocene is to constrain the Cp rings in a particular conformer. Within the normal range of *ansa* metallocene $\text{Cp}_{\text{cent}}\text{-Zr-Cp}_{\text{cent}}$ angles, there is no measurable effect on the energy of the $1a_1$ orbital and hence the reduction potentials and Zr(II) carbonyl stretching frequencies remain unchanged.

Anion Dissociation.

The kinetic studies of $[\text{MeB}(\text{C}_6\text{F}_5)_3]^-$ from the zirconocene alkoxy cations also yielded interesting information. Though the original intent of this study was for comparison with the carbonyl and electrochemistry, it is clear that the original premise for comparison was flawed. The carbonyl stretching frequencies and zirconocene dichloride reduction potentials are in fact a measure of the stability of the $1a_1$ orbital. If the binding affinity of some ligand into this vacant orbital was measured, then a reasonable expectation of correlation could exist, but the anion binds instead to an orbital that is a linear combination of the $1b_2$ and $2a_1$ orbitals.

As shown in the Results, there is a steady increase in the binding energy of the anion as one moves from unlinked Cp ligands to the very strained doubly-linked *ansa* metallocene. By inspection of the Walsh diagram (Figure 8), it can be determined that there is no correlation with the variation in energy of the $1a_1$ orbital. Neither does the sum of energies of the $1b_2$ and $2a_1$ orbitals correlate with the anion binding trend. Only one of the geometric parameters, β , increases in a similar fashion to the anion binding energy. Most likely this

measurement is consistent with the exposure of the metal to ligands such as the $[\text{MeB}(\text{C}_6\text{F}_5)_3]^-$ anion.

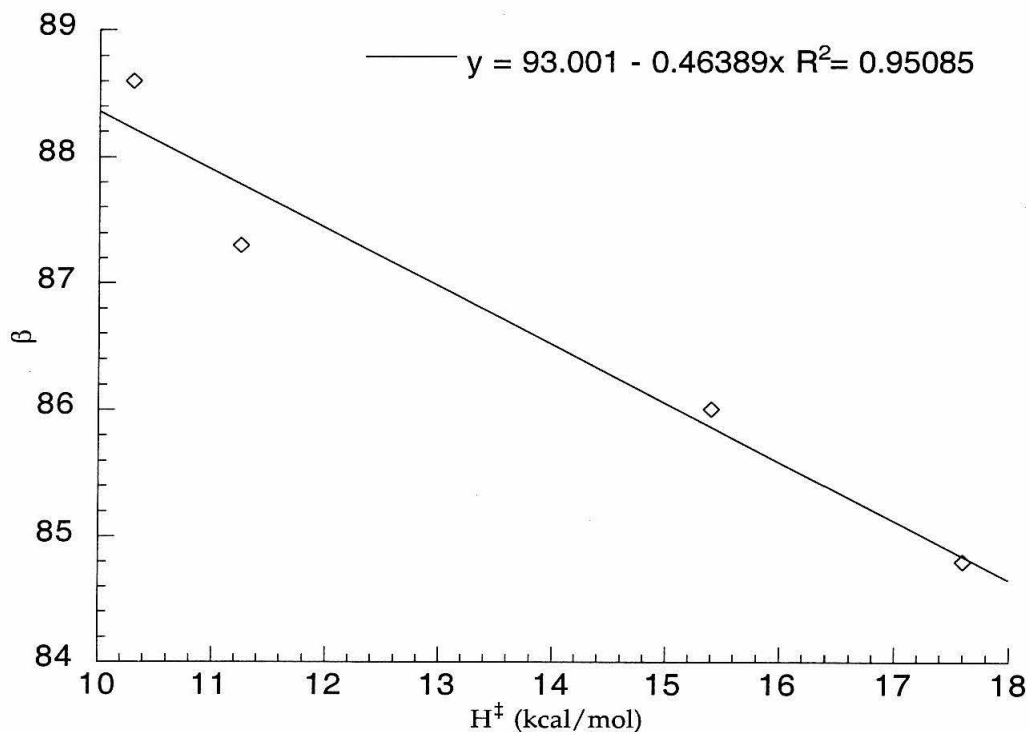


Figure 29. Plot of zirconocene geometric parameter β versus binding energy.

Conclusions

A number of novel *ansa* zirconocene dicarbonyl complexes were prepared and the carbonyl stretching frequencies were measured. The reduction potentials for several zirconocene dichloride complexes were also measured. Both of these measurements of the $1a_1$ orbital are consistent with each other. By comparing the reduction potentials of the dichloride complexes with the sum of the substituents' Hammett parameters, we showed that the stability of the $1a_1$ orbital is not affected by the $\text{Cp}_{\text{cent}}\text{-Zr-Cp}_{\text{cent}}$ angle. Our data indicates that the orientation of the cyclopentadiene rings affects the orbital's stability. The orbital is most stable when the edges of the two cyclopentadiene rings face the zirconocene wedge, as they do in a singly linked zirconocene. The orbital is least stable when the vertices of each cyclopentadiene ring face the zirconocene

wedge as they do in doubly bridged zirconocenes. The orbital has stability between these two extremes in Unlinked zirconocenes, whose cyclopentadiene rings adopt an intermediate orientation. The density functional calculations of Green and co-workers provide an excellent description of the orbital energies that correlate well to experimental data. The distinction between the three series of zirconocenes arises from their differing cyclopentadienyl rotational conformations. Changes in the $\text{Cp}_{\text{cent}}\text{-Zr-Cp}_{\text{cent}}$ angle contributes very little to the reduction potentials.

We also prepared an isosteric series of cationic alkoxy zirconocenes and studied the kinetics of anion dissociation for these complexes. We found that in this case, the increase in anion binding energy correlated linearly with the "tilting" of the Cp rings on the metallocenes. That is, as the Cp plane deviates from perpendicularity to the Cp-Zr axis (i.e., as β becomes more acute, the anion is bound more tightly).

Experimental

Electrochemistry. Electrochemical measurements were conducted with a BAS-100A Electrochemical Analyzer. The cell was a homemade one-compartment, glass cell with gas inlets for argon gas and three 10/18 female joints through which the electrodes were inserted. The working electrode was a gold disk (1.6 mm diameter, BAS). The auxiliary electrode was a Pt wire, inserted through a rubber septum. A silver wire (inserted through a rubber septum) was used as a pseudo-reference electrode; potentials are referenced to an internal ferrocene standard (0 V). All solutions are 0.1 M tetrabutylammonium hexafluoro phosphate in THF (freshly distilled under nitrogen from sodium/benzophenone) with 1 mM ferrocene and 1 mM analyte. Compensation for iR drop was employed. Typically, the potential was scanned, and then the cathodic and anodic limits were set to contain the 1-e reduction of the Zr species and ferrocene oxidation. Then scans were recorded at scan rates of 100, 200, 400, 800 mV/s (or higher to obtain chemical reversibility).

(1-Me₂Si)(2-Me₂C)(C₅H₂-4-CMe₃)₂ZrCl₂. In an inert atmosphere glove box, Li₂[Me₂C(C₅H₃CMe₃)₂] (4.6 g, 15.85 mmol) was loaded into a 500 mL round bottom flask, which was attached to a swivel frit assembly. This sealed assembly was attached to a high vacuum line and 250 mL of THF were vacuum transferred

and the solid was dissolved producing a yellow solution. SiCl_2Me_2 (2.12 mL, 17.43 mmol) was vacuum transferred into a calibrated finger and vacuum transferred at $-78\text{ }^\circ\text{C}$ onto the yellow solution, which was cooled by a dry ice/acetone slurry. The slurry was removed and the reaction mixture was allowed to warm to room temperature. After stirring overnight, all volatiles were removed *in vacuo*, leaving a yellowish oil with white precipitate. 100 mL of petroleum ether was condensed onto this solid and this was stirred at room temperature and filtered, leaving a white solid behind. The solid was rinsed 3 times with petroleum ether. In the inert atmosphere glove box, the round bottom flask was removed from the swivel frit assembly and $\text{Zr}(\text{NMe}_2)_4$ (3.88 g, 14.5 mmol) was added. A reflux condenser and 180° valve was attached to the round bottom flask. 100 mL of toluene was condensed onto this mixture. After flushing with Ar, the mixture was stirred at $130\text{ }^\circ\text{C}$ for 18 hours while open to a mercury bubbler, allowing NMe_2H to escape. Trimethylsilylchloride (7 mL, 56 mmol) was condensed onto the resulting orange solution. This stirred for 24 hours and then all volatiles were removed. In the inert atmosphere glove box, the solid was taken up in a minimum amount of toluene and cooled to $-30\text{ }^\circ\text{C}$. ^1H NMR (500 MHz, C_6D_6 , δ): 0.37 (s, 3H, SiCH_3), 0.60 (s, 3H, SiCH_3), 1.17 (s, 3H, CCH_3), 1.44 (s, 18H, $\text{C}(\text{CH}_3)_3$), 1.77 (s, 3H, CCH_3), 6.42 (d, 2H, CpH , $J_{\text{HH}}=1.9\text{ Hz}$), 6.62 (d, 2H, CpH , $J_{\text{HH}}=1.9\text{ Hz}$).

$(\text{C}_5\text{H}_4\text{CMe}_3)_2\text{Zr}(\text{CO})_2$. In an inert atmosphere glove box, $(\text{C}_5\text{H}_4\text{CMe}_3)_2\text{ZrCl}_2$ (500 mg, 1.24 mmol) was loaded into a 100 ml round bottom flask. A 180° adapter with a teflon stopcock was attached, and the assembly was evacuated on a high vacuum line. This was evacuated and cooled to $-80\text{ }^\circ\text{C}$ until the Na/Hg amalgam was frozen (occasionally it was necessary to condense a small amount of THF first as the amalgam would not freeze otherwise). THF (25 mL) was slowly condensed onto the mixture and then the solution was stirred rapidly. The evacuated line and flask were filled with CO gas. The dry ice bath was removed, and the flask was covered with aluminum foil. Upon warming, the solution darkened from pale green to dark blue to dark green. This was allowed to stir under a CO atmosphere for 18 hours. All volatiles were removed *in vacuo*. In an inert atmosphere glove box, the solid was transferred into a vacuum sublimator. The solid was sublimed onto a cold finger condenser at $65\text{ }^\circ\text{C}$ at 0.01 mm Hg. The green solid was obtained in 33% yield. ^1H NMR (300 MHz, C_6D_6 ,

δ): 1.04 (s, 18H, CCH₃), 4.96 (t, 4H, CpH, J_{HH}=2.5 Hz), 5.01 (t, 4H, CpH, J_{HH}=2.5 Hz) IR (cm⁻¹): 1968, 1881.

meso-Me₂Si(C₅H₃-3-CMe₃)₂Zr(CO)₂. ¹H NMR (500 MHz, C₆D₆, δ): 0.04 (s, 3H, SiCH₃), 0.11 (s, 3H, SiCH₃), 1.15 (s, 18H, CCH₃), 5.08 (s, 2H, CpH), 5.14 (s, 2H, CpH), 5.17 (s, 2H, CpH). IR (cm⁻¹): 1969, 1892.

rac-Me₂C(C₅H₃-3-CMe₃)₂Zr(CO)₂. ¹H NMR (400 MHz, C₆D₆, δ): 1.04 (s, 6H, C(CH₃)₂), 1.19 (s, 18H, C(CH₃)₃), 4.89 (t, 2H, CpH, J_{HH}=2.2 Hz), 5.03 (t, 2, CpH, J_{HH}=2.2 Hz), 5.12 (t, 2, CpH, J_{HH}=2.2 Hz). IR (cm⁻¹): 1878, 1967.

1,2-(Me₂Si)₂(C₅H₂-4-CMe₃)₂Zr(CO)₂. ¹H NMR (500 MHz, C₆D₆, δ): 0.25 (s, 6H, Si(CH₃)(CH₃)), 0.48 (s, 6H, Si(CH₃)(CH₃)), 1.07 (s, 18H, C(CH₃)₃), 6.01 (s, 4H, CpH). IR (cm⁻¹): 1869, 1962. IR (cm⁻¹): 1962, 1867.

(1-Me₂Si)(2-Me₂C)(C₅H₂-4-CMe₃)₂Zr(CO)₂. ¹H NMR (500 MHz, C₆D₆, δ): 0.42 (s, 3H, SiCH₃), 0.58 (s, 3H, SiCH₃), 0.93 (s, 3H, CCH₃), 0.99 (s, 18H, C(CH₃)₃), 1.64 (s, 3H, CCH₃), 5.64 (d, 2H, CpH, J_{HH}=18 Hz), 5.70 (d, 2H, CpH, J_{HH}=18 Hz). IR (cm⁻¹): 1967, 1888.

Me₂Si(C₅H₃-2-SiMe₃-4-CMe₃)₂Zr(CO)₂. ¹H NMR (300 MHz, C₆D₆, δ): 0.31 (s, 18H, Si(CH₃)₃), 0.40 (s, 6H, Si(CH₃)₂), 1.19 (s, 18H, C(CH₃)₃), 5.36 (s, 2H, CpH), 5.43 (s, 2H, CpH). IR (cm⁻¹): 1967, 1888.

Me₂Si(C₅H₄)₂Zr(CO)₂. IR (cm⁻¹): 1980, 1896.

Me₂C(C₅H₄)₂Zr(CO)₂. IR (cm⁻¹): 1978, 1892.

[(MeC₅H₄)₂Zr(OCMe₃)] [MeB(C₆F₅)₃]. In an inert atmosphere glove box, (MeCp)₂ZrMe₂ (50 mg, 179 μ mol) was dissolved in 10 mL of CH₂Cl₂ in a 25 ml round bottom flask. *t*-Butanol (18 μ L, 189 μ mol) was quickly added to this solution *via* syringe. The solution was allowed to stir for 10 minutes during which a gas was evolved. A 180° adapter with a teflon stopcock was attached, and the sealed assembly was attached to a high-vacuum line. The volatiles were removed *in vacuo* leaving a white solid in quantitative yield. The solid was taken up in 0.5 mL CD₂Cl₂ and B(C₆F₅)₃ (91.5 mg, 179 μ mol) was added, resulting in a yellow solution. ¹H NMR (500 MHz, CD₂Cl₂, -80 °C, δ): 0.67 (s, 3H, BCH₃), 1.05

(s, 9H, C(CH₃)₃), 2.12 (s, 6H, CpCH₃), 6.07 (s, 2H, CpH), 6.08 (s, 2H, CpH), 6.23 (s, 2H, CpH), 6.28 (s, 2H, CpH).

[Me₂Si(C₅H₅)₂Zr(OCMe₃)] [MeB(C₆F₅)₃]. ¹H NMR (500 MHz, CD₂Cl₂, -80 °C, δ): 0.67 (s, 3H, BCH₃), 0.76 (s, 3H, SiCH₃), 0.80 (s, 3H, SiCH₃), 0.96 (s, 9H, C(CH₃)₃), 5.92 (s, 2H, CpH), 6.20 (s, 2H, CpH), 6.50 (s, 2H, CpH), 6.68 (s, 2H, CpH).

[Me₂C(C₅H₅)₂Zr(OCMe₃)] [MeB(C₆F₅)₃]. ¹H NMR (300 MHz, C₆D₆, δ): 0.67 (s, 3H, BCH₃), 1.80 (s, 3H, CCH₃), 1.84 (s, 3H, SiCH₃), 1.03 (s, 9H, C(CH₃)₃), 5.75 (s, 2H, CpH), 6.05 (s, 2H, CpH), 6.29 (s, 2H, CpH), 6.35 (s, 2H, CpH).

(1,2-Me₂Si)₂(C₅H₅)₂Zr(OCMe₃)] [MeB(C₆F₅)₃]. In an inert atmosphere glove box, (1,2-Me₂Si)₂(C₅H₅)₂ZrMe₂ (27 mg, 74 μmol) and B(C₆F₅)₃ (38 mg, 74 μmol) were loaded into a 25 ml round bottom flask. A 180° adapter with a teflon stopcock was attached and the sealed assembly was attached to a high-vacuum line. This was evacuated, cooled to -78 °C with a dry ice-acetone slurry, and 10 mL of toluene was vacuum transferred onto this mixture. The mixture continued stirring at -78 °C for 15 minutes, producing a bright yellow solution. Acetone (32.4 ml at 42.5 mm Hg, 74 μmol), which had been dried over CaH₂, was measured in a gas bulb on the vacuum line and was vacuum transferred onto the solution. This solution stirred for an additional 30 minutes and then the volatiles were removed *in vacuo*. The resulting tan solid was dissolved in C₆D₅Br and used without further purification. ¹H NMR (500 MHz, C₆D₅Br, 27 °C, δ): 0.28 (s, 3H, SiCH₃), 0.60 (s, 3H, SiCH₃), 0.75 (s, 3H, BCH₃), 0.89 (s, 3H, SiCH₃), 1.05 (s, 9H, CCH₃), 1.27 (s, 3H, SiCH₃), 6.28 (s, 2H, CpH), 6.58 (s, 2H, CpH), 6.90 (s, 2H, CpH).

-
1. Ziegler, K.; Holzcamp, E.; Breil, H.; Martin, H. *Angew. Chem.* **1955**, *67*, 541.
 2. Breslow, D. S.; Newburg, N. R. *J. Am. Chem. Soc.* **1957**, *79*, 5072.
 3. Kaminsky, W.; Kulper, K.; Brintzinger, H. H.; Wild, F. R. W. P. *Angew. Chem. Int. Ed. Engl.* **1985**, *24*, 507.
 4. Ewen, J. A. *J. Mol. Catal. A-Chem.* **1998**, *128*, 103.

-
5. Smith, J. A.; von Seyerl, J.; Huttner, G.; Brintzinger, H.-H. *J. Organomet. Chem.* **1984**, *106*, 6355.
 6. Brintzinger, H.-H.; Fischer, D.; Müllhaupt, R.; Rieger, B.; Waymouth, R. M. *Angew. Chem. Int. Ed. Engl.* **1995**, *34*, 1143.
 7. Casey and co-workers have recently addressed this problem: Liu, Z.; Somsook, E.; Landis, C. R. *J. Am. Chem. Soc.* **2001**, *123*, 2915.
 8. Deeming, A. J. Mononuclear Iron Compounds with η^2 - η^6 Hydrocarbon Ligands. In *Comprehensive Organometallic Chemistry*, 1st ed.; Wilkinson, G.; Stone, F. G. A.; Abel, E. A.; Pergamon Press: Oxford, 1982; Vol. 4, pp 478-480.
 9. Wilkinson, G. *J. Organomet. Chem.* **1975**, *100*, 273.
 10. Bercaw, J. E. **1974**, *96*, 5087.
 11. Lauher, J. W.; Hoffman, R. *J. Am. Chem. Soc.* **1976**, *98*, 1729.
 12. Jardine, C. N. Density Functional Studies of *Ansa*-metallocenes and Related Compounds. Doctor of Philosophy, St. Catherine's College-Oxford University, Oxford, U.K., 2000
 13. (a) Shaltout, R. M.; Corey, J. Y.; Rath, N. P. *J. Organomet. Chem.* **1984**, *106*, 6355.

(b) Cano, A.; Cuenca, T.; Gómez-Sal, P.; Royo, B.; Royo, P. *Organometallics* **1993**, *13*, 1688.
 14. Kelsey, B. A.; Ellis, J. E. *J. Am. Chem. Soc.* **1986**, *108*, 1344.
 15. Diamond, G. M.; Jordan, R. F.; Petersen, J. L. *Organometallics* **1996**, *15*, 4045.
 16. $\text{Me}_2\text{Si}(\text{C}_5\text{H}_2\text{-2-TMS-4-}t\text{-Bu})_2\text{Zr}(\text{CO})_2$ was not included because the ancillary substitution is extremely crowded and introduces distortions that probably mask the *ansa* effects that we want to study.

-
17. A DFT calculation confirmed that the preferred geometry of zirconocene hydroxy cation is a planar geometry with the oxygen in the middle of the metallocene wedge. The bond length is extremely short (1.94 Å) in this structure confirming that there is a Zr-O multiple bond.
 18. Carpentier, J.-F.; Wu, Z.; Lee, C. W.; Strömberg, S.; Christopher, J. N.; Jordan, R. F. *J. Am. Chem. Soc.* **2000**, *122*, 7750.
 19. Wu, Z.; Jordan, R. F.; Petersen, J. L. *J. Am. Chem. Soc.* **1995**, *117*, 5867.
 20. Sita, L. R.; Babcock, J. R. *Organometallics* **1998**, *17*, 5228.
 21. Unpublished results.
 22. Beck, S.; Lieber, S.; Schaper, F.; Geyer, A.; Brintzinger, H.-H. *J. Am. Chem. Soc.* **2001**, *123*, 1483. (*and references therein*)

Appendix B. Carbonyl stretching frequencies for zirconocene dicarbonyl complexes.

Complex	Assym. Stretch (cm ⁻¹)	Sym.Stretch Mode (cm ⁻¹)
Cp ₂ Zr(CO) ₂	1975	1886
Me ₂ SiCp ₂ Zr(CO) ₂	1980	1896
Me ₂ CCp ₂ Zr(CO) ₂	1978	1892
(<i>t</i> -BuCp) ₂ Zr(CO) ₂	1967	1879
Me ₂ Si(<i>t</i> -BuCp) ₂ Zr(CO) ₂	1969	1881
Me ₂ C(<i>t</i> -BuCp) ₂ Zr(CO) ₂	1967	1878
(Me ₂ Si) ₂ (<i>t</i> -BuCp) ₂ Zr(CO) ₂	1962	1867
(Me ₂ Si) ₂ (TMS- <i>t</i> -BuCp)- Zr(CO) ₂	1967	1878
(Me ₂ Si)(Me ₂ C) ₂ (<i>t</i> -BuCp)- Zr(CO) ₂	1962	1869
(Me ₅ C ₅) ₂ Zr(CO) ₂ ¹	1945	1852
(Me ₅ C ₅)(Cp)Zr(CO) ₂ ²	1965	1875
(TMSCp) ₂ Zr(CO) ₂ ³	1970	1880
(TMS ₂ Cp) ₂ Zr(CO) ₂ ³	1962	1875

-
1. Sikora, D. J.; Moriarty, K. J.; Rausch, M. D. *Inorg. Synth.* **1986**, *24*, 147.

-
2. Sikora, D. J.; Macomber, D. W.; Rausch, M. D. *Adv. Organomet. Chem.* **1986**, *25*, 318.
 3. Antinolo, A.; Lappert, M. F.; Winterborn, D. J. W. *J. Organomet. Chem.* **1984**, *272*, C37.

Appendix C.

Crystal Structure Analysis of:



Contents

Table 1.	Crystal data
Table 2.	Atomic Coordinates
Table 3.	Selected bond distances and angles
Table 4.	Full bond distances and angles (for deposit)
Table 5.	Anisotropic displacement parameters
Table 6.	Hydrogen atomic coordinates
Table 7.	Observed and calculated structure factors (for deposit)



Note: The crystallographic data has been deposited in the Cambridge Database (CCDC) and has been placed on hold pending further instructions from me. The deposition number is 103280. Ideally the CCDC would like the publication to contain a footnote of the type: "Crystallographic data have been deposited at the CCDC, 12 Union Road, Cambridge CB2 1EZ, UK and copies can be obtained on request, free of charge, by quoting the publication citation and the deposition number 103280."

Table 1. Crystal data and structure refinement for CGB1.

Empirical formula	$C_{35}H_{26}BF_{15}OSiZr$
Formula weight	877.68
Crystallization Solvent	CD_2Cl_2
Crystal Habit	Plate
Crystal size	0.44 x 0.22 x 0.15 mm ³
Crystal color	Colorless

Data Collection

Preliminary Photos	None
Type of diffractometer	CAD-4
Wavelength	0.71073 Å MoKa
Data Collection Temperature	85 K
Theta range for reflections used in lattice determination	11.0 to 13.1°
Unit cell dimensions	a = 10.900(6) Å b = 16.134(13) Å b = 96.73(6)° c = 20.43(2) Å
Volume	3568(5) Å ³
Z	4
Crystal system	Monoclinic
Space group	P2 ₁ /n
Density (calculated)	1.634 Mg/m ³
F(000)	1752

Theta range for data collection	1.61 to 25.00°
Completeness to $\theta = 25.00^\circ$	99.9 %
Index ranges	$-12 \leq h \leq 12, -19 \leq k \leq 19, 0 \leq l \leq 24$
Data collection scan type	ω scans
Reflections collected	13385
Independent reflections	6274 [$R_{\text{int}} = 0.037$; $\text{GOF}_{\text{merge}} = 1.17$]
Absorption coefficient	0.450 mm ⁻¹
Number of standards	3 reflections measured every 75 min.
Variation of standards	-1.31%.

Structure solution and Refinement

Structure solution program	SHELXS-97 (Sheldrick, 1990)
Primary solution method	Direct methods
Secondary solution method	Difference Fourier map
Hydrogen placement	Difference Fourier map
Structure refinement program	SHELXL-97 (Sheldrick, 1997)
Refinement method	Full matrix least-squares on F^2
Data / restraints / parameters	6274 / 0 / 591
Treatment of hydrogen atoms	Unrestrained
Goodness-of-fit on F^2	1.245
Final R indices [$I > 2s(I)$]	$R1 = 0.0343, wR2 = 0.0603$
R indices (all data)	$R1 = 0.0549, wR2 = 0.0660$
Type of weighting scheme used	Sigma

Weighting scheme used	$w=1/\sigma^2(Fo^2)$
Max shift/error	0.001
Average shift/error	0.000
Largest diff. peak and hole	0.419 and -0.427 e.Å ⁻³

Special Refinement Details

The variances [$\sigma^2(Fo^2)$] were derived from counting statistics plus an additional term, $(0.014I)^2$, and the variances of the merged data were obtained by propagation of error plus the addition of another term, $(0.014\langle I \rangle)^2$.

Refinement of F^2 against ALL reflections. The weighted R-factor (wR) and goodness of fit (S) are based on F^2 , conventional R-factors (R) are based on F , with F set to zero for negative F^2 . The threshold expression of $F^2 > 2\sigma(F^2)$ is used only for calculating R-factors(gt) etc. and is not relevant to the choice of reflections for refinement. R-factors based on F^2 are statistically about twice as large as those based on F , and R-factors based on ALL data will be even larger.

All esds (except the esd in the dihedral angle between two l.s. planes) are estimated using the full covariance matrix. The cell esds are taken into account individually in the estimation of esds in distances, angles and torsion angles; correlations between esds in cell parameters are only used when they are defined by crystal symmetry. An approximate (isotropic) treatment of cell esds is used for estimating esds involving l.s. planes.

Table 2. Atomic coordinates ($\times 10^4$) and equivalent isotropic displacement parameters ($\text{\AA}^2 \times 10^3$) for CGB1. $U(\text{eq})$ is defined as the trace of the orthogonalized U^{ij} tensor.

	x	y	z	U_{eq}
Zr	6816(1)	7818(1)	2218(1)	11(1)
Si	9563(1)	7025(1)	1906(1)	14(1)
O	5794(2)	8286(1)	2812(1)	16(1)
B	4198(3)	7853(2)	507(2)	12(1)
F(22)	3045(2)	6698(1)	1343(1)	20(1)
F(23)	2483(2)	5121(1)	1111(1)	32(1)
F(24)	2936(2)	4384(1)	-44(1)	33(1)
F(25)	4003(2)	5280(1)	-957(1)	26(1)
F(26)	4557(2)	6850(1)	-755(1)	20(1)
F(32)	6555(1)	7213(1)	242(1)	15(1)
F(33)	8147(1)	7845(1)	-492(1)	20(1)
F(34)	7584(2)	9264(1)	-1218(1)	21(1)
F(35)	5379(2)	10024(1)	-1130(1)	21(1)
F(36)	3804(1)	9444(1)	-362(1)	17(1)
F(42)	2425(1)	7987(1)	-649(1)	15(1)

F(43)	204(1)	8704(1)	-763(1)	20(1)
F(44)	-680(1)	9386(1)	311(1)	19(1)
F(45)	781(1)	9385(1)	1506(1)	18(1)
F(46)	2977(1)	8677(1)	1634(1)	18(1)
C(1)	8157(3)	6540(2)	2196(1)	14(1)
C(2)	7053(3)	6350(2)	1791(2)	14(1)
C(3)	6061(3)	6307(2)	2192(2)	17(1)
C(4)	6552(3)	6472(2)	2847(2)	16(1)
C(5)	7822(3)	6641(2)	2849(1)	15(1)
C(6)	8942(3)	8105(2)	1928(1)	14(1)
C(7)	8125(3)	8480(2)	1427(2)	17(1)
C(8)	7530(3)	9160(2)	1696(2)	20(1)
C(9)	7963(3)	9206(2)	2368(2)	21(1)
C(10)	8797(3)	8546(2)	2522(2)	15(1)
C(11)	10956(3)	6893(2)	2514(2)	24(1)
C(12)	9780(3)	6713(2)	1051(2)	21(1)
C(13)	5049(3)	8741(2)	3222(1)	20(1)
C(14)	5793(5)	8853(3)	3895(2)	46(1)
C(15)	3882(3)	8241(2)	3265(2)	29(1)
C(16)	4742(3)	9576(2)	2900(2)	22(1)
C(17)	5034(3)	7919(2)	1246(1)	12(1)
C(21)	3899(2)	6862(2)	327(1)	13(1)

C(22)	3338(3)	6374(2)	762(1)	14(1)
C(23)	3022(3)	5554(2)	657(2)	20(1)
C(24)	3254(3)	5180(2)	80(2)	21(1)
C(25)	3791(3)	5633(2)	-381(2)	17(1)
C(26)	4085(2)	6454(2)	-255(1)	14(1)
C(31)	5076(2)	8281(2)	-9(1)	11(1)
C(32)	6213(2)	7933(2)	-82(1)	12(1)
C(33)	7061(2)	8236(2)	-469(1)	14(1)
C(34)	6793(3)	8949(2)	-829(1)	14(1)
C(35)	5670(3)	9323(2)	-783(1)	13(1)
C(36)	4857(2)	8999(2)	-380(1)	13(1)
C(41)	2830(2)	8297(2)	495(1)	11(1)
C(42)	2034(2)	8316(2)	-93(1)	12(1)
C(43)	881(3)	8674(2)	-164(1)	14(1)
C(44)	447(3)	9026(2)	374(2)	15(1)
C(45)	1177(3)	9027(2)	976(1)	13(1)
C(46)	2334(3)	8658(2)	1019(1)	12(1)

Table 3. Selected bond lengths [\AA] and angles [$^\circ$] for CGB1.

Zr-Pln(1)	2.229(2)	Zr-Cent(1)	2.231(2)
Zr-Pln(2)	2.219(1)	Zr-Cent(2)	2.222(1)
Zr-O	1.898(2)		
Zr-C(17)	2.615(4)		
Zr-H(17A)	2.62(2)		
Zr-H(17B)	2.62(3)		
Zr-H(17C)	2.29(2)		
Pln(1)-Zr-Pln(2)	119.4(1)	Cent(1)-Zr-Cent(2)	123.9(1)
O-Zr-C(17)	91.24(11)		
B-C(17)-Zr	163.5(2)		
B-C(17)-H(17A)	110.5(15)	Zr-C(17)-H(17A)	79.2(14)
B-C(17)-H(17B)	107.2(17)	Zr-C(17)-H(17B)	80.3(17)
B-C(17)-H(17C)	103.5(14)	Zr-C(17)-H(17C)	60.0(14)
H(17A)-C(17)-H(17B)	111(2)		

H(17A)-C(17)-H(17C) 114(2)

H(17B)-C(17)-H(17C) 110(2)

Cent(1) is the centroid formed by C(1), C(2), C(3), C(4) and C(5).

Cent(2) is the centroid formed by C(6), C(7), C(8), C(9) and C(10).

Pln(1) is the plane formed by C(1), C(2), C(3), C(4) and C(5).

Pln(2) is the plane formed by C(6), C(7), C(8), C(9) and C(10).

Table 4. Bond lengths [Å] and angles [°] for CGB1.

Zr-Pln(1)	2.231(2)	Zr-C(4)	2.556(3)
Zr-Pln(2)	2.216(1)	Zr-C(9)	2.566(3)
Zr-Cent(1)	2.231(2)	Zr-C(3)	2.571(3)
Zr-Cent(2)	2.216(1)	Zr-C(8)	2.574(3)
Zr-O	1.898(2)	Zr-C(17)	2.615(4)
Zr-C(10)	2.473(3)	Zr-H(17A)	2.62(2)
Zr-C(5)	2.477(3)	Zr-H(17B)	2.62(3)
Zr-C(6)	2.502(3)	Zr-H(17C)	2.29(2)
Zr-C(7)	2.516(3)	Si-C(11)	1.858(4)
Zr-C(1)	2.531(3)	Si-C(6)	1.871(3)
Zr-C(2)	2.548(3)	Si-C(1)	1.877(3)

Si-C(12)	1.860(4)	C(1)-C(2)	1.412(4)
O-C(13)	1.435(3)	C(1)-C(5)	1.434(4)
B-C(41)	1.652(4)	C(2)-C(3)	1.433(4)
B-C(31)	1.654(4)	C(2)-H(2)	0.92(3)
B-C(21)	1.663(4)	C(3)-C(4)	1.408(4)
B-C(17)	1.672(4)	C(3)-H(3)	0.94(3)
F(22)-C(22)	1.368(3)	C(4)-C(5)	1.410(4)
F(23)-C(23)	1.349(3)	C(4)-H(4)	0.95(3)
F(24)-C(24)	1.347(3)	C(5)-H(5)	0.95(3)
F(25)-C(25)	1.353(3)	C(6)-C(7)	1.413(4)
F(26)-C(26)	1.356(3)	C(6)-C(10)	1.431(4)
F(32)-C(32)	1.367(3)	C(7)-C(8)	1.417(4)
F(33)-C(33)	1.347(3)	C(7)-H(7)	0.89(3)
F(34)-C(34)	1.338(3)	C(8)-C(9)	1.399(5)
F(35)-C(35)	1.351(3)	C(8)-H(8)	0.93(3)
F(36)-C(36)	1.357(3)	C(9)-C(10)	1.411(4)
F(42)-C(42)	1.367(3)	C(9)-H(9)	0.93(3)
F(43)-C(43)	1.354(3)	C(10)-H(10)	0.92(3)
F(44)-C(44)	1.350(3)	C(11)-H(11A)	0.94(3)
F(45)-C(45)	1.343(3)	C(11)-H(11B)	1.00(3)
F(46)-C(46)	1.364(3)	C(11)-H(11C)	0.89(4)

C(12)-H(12A)	0.90(3)	C(23)-C(24)	1.375(4)
C(12)-H(12B)	0.94(3)	C(24)-C(25)	1.374(4)
C(12)-H(12C)	1.02(4)	C(25)-C(26)	1.381(4)
C(13)-C(16)	1.519(4)	C(31)-C(32)	1.385(4)
C(13)-C(15)	1.517(5)	C(31)-C(36)	1.391(4)
C(13)-C(14)	1.523(5)	C(32)-C(33)	1.375(4)
C(14)-H(14A)	0.98(3)	C(33)-C(34)	1.378(4)
C(14)-H(14B)	1.01(4)	C(34)-C(35)	1.378(4)
C(14)-H(14C)	0.91(4)	C(35)-C(36)	1.382(4)
C(15)-H(15A)	0.95(3)	C(41)-C(46)	1.384(4)
C(15)-H(15B)	1.04(3)	C(41)-C(42)	1.397(4)
C(15)-H(15C)	0.95(4)	C(42)-C(43)	1.375(4)
C(16)-H(16A)	0.96(3)	C(43)-C(44)	1.370(4)
C(16)-H(16B)	0.93(3)	C(44)-C(45)	1.383(4)
C(16)-H(16C)	0.94(3)	C(45)-C(46)	1.388(4)
C(17)-H(17A)	1.00(3)		
C(17)-H(17B)	0.90(3)	Pln(1)-Zr-Pln(2)	119.4(1)
C(17)-H(17C)	0.99(3)	Cent(1)-Zr-Cent(2)	123.9(1)
C(21)-C(22)	1.382(4)	O-Zr-C(10)	102.18(10)
C(21)-C(26)	1.395(4)	O-Zr-C(5)	103.26(10)
C(22)-C(23)	1.378(4)	C(10)-Zr-C(5)	85.01(11)

O-Zr-C(6)	135.00(9)	C(6)-Zr-C(4)	115.98(10)
C(10)-Zr-C(6)	33.43(9)	C(7)-Zr-C(4)	142.13(10)
C(5)-Zr-C(6)	84.20(10)	C(1)-Zr-C(4)	54.29(10)
O-Zr-C(7)	131.38(10)	C(2)-Zr-C(4)	53.47(11)
C(10)-Zr-C(7)	54.19(11)	O-Zr-C(9)	83.72(10)
C(5)-Zr-C(7)	114.21(10)	C(10)-Zr-C(9)	32.46(10)
C(6)-Zr-C(7)	32.70(9)	C(5)-Zr-C(9)	115.27(11)
O-Zr-C(1)	135.99(9)	C(6)-Zr-C(9)	54.17(10)
C(10)-Zr-C(1)	84.39(11)	C(7)-Zr-C(9)	53.16(11)
C(5)-Zr-C(1)	33.24(10)	C(1)-Zr-C(9)	116.01(11)
C(6)-Zr-C(1)	66.00(10)	C(2)-Zr-C(9)	141.67(10)
C(7)-Zr-C(1)	87.85(10)	C(4)-Zr-C(9)	139.77(11)
O-Zr-C(2)	132.86(9)	O-Zr-C(3)	100.41(10)
C(10)-Zr-C(2)	114.00(10)	C(10)-Zr-C(3)	136.35(10)
C(5)-Zr-C(2)	53.81(11)	C(5)-Zr-C(3)	53.53(11)
C(6)-Zr-C(2)	87.51(10)	C(6)-Zr-C(3)	118.26(9)
C(7)-Zr-C(2)	94.98(11)	C(7)-Zr-C(3)	126.40(10)
C(1)-Zr-C(2)	32.28(9)	C(1)-Zr-C(3)	53.95(10)
O-Zr-C(4)	84.70(10)	C(2)-Zr-C(3)	32.51(10)
C(10)-Zr-C(4)	115.08(11)	C(4)-Zr-C(3)	31.87(10)
C(5)-Zr-C(4)	32.50(9)	C(9)-Zr-C(3)	168.60(10)

O-Zr-C(8)	99.12(11)	O-Zr-H(17C)	113.2(7)
C(10)-Zr-C(8)	53.60(10)	C(10)-Zr-H(17C)	126.2(6)
C(5)-Zr-C(8)	136.31(10)	C(5)-Zr-H(17C)	121.9(6)
C(6)-Zr-C(8)	54.04(10)	C(6)-Zr-H(17C)	98.6(6)
C(7)-Zr-C(8)	32.30(10)	C(7)-Zr-H(17C)	72.0(6)
C(1)-Zr-C(8)	118.32(11)	C(1)-Zr-H(17C)	95.8(6)
C(2)-Zr-C(8)	126.31(12)	C(2)-Zr-H(17C)	68.3(6)
C(4)-Zr-C(8)	168.51(10)	C(4)-Zr-H(17C)	107.6(6)
C(9)-Zr-C(8)	31.59(11)	C(9)-Zr-H(17C)	112.4(6)
C(3)-Zr-C(8)	154.21(10)	C(3)-Zr-H(17C)	75.9(6)
O-Zr-C(17)	91.24(11)	C(8)-Zr-H(17C)	81.0(6)
C(10)-Zr-C(17)	135.22(10)	C(17)-Zr-H(17C)	22.0(6)
C(5)-Zr-C(17)	133.41(10)	C(11)-Si-C(6)	111.13(15)
C(6)-Zr-C(17)	115.78(11)	C(11)-Si-C(1)	112.05(16)
C(7)-Zr-C(17)	84.97(11)	C(6)-Si-C(1)	94.01(13)
C(1)-Zr-C(17)	114.61(10)	C(11)-Si-C(12)	114.36(17)
C(2)-Zr-C(17)	83.92(10)	C(6)-Si-C(12)	111.14(14)
C(4)-Zr-C(17)	108.51(10)	C(1)-Si-C(12)	112.43(15)
C(9)-Zr-C(17)	110.13(10)	C(13)-O-Zr	172.59(19)
C(3)-Zr-C(17)	80.56(10)	C(41)-B-C(31)	113.4(2)
C(8)-Zr-C(17)	82.34(10)	C(41)-B-C(21)	105.1(2)

C(31)-B-C(21)	111.9(2)	Zr-C(3)-H(3)	119.9(17)
C(41)-B-C(17)	112.4(2)	C(3)-C(4)-C(5)	107.7(3)
C(31)-B-C(17)	104.7(2)	C(3)-C(4)-Zr	74.66(17)
C(21)-B-C(17)	109.4(2)	C(5)-C(4)-Zr	70.69(16)
C(2)-C(1)-C(5)	106.2(3)	C(3)-C(4)-H(4)	126.1(17)
C(2)-C(1)-Si	125.2(2)	C(5)-C(4)-H(4)	126.3(17)
C(5)-C(1)-Si	123.5(2)	Zr-C(4)-H(4)	120.8(16)
C(2)-C(1)-Zr	74.51(16)	C(4)-C(5)-C(1)	109.4(3)
C(5)-C(1)-Zr	71.32(16)	C(4)-C(5)-Zr	76.81(17)
Si-C(1)-Zr	99.24(12)	C(1)-C(5)-Zr	75.44(16)
C(1)-C(2)-C(3)	108.9(3)	C(4)-C(5)-H(5)	124.0(17)
C(1)-C(2)-Zr	73.21(16)	C(1)-C(5)-H(5)	126.6(17)
C(3)-C(2)-Zr	74.64(16)	Zr-C(5)-H(5)	116.6(17)
C(1)-C(2)-H(2)	127.6(17)	C(7)-C(6)-C(10)	106.1(3)
C(3)-C(2)-H(2)	123.5(17)	C(7)-C(6)-Si	125.6(2)
Zr-C(2)-H(2)	116.6(17)	C(10)-C(6)-Si	124.0(2)
C(4)-C(3)-C(2)	107.8(3)	C(7)-C(6)-Zr	74.22(17)
C(4)-C(3)-Zr	73.46(16)	C(10)-C(6)-Zr	72.19(16)
C(2)-C(3)-Zr	72.85(16)	Si-C(6)-Zr	100.43(12)
C(4)-C(3)-H(3)	125.1(17)	C(6)-C(7)-C(8)	109.2(3)
C(2)-C(3)-H(3)	127.1(17)	C(6)-C(7)-Zr	73.08(17)

C(8)-C(7)-Zr	76.09(18)	Zr-C(10)-H(10)	116.7(18)
C(6)-C(7)-H(7)	126.7(19)	Si-C(11)-H(11A)	111(2)
C(8)-C(7)-H(7)	124.0(19)	Si-C(11)-H(11B)	111.7(19)
Zr-C(7)-H(7)	119.5(19)	H(11A)-C(11)-H(11B)	111(3)
C(9)-C(8)-C(7)	107.7(3)	Si-C(11)-H(11C)	114(3)
C(9)-C(8)-Zr	73.90(18)	H(11A)-C(11)-H(11C)	105(3)
C(7)-C(8)-Zr	71.60(18)	H(11B)-C(11)-H(11C)	102(3)
C(9)-C(8)-H(8)	128.1(19)	Si-C(12)-H(12A)	109.9(19)
C(7)-C(8)-H(8)	124.1(19)	Si-C(12)-H(12B)	112.4(19)
Zr-C(8)-H(8)	119.4(19)	H(12A)-C(12)-H(12B)	104(3)
C(8)-C(9)-C(10)	108.2(3)	Si-C(12)-H(12C)	111.7(19)
C(8)-C(9)-Zr	74.51(17)	H(12A)-C(12)-H(12C)	111(3)
C(10)-C(9)-Zr	70.13(17)	H(12B)-C(12)-H(12C)	108(3)
C(8)-C(9)-H(9)	123.8(19)	O-C(13)-C(16)	108.1(3)
C(10)-C(9)-H(9)	127.9(19)	O-C(13)-C(15)	107.3(3)
Zr-C(9)-H(9)	118.5(19)	C(16)-C(13)-C(15)	110.7(3)
C(9)-C(10)-C(6)	108.6(3)	O-C(13)-C(14)	108.1(3)
C(9)-C(10)-Zr	77.41(18)	C(16)-C(13)-C(14)	110.7(3)
C(6)-C(10)-Zr	74.38(17)	C(15)-C(13)-C(14)	111.8(3)
C(9)-C(10)-H(10)	126.9(18)	C(13)-C(14)-H(14A)	112.2(18)
C(6)-C(10)-H(10)	124.5(18)	C(13)-C(14)-H(14B)	110(2)

H(14A)-C(14)-H(14B)	105(3)	Zr-C(17)-H(17B)	80.3(17)
C(13)-C(14)-H(14C)	110(3)	Zr-C(17)-H(17C)	60.0(14)
H(14A)-C(14)-H(14C)	114(3)	H(17A)-C(17)-H(17B)	111(2)
H(14B)-C(14)-H(14C)	105(3)	H(17A)-C(17)-H(17C)	114(2)
C(13)-C(15)-H(15A)	111.0(19)	H(17B)-C(17)-H(17C)	110(2)
C(13)-C(15)-H(15B)	111.5(17)	C(22)-C(21)-C(26)	113.5(3)
H(15A)-C(15)-H(15B)	106(2)	C(22)-C(21)-B	119.7(2)
C(13)-C(15)-H(15C)	111(2)	C(26)-C(21)-B	126.7(2)
H(15A)-C(15)-H(15C)	108(3)	F(22)-C(22)-C(23)	114.9(3)
H(15B)-C(15)-H(15C)	108(3)	F(22)-C(22)-C(21)	120.3(3)
C(13)-C(16)-H(16A)	110(2)	C(23)-C(22)-C(21)	124.7(3)
C(13)-C(16)-H(16B)	109.6(18)	F(23)-C(23)-C(22)	120.8(3)
H(16A)-C(16)-H(16B)	108(3)	F(23)-C(23)-C(24)	120.1(3)
C(13)-C(16)-H(16C)	110.8(18)	C(22)-C(23)-C(24)	119.1(3)
H(16A)-C(16)-H(16C)	106(3)	F(24)-C(24)-C(25)	119.9(3)
H(16B)-C(16)-H(16C)	113(2)	F(24)-C(24)-C(23)	120.7(3)
B-C(17)-Zr	163.5(2)	C(25)-C(24)-C(23)	119.3(3)
B-C(17)-H(17A)	110.5(15)	F(25)-C(25)-C(24)	120.2(3)
B-C(17)-H(17B)	107.2(17)	F(25)-C(25)-C(26)	120.4(3)
B-C(17)-H(17C)	103.5(14)	C(24)-C(25)-C(26)	119.5(3)
Zr-C(17)-H(17A)	79.2(14)	F(26)-C(26)-C(25)	114.4(3)

F(26)-C(26)-C(21)	121.7(2)	C(35)-C(36)-C(31)	124.0(3)
C(25)-C(26)-C(21)	123.9(3)	C(46)-C(41)-C(42)	113.3(2)
C(32)-C(31)-C(36)	112.2(2)	C(46)-C(41)-B	127.2(2)
C(32)-C(31)-B	119.4(2)	C(42)-C(41)-B	119.4(2)
C(36)-C(31)-B	128.3(2)	F(42)-C(42)-C(43)	116.5(2)
F(32)-C(32)-C(33)	114.7(2)	F(42)-C(42)-C(41)	118.9(2)
F(32)-C(32)-C(31)	119.3(2)	C(43)-C(42)-C(41)	124.6(3)
C(33)-C(32)-C(31)	126.0(3)	F(43)-C(43)-C(42)	120.3(3)
F(33)-C(33)-C(32)	120.4(2)	F(43)-C(43)-C(44)	120.5(2)
F(33)-C(33)-C(34)	120.3(3)	C(42)-C(43)-C(44)	119.2(3)
C(32)-C(33)-C(34)	119.3(3)	F(44)-C(44)-C(43)	119.8(3)
F(34)-C(34)-C(35)	120.9(3)	F(44)-C(44)-C(45)	120.4(3)
F(34)-C(34)-C(33)	121.5(3)	C(43)-C(44)-C(45)	119.7(3)
C(35)-C(34)-C(33)	117.6(3)	F(45)-C(45)-C(44)	120.7(3)
F(35)-C(35)-C(34)	119.1(2)	F(45)-C(45)-C(46)	120.5(3)
F(35)-C(35)-C(36)	120.1(3)	C(44)-C(45)-C(46)	118.7(3)
C(34)-C(35)-C(36)	120.8(3)	F(46)-C(46)-C(41)	121.1(2)
F(36)-C(36)-C(35)	114.8(2)	F(46)-C(46)-C(45)	114.5(2)
F(36)-C(36)-C(31)	121.2(2)	C(41)-C(46)-C(45)	124.4(3)

Cent(1) is the centroid formed by C(1), C(2), C(3), C(4) and C(5).

Cent(2) is the centroid formed by C(6), C(7), C(8), C(9) and C(10).

Pln(1) is the plane formed by C(1), C(2), C(3), C(4) and C(5).

Pln(2) is the plane formed by C(6), C(7), C(8), C(9) and C(10).

Table 5. Anisotropic displacement parameters ($\text{\AA}^2 \times 10^4$) for CGB1. The anisotropic displacement factor exponent takes the form: $-2p^2 [h^2 a^*2U^{11} + \dots + 2 h k a^* b^* U^{12}]$

	U ¹¹	U ²²	U ³³	U ²³	U ¹³	U ¹²
Zr	127(1)	80(1)	114(1)	-4(1)	0(1)	0(1)
Si	138(4)	140(4)	154(4)	2(3)	5(3)	12(3)
O	184(11)	154(11)	128(11)	-43(9)	9(9)	19(9)
B	120(16)	116(16)	113(16)	3(14)	0(13)	1(14)
F(22)	234(9)	179(9)	195(9)	13(7)	71(8)	-46(7)
F(23)	398(12)	170(10)	418(12)	52(9)	172(10)	-101(9)
F(24)	410(12)	88(9)	507(13)	-70(9)	70(10)	-87(8)
F(25)	309(11)	183(9)	283(11)	-129(8)	19(8)	1(8)
F(26)	271(10)	179(9)	140(9)	-25(7)	35(7)	-41(7)
F(32)	172(8)	110(8)	175(9)	32(7)	21(7)	33(7)

F(33)	168(9)	187(9)	239(9)	9(8)	68(7)	28(8)
F(34)	202(9)	221(10)	220(10)	45(8)	87(8)	-47(8)
F(35)	252(10)	144(9)	224(10)	100(7)	25(8)	2(8)
F(36)	153(9)	117(8)	230(10)	39(7)	34(7)	32(7)
F(42)	156(8)	191(9)	104(8)	-33(7)	3(7)	17(7)
F(43)	146(9)	288(10)	139(9)	46(8)	-35(7)	24(7)
F(44)	123(9)	197(9)	263(10)	67(8)	46(7)	40(7)
F(45)	177(9)	200(9)	187(9)	-45(7)	72(7)	-5(7)
F(46)	171(9)	242(9)	111(9)	-45(7)	-12(7)	9(7)
C(1)	183(16)	72(14)	165(16)	4(12)	7(13)	47(12)
C(2)	217(16)	51(14)	130(16)	-15(12)	-5(13)	23(12)
C(3)	185(17)	61(14)	252(18)	20(13)	12(14)	2(12)
C(4)	222(17)	102(15)	155(16)	46(12)	50(14)	14(12)
C(5)	197(16)	122(15)	113(15)	38(12)	-20(13)	12(12)
C(6)	121(15)	151(15)	140(15)	-10(12)	12(12)	-55(12)
C(7)	183(16)	137(16)	172(17)	30(13)	-6(14)	-55(13)
C(8)	140(16)	88(15)	350(20)	71(14)	-37(14)	-35(12)
C(9)	169(17)	116(16)	340(20)	-55(15)	43(15)	-47(13)
C(10)	137(15)	165(16)	147(16)	-1(13)	-33(13)	-68(12)
C(11)	175(18)	260(20)	280(20)	33(16)	-15(15)	43(15)
C(12)	206(18)	200(18)	240(19)	-16(15)	81(15)	6(15)
C(13)	224(17)	210(17)	151(16)	-52(13)	23(13)	77(13)

C(22)	136(15)	131(15)	159(16)	-8(12)	14(12)	25(12)
C(23)	162(16)	161(16)	282(18)	79(14)	61(14)	-32(13)
C(24)	187(17)	83(15)	360(20)	-30(14)	-16(15)	-18(12)
C(25)	156(16)	144(16)	194(17)	-71(13)	-33(13)	43(12)
C(26)	119(15)	144(15)	149(16)	5(12)	-6(12)	-21(12)
C(31)	118(14)	112(14)	89(14)	-32(11)	-13(11)	-20(12)
C(32)	168(15)	67(14)	106(14)	23(11)	-5(12)	-7(12)
C(33)	108(15)	126(15)	168(16)	-55(12)	-13(12)	3(12)
C(34)	161(16)	141(15)	125(15)	2(12)	34(12)	-87(12)
C(35)	190(16)	81(14)	121(15)	34(12)	-22(12)	-26(12)
C(36)	103(14)	141(15)	128(15)	-36(12)	-7(12)	11(12)
C(41)	128(15)	63(14)	130(15)	15(11)	7(12)	-29(11)
C(42)	136(15)	98(14)	132(15)	12(12)	30(12)	-12(12)
C(43)	126(15)	132(15)	153(16)	50(12)	-15(12)	-10(12)
C(44)	125(15)	110(15)	227(17)	55(13)	55(13)	6(12)
C(45)	166(15)	92(14)	134(15)	15(12)	80(12)	-31(12)
C(46)	161(15)	104(14)	93(15)	29(11)	-18(12)	-32(12)

Table 6. Hydrogen coordinates ($\times 10^4$) and isotropic displacement parameters ($\text{\AA}^2 \times 10^3$) for CGB1.

Table 6. Hydrogen coordinates ($\times 10^4$) and isotropic displacement parameters ($\text{\AA}^2 \times 10^3$) for CGB1.

	x	y	z	U_{iso}
H(2)	6950(20)	6282(17)	1338(14)	12(8)
H(3)	5230(30)	6186(16)	2052(13)	13(8)
H(4)	6110(20)	6465(16)	3219(13)	11(7)
H(5)	8360(30)	6777(18)	3235(14)	21(8)
H(7)	8010(30)	8339(18)	1004(14)	15(8)
H(8)	6950(30)	9497(19)	1455(15)	25(9)
H(9)	7690(30)	9597(19)	2654(15)	23(9)
H(10)	9210(30)	8424(18)	2928(15)	19(8)
H(11A)	11640(30)	7170(20)	2380(16)	36(10)
H(11B)	10800(30)	7070(20)	2967(17)	38(10)
H(11C)	11200(30)	6370(30)	2576(19)	58(13)
H(12A)	10410(30)	7002(18)	912(15)	22(9)
H(12B)	10030(30)	6160(20)	1026(15)	25(9)

H(12C)	8990(30)	6790(20)	735(17)	41(10)
H(14A)	5320(30)	9131(19)	4209(15)	23(9)
H(14B)	6010(30)	8290(20)	4098(17)	41(11)
H(14C)	6530(40)	9100(20)	3850(20)	55(15)
H(15A)	3360(30)	8506(19)	3541(15)	24(9)
H(15B)	3370(30)	8182(18)	2808(16)	27(9)
H(15C)	4070(30)	7700(20)	3437(18)	49(11)
H(16A)	4290(30)	9500(20)	2468(17)	37(10)
H(16B)	5470(30)	9856(18)	2845(14)	17(8)
H(16C)	4220(30)	9881(17)	3141(14)	15(8)
H(17A)	4600(20)	7642(16)	1587(13)	6(7)
H(17B)	5150(20)	8462(18)	1338(13)	11(7)
H(17C)	5830(20)	7655(15)	1175(12)	2(6)

Chapter 4

Ancillary Ligand and Olefin Substituent Effects on Olefin Dissociation for Cationic Zirconocene Complexes Bearing a Coordinated Pendant Olefin

Abstract

A series of zirconocene complexes bearing 2,2-dimethyl-2-sila-4-pentenyl substituents (and methyl-substituted olefin variants) $((\eta^5\text{-C}_5\text{H}_5)_2\text{Zr}(\text{CH}_3)(\text{CH}_2\text{SiMe}_2\text{CH}_2\text{CR}^1=\text{CR}^2\text{R}^3)$, ($\text{R}^1, \text{R}^2, \text{R}^3 = \text{H}, \text{CH}_3$, **1**, **5** - **7**), $(\eta^5\text{-C}_5\text{H}_4\text{CMe}_3)_2\text{Zr}(\text{CH}_3)(\text{CH}_2\text{SiMe}_2\text{CH}_2\text{CH}=\text{CH}_2)$ (**2**), $\{\text{Me}_2\text{Si}(\eta^5\text{-C}_5\text{H}_4)_2\}\text{Zr}(\text{CH}_3)(\text{CH}_2\text{SiMe}_2\text{CH}_2\text{CH}=\text{CH}_2)$ (**3**) and 1,2- $(\text{SiMe}_2)_2(\eta^5\text{-C}_5\text{H}_3)_2\text{Zr}(\text{CH}_3)(\text{CH}_2\text{SiMe}_2\text{CH}_2\text{CH}=\text{CH}_2)$ (**4**) has been prepared. Methide abstraction with $\text{B}(\text{C}_6\text{F}_5)$ results in reversible coordination of the tethered olefin to the cationic zirconium center. The kinetics of olefin dissociation has been examined using NMR methods, and the effects of ligand variation for unlinked, singly $[\text{SiMe}_2]$ -linked and doubly $[\text{SiMe}_2]$ -linked bis(cyclopentadienyl) arrangements have been compared (ΔG^\ddagger for olefin dissociation varies from 12.8 to 15.6 kcal.mol⁻¹). The binding of the pendant olefins with different methyl substitution has also been investigated. For the cation derived from **4**, the kinetics for olefin dissociation and site epimerization (inversion at zirconium) can be distinguished. Additionally, with this ligand system competitive binding of the olefin and the $[\text{CH}_3\text{B}(\text{C}_6\text{F}_5)_3]$ anion is observed. Methide abstraction from 1,2- $(\text{SiMe}_2)_2(\eta^5\text{-C}_5\text{H}_3)_2\text{Zr}(\text{CH}_3)(\text{CH}_2\text{CMe}_2\text{CH}_2\text{CH}=\text{CH}_2)$ (**15**) results in rapid β -allyl elimination with loss of isobutene to cleanly afford the allyl cation $[\{1,2\text{-}(\text{SiMe}_2)_2(\eta^5\text{-C}_5\text{H}_3)_2\text{Zr}(\eta^3\text{-CH}_2\text{CH}=\text{CH}_2)\}^+]$ (**17**).

Introduction

Ziegler-Natta polymerization catalysis for the production of polyolefins is practiced on a large scale with both heterogeneous and homogeneous catalysts. Homogeneous metallocene-based catalysts allow a more careful study of the mechanism than was possible with heterogeneous catalysts.¹ One proposed intermediate that has defied careful study is the d^0 olefin complex.² While olefin complexes are well known throughout organometallic chemistry, no evidence of stable d^0 olefin complexes existed until recently. In order to understand this, it would be helpful to discuss olefin binding to transition metals.

The first isolated transition-metal organometallic complex, Zeise's salt $K[PtCl_3(C_2H_4)]$, was prepared in 1827, though its identity was unknown until the 1950's. Classical transition-metal olefin complexes arise from an olefin binding facially to a transition metal that has at least one electron in a d orbital. The most common model used to describe this bonding is the *Dewar-Chatt* model (Figure 1).³ The electron pair in the olefin π -bond forms a dative bond with an empty d orbital having σ symmetry along the M-(C₂H₄) axis. At the same time, the electrons in a d orbital with π symmetry along the M-(C₂H₄) axis form a bonding interaction with the olefin π^* orbital (backbonding). This weakens the C=C bond, thus lengthened C=C bonds are a common feature of these complexes. The C=C bond distances for these complexes vary from 1.35 to 1.45 Å. The longer bond distances correlate with higher degrees of backbonding.⁴ In cases of extreme backbonding the M(C₂H₄) moiety can be considered a metallocyclopropane, as though the C-C π bond is replaced by two σ -bonds to the metal. The contribution of transition-metal electrons to the bonding is considered a very important stabilizing interaction. In fact, it was thought that without metal backbonding an olefin could not bind to the metal.³

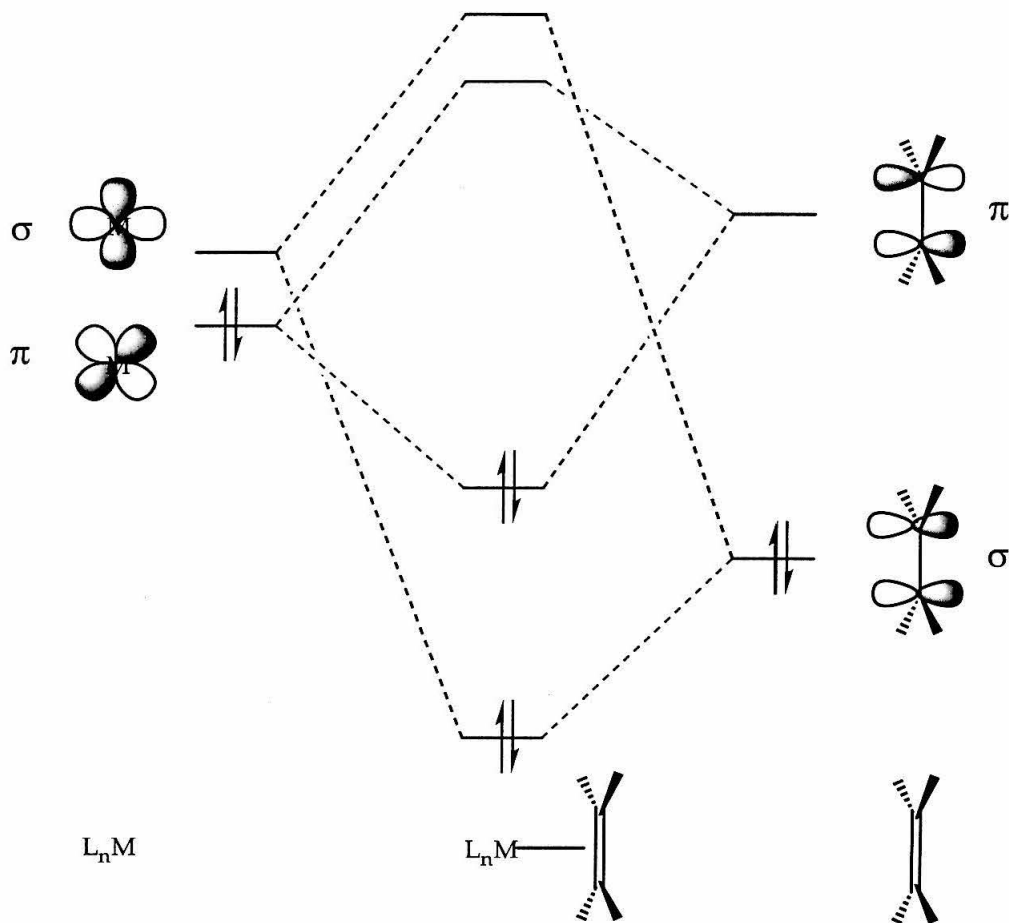


Figure 1. Molecular orbital diagram of transition-metal olefin complex.

While claiming that d^0 metals cannot bind olefins may overstate the weakness of the dative bond that an olefin forms with a metal, there are indeed few examples of this type of binding.⁵ Transition-metal complexes that have no d electrons must bind olefins simply as σ -donor ligands. In analogy to the bonding in protonated olefins,⁶ the metal-olefin bonding can be described in two different ways. The olefin could simply form a 3 center-2 electron bond with the metal, similar to nonclassical carbocations. However, ethylene is a poor σ -donor, because the σ -symmetry metal orbital points directly between the olefin p -orbitals that comprise the π -bond, and neither p orbitals nor d orbitals are as diffuse as an s orbital.⁷ Shifting the olefin along the C=C axis might improve the orbital overlap similar to a classical carbocation (Figure 2). The pure σ -donor bonding picture would not lead to significant distortions of the ethylene, while

the polarized ethylene bonding model would lead to a lengthening of the C=C bond and unsymmetric olefin binding.

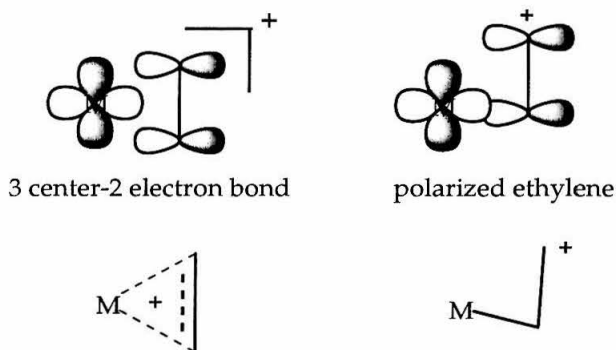


Figure 2. Bonding descriptions of d^0 transition-metal olefin complexes.

Most research in the coordination chemistry of olefins has focused on the complexes of d^n transition metals. However, two d^0 transition-metal olefin complexes are known that bind untethered olefin. The first is a cationic W(VI) alkylidene, **A**, which binds cyclooctene at low temperatures. The olefin can be displaced by anion or it can form a metallocyclobutane with the $W=CR_2$ fragment. This complex, however, may not be a truly d^0 complex because alkylidene complexes can be considered either neutral 2 electron donors or 4 electron dianionic donors. In this complex the ^{13}C chemical shift of the olefin is slightly upfield from free cyclooctene. If the olefin were to coordinate to a purely d^0 metal, then the chemical shift should be downfield of the free olefin chemical shift due to a build up of positive charge resulting from a lower electron density on the olefinic carbons. The other example of a d^0 transition-metal olefin complex, $[\eta^5, \eta^1-(C_5H_4C_2H_4NCHMe_2)Zr(=NCMe_3)(C_2H_4)]^+$, **B**, has a tightly bound ethylene that does not exchange with other olefins below 60 °C.

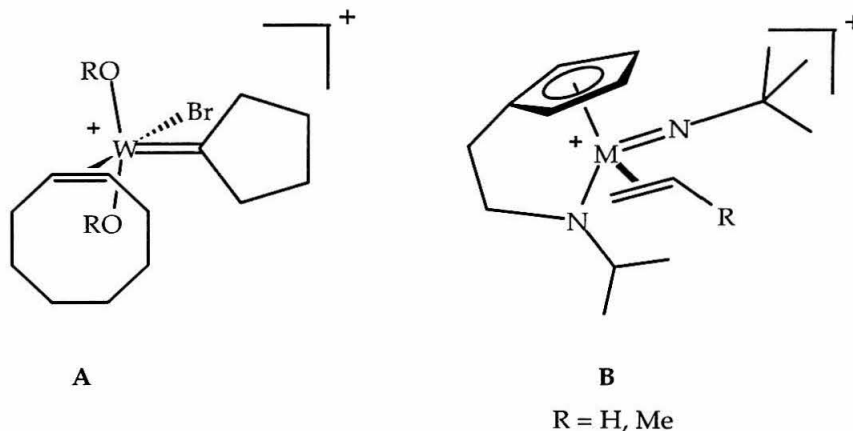


Figure 3. d^0 Complexes that bind free olefin.

In order to study the d^0 olefin complex that has been implicated as an intermediate in Ziegler-Natta polymerization catalysts, it is necessary to prepare a cationic zirconocene alkyl-olefin complex. A common technique for stabilizing olefin complexes is to prepare ligands with pendant olefins, taking advantage of the chelate effect (such tethering lowers entropy loss upon olefin binding).⁸ The first example of such a compound, prepared by Jordan and co-workers, was a cationic zirconocene alkoxide complex, C, with a pendant olefin that intramolecularly displaces the anion.⁹ In this work they studied the kinetics of olefin dissociation from the zirconocene and measured a free energy of activation of $10.7 \text{ kcal}\cdot\text{mol}^{-1}$. In subsequent publications,¹⁰ the authors synthesized a variety of cyclopentadienyl derivatives of zirconium and titanium.

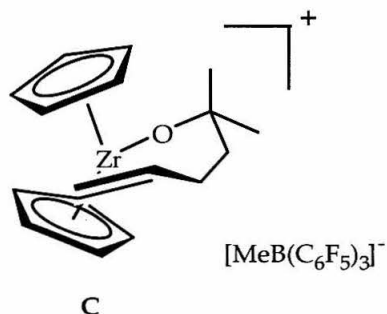


Figure 4. Cationic zirconocene alkoxy-olefin complex.

Some of these complexes were structurally characterized by X-ray crystallography and, as expected for an olefin complex with no metal

backbonding, the olefin moiety was nearly planar. Unfortunately, the C=C bond distance could not be resolved. Though later, a crystal structure of an analogous olefin complex confirmed that the C=C bond distance was virtually unchanged from that of a free olefin.^{10a} These alkoxy olefin complexes are the only structurally characterized d^0 olefin complexes to date.

The next advance in the study of tethered alkyl-olefin complexes was the preparation by Casey and co-workers of a d^0 alkyl yttrocene with a bound pendant olefin, **D**, which could be observed by NMR spectroscopy.¹¹ Olefin insertion, which is typically too fast to observe by common spectroscopic techniques, is slowed in these complexes by the instability of the methylenecyclobutane product (Figure 5). The free energy of olefin dissociation was low ($\Delta G^\ddagger < 8 \text{ kcal}\cdot\text{mol}^{-1}$), and a small barrier ($\Delta G^\ddagger = \text{ca. } 3 \text{ kcal}\cdot\text{mol}^{-1}$) was measured for the alkyl substituent to move from one side of the metallocene wedge to the other (site epimerization).

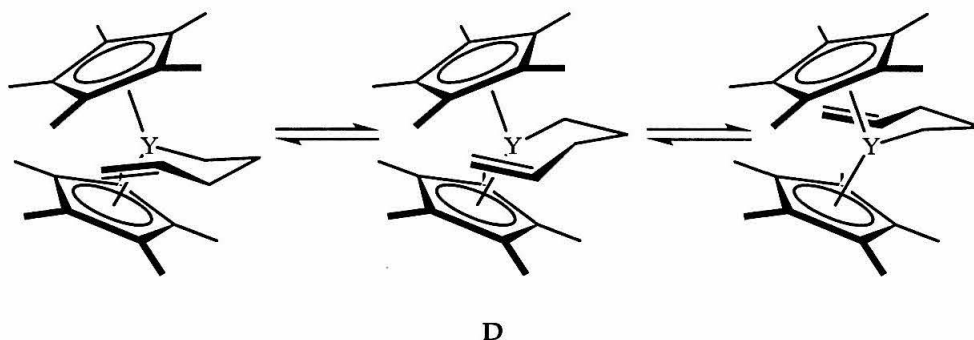


Figure 5. d^0 Yttrocene alkyl-olefin complex.

The first report of a cationic metallocene alkyl olefin complex was by Royo and co-workers.¹² Their strategy was to tether a pendant olefin to a cyclopentadienyl ring and to activate the zirconium center, allowing the olefin to bind. The barrier for olefin dissociation that they measured was higher than any reported previously ($\Delta G^\ddagger = 11.7 \text{ kcal}\cdot\text{mol}^{-1}$). Subsequently, Casey and co-workers prepared a zwitterionic zirconocene olefin complex, **F**, and a cationic zirconocene olefin complex, **G**.¹³ The olefin dissociation energy for the olefin in **F** ($\Delta G^\ddagger = 11.7 \text{ kcal}\cdot\text{mol}^{-1}$) was similar to the one in **E**, but for the cationic complex **G** the dissociation energy was much higher ($\Delta G^\ddagger = 14.1 \text{ kcal}\cdot\text{mol}^{-1}$). Olefin insertion into the Zr-C bond was not observed in any of these zirconocene complexes.

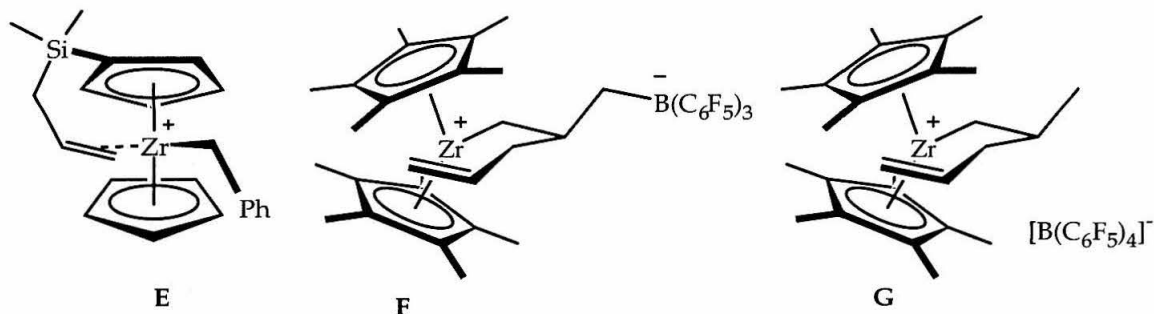


Figure 6. Cationic zirconocene alkyl-olefin complexes.

These studies have shed light on the nature of d^0 olefin complexes. In all of these compounds, ^1H and ^{13}C NMR data indicates increasing positive charge on the internal olefinic carbon. This is consistent with the polarized model of d^0 olefin binding, but the structural data of C does not indicate a lengthening of the C=C bond that is expected for this type of bonding. NMR data suggests a stronger polarization in complexes E, F, and G, for which there is no structural data available.

These studies have also shed light on d^0 olefin intermediates in Ziegler-Natta polymerization. Olefin binding to cationic Group IV alkyl metallocenes is stronger than it is to neutral Group III alkyl metallocenes. Olefin insertion into a M-C bond occurs from the bound olefin intermediate. But other questions about these intermediates remain unanswered. The mechanism of olefin dissociation might be either associative or dissociative. The effect of cyclopentadienyl ligand variations on olefin binding is unclear. Lastly, the effect pendant-olefin substituent variations on olefin binding is unknown. We have prepared a series of 2-sila-4-pentenyl zirconocene cations and have studied the dynamic behavior of these olefin complexes in an effort to address these questions. This series, shown in Figure 7, spans a limited range of unlinked, singly linked and doubly linked *bis*(cyclopentadienyl) ligands as well as methyl substitution of the coordinated olefin.

Results and Discussion

Synthesis of Pentenyl- and Hexenyl-Iodides and Methyl(4-pentenyl)zirconocenes.

The syntheses of both 4,4-dimethyl-5-iodo-4-sila-1-pentene and 2,4,4-trimethyl-5-iodo-4-sila-1-pentene were accomplished according to literature

precedent by the reaction of the respective Grignard reagent with $\text{ClCH}_2\text{Si}(\text{CH}_3)\text{Cl}$ in ethereal solvent, followed by reaction with NaI .¹⁴ On the other hand, the preparations of the *cis*- and *trans*-5,5-dimethyl-6-iodo-5-sila-2-hexenes were not as straightforward. In both cases the respective 2-butenyltrichlorosilane was prepared according to literature methods.¹⁵

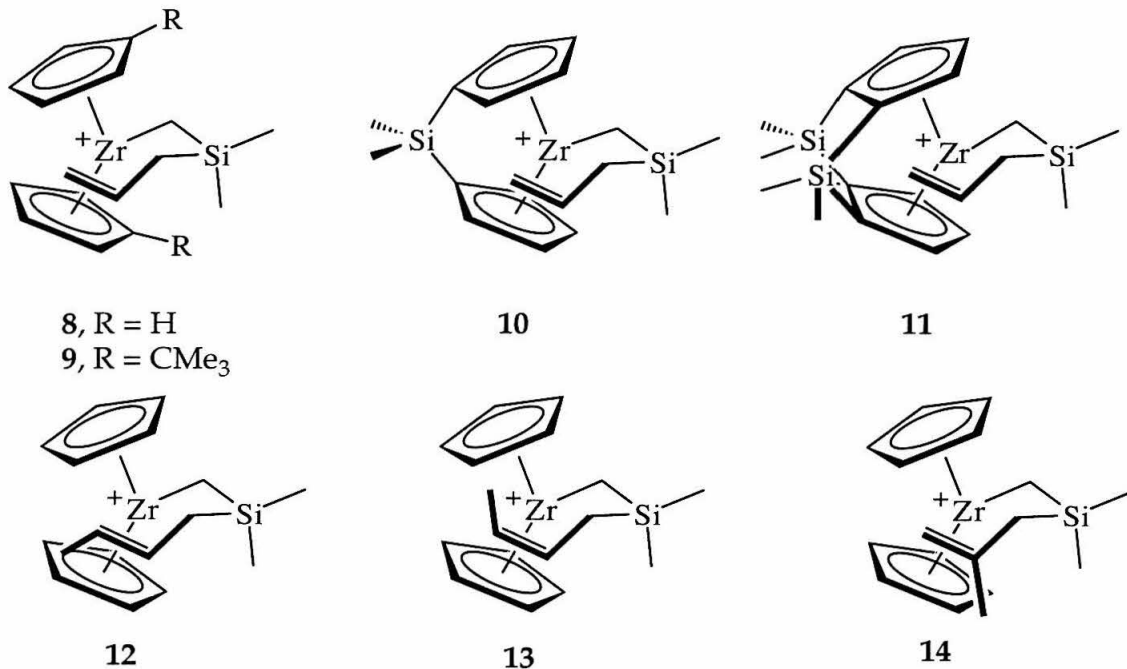


Figure 7. Cationic zirconocene olefin complexes studied in this chapter.

These were treated with 2 equivalents of methylmagnesiumchloride to yield the respective 2-butenyldimethylchlorosilane, followed by addition of BrCH_2Li . BrCH_2Li was prepared *in situ* from the reaction of CH_2Br_2 with *n*-BuLi in the presence of the silylchloride at -78°C . Much lower yields were obtained if the silyl chloride was added after the preparation of BrCH_2Li . We note in passing that this appears to be a novel use of this reagent, which previously has been studied extensively as a $[\text{CH}_2]$ homologation reagent with alkyl-catechol boranes,¹⁶ and offers a useful alternative to current methods for preparing halomethyl(trialkyl)silanes.¹⁷ After purification by column separation on silica gel, the hexenyl bromide was treated with NaI to give the hexenyl iodide.

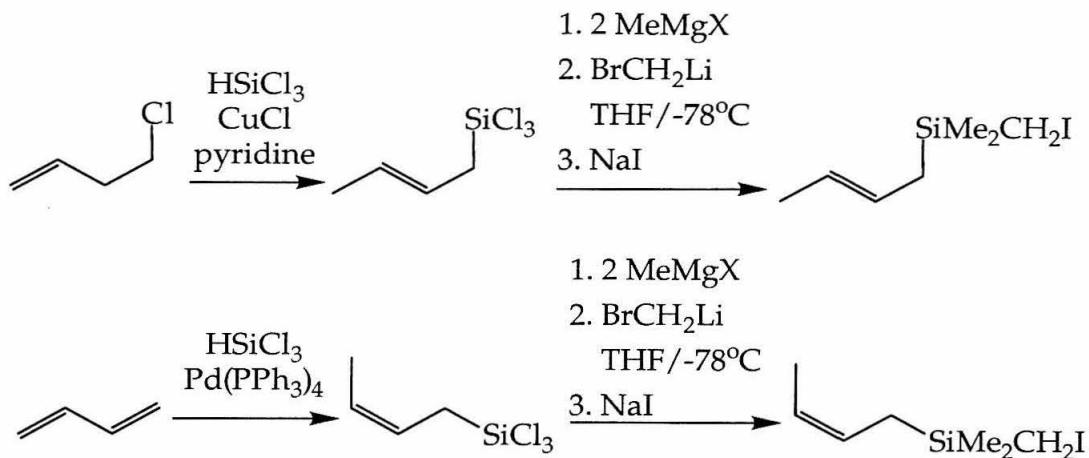


Figure 8. Synthesis of *cis* and *trans* 2-butenyl halomethyl(dialkyl)silanes.

The methyl(4-pentenyl)zirconocenes were generally obtained as oils via treatment of the appropriate 4-pentenyl-lithium reagent, generated *in situ* by lithium-halogen exchange, with a methyl-chlorozirconocene (Figure 9):

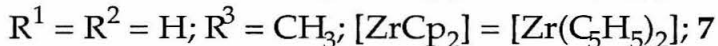
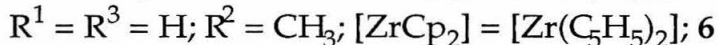
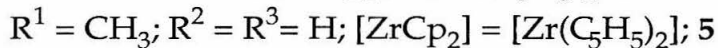
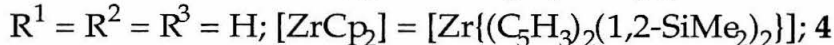
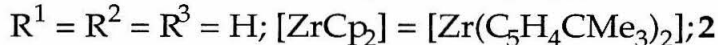
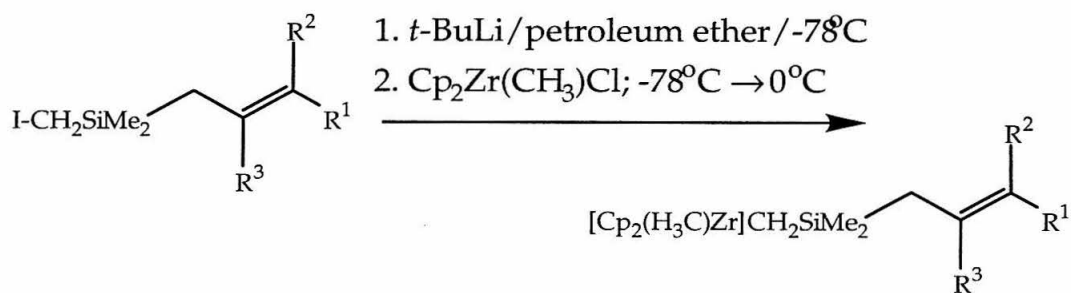


Figure 9. Preparation of methyl(4-pentenyl)zirconocene.

The complex $\text{Me}_2\text{Si}(\eta^5\text{-C}_5\text{H}_4)_2\text{Zr}(\text{CH}_3)(\text{CH}_2\text{SiMe}_2\text{CH}_2\text{CH}=\text{CH}_2)$, **3**, was prepared by an alternate route because the starting material,

$\text{Me}_2\text{Si}(\eta^5\text{-C}_5\text{H}_4)_2\text{Zr}(\text{CH}_3)\text{Cl}$, could not be prepared with satisfactory purity. Treatment of $\text{Me}_2\text{Si}(\eta^5\text{-C}_5\text{H}_4)_2\text{ZrCl}_2$ with 4-pentenyl-magnesiumchloride in CH_2Cl_2 yielded $\text{Me}_2\text{Si}(\eta^5\text{-C}_5\text{H}_4)_2\text{Zr}(\text{Cl})(\text{CH}_2\text{SiMe}_2\text{CH}_2\text{CH}=\text{CH}_2)$ upon recrystallization (Figure 10). Addition of MeLi and filtration yielded **3** as a yellow oil.

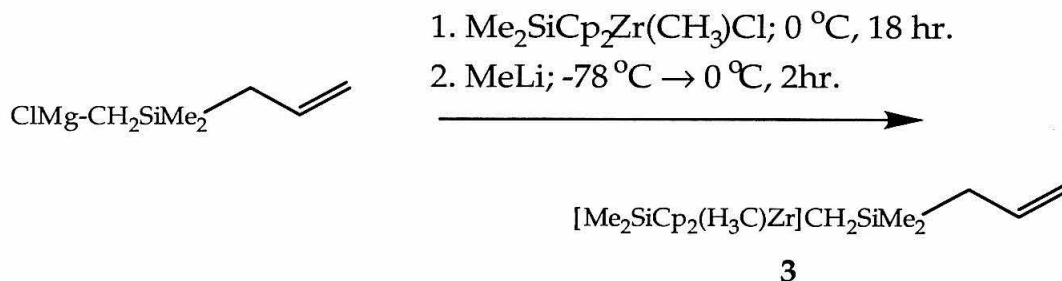


Figure 10. Preparation of $\text{Me}_2\text{Si}(\eta^5\text{-C}_5\text{H}_4)_2\text{Zr}(\text{CH}_3)(\text{CH}_2\text{SiMe}_2\text{CH}_2\text{CH}=\text{CH}_2)$

Preparation and Kinetic Studies of Cationic Pendant Olefin Complexes.

Abstraction of the methyl group from **1** with $\text{B}(\text{C}_6\text{F}_5)_3$ at $-78\text{ }^\circ\text{C}$ results in the immediate formation of **8** (Figure 11).

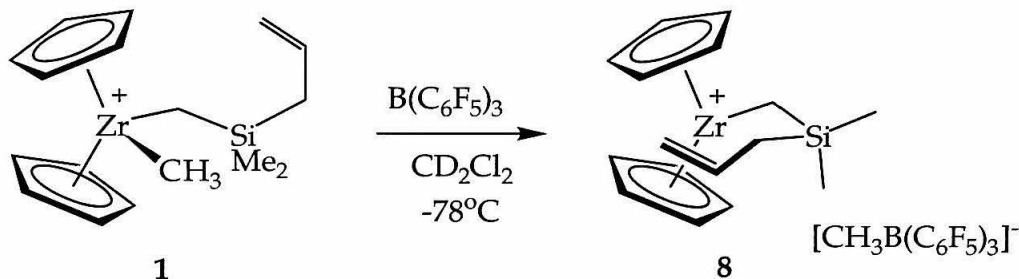


Figure 11. Activation of methyl(4-pentenyl)zirconocene complexes.

Several features in the static ^1H NMR spectrum, shown below in Figure 12, (CD_2Cl_2 , $-78\text{ }^\circ\text{C}$) of **8** are notable: (1) the two protons on the α -carbon display a chemical shift difference of 2.3 ppm, (2) the protons on the terminal vinyl carbon are separated 3.6 ppm, (3) the proton on the internal olefin carbon is at 8.6 ppm, 2 ppm downfield from its position for **1**. The first two features suggest differing proton positions relative to the magnetic fields resulting from cyclopentadienyl ring currents. The large downfield shift for proton of the internal vinylic carbon has been suggested to result from resonance structures with a positive charge on

this carbon^{9,13a}, a suggestion that is certainly supported by the very downfield chemical shift for this proton of **8**.

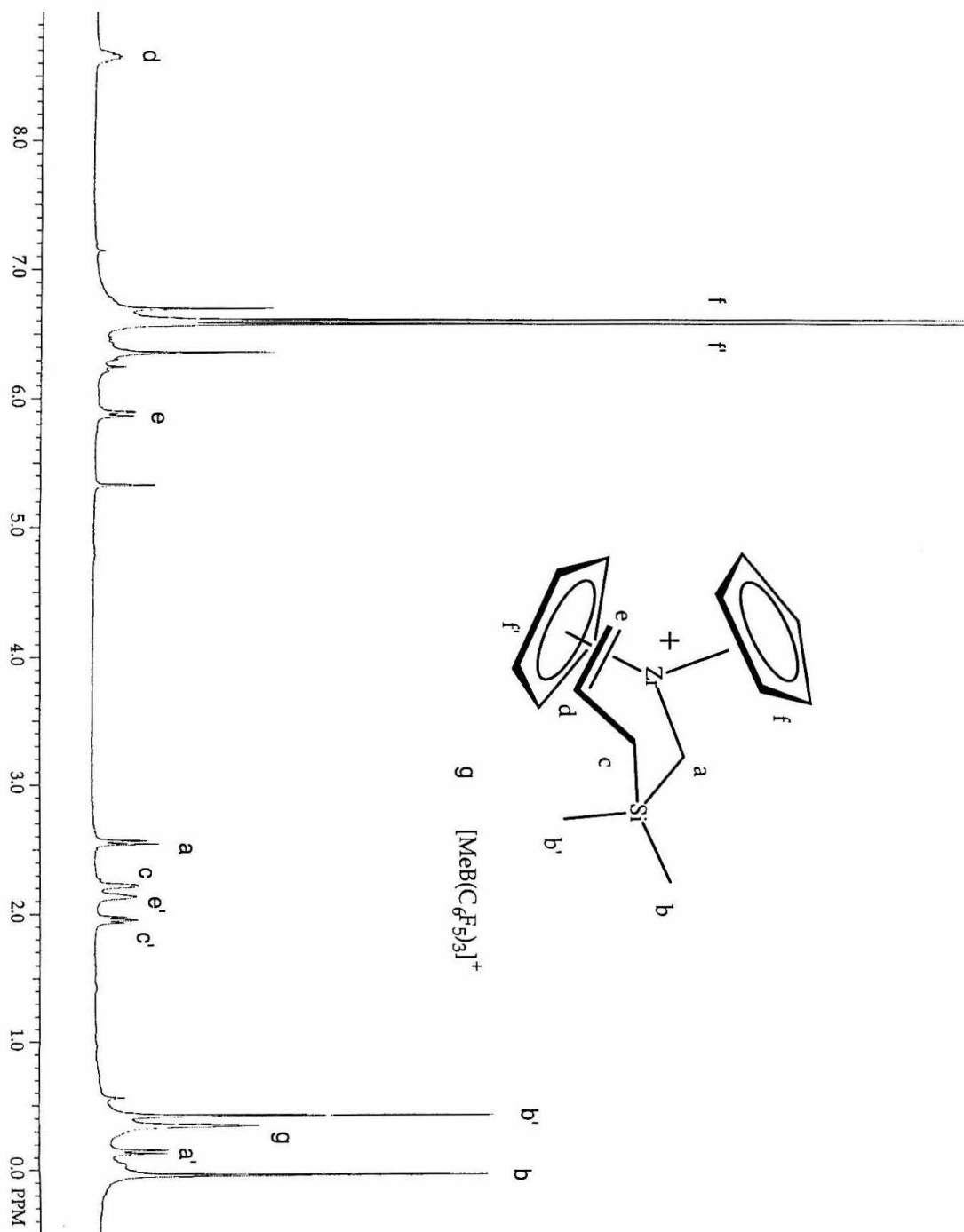


Figure 12. Static ^1H NMR spectra of **8**.

Additionally, the ^{13}C chemical shift of the internal olefin is shifted downfield to 175 ppm from 137 ppm, where it is found for the neutral metallocene. The ^{13}C chemical shift of the terminal olefin carbon does not shift significantly upon activation however. The presence of a β -silicon would further stabilize such a resonance structure.

When solutions of **8** are warmed, a dynamic process ensues, which we attribute to olefin dissociation followed by fast recoordination. The $\Delta G^\ddagger(248\text{ K}) = 13.1\text{ kcal}\cdot\text{mol}^{-1}$. We have modeled the coalescence using GNMR line shape analysis¹⁸ and determined that the activation parameters for this process are $\Delta H^\ddagger = 13.4\text{ kcal}\cdot\text{mol}^{-1}$, $\Delta S^\ddagger = 0.7\text{ e.u.}$ The activation parameters for most cases are obtained over only 20-25°C ranges, and while our Eyring plots have an excellent fit to the data, we do not have enough confidence in activation parameters derived from this limited temperature range to draw conclusions from them. Hence, we confident only to compare free energies of activation.

We attempted to investigate the possibility of a counter-anion effect on the olefin dissociation by utilizing $[\text{Ph}_3\text{C}][\text{B}(\text{C}_6\text{F}_5)_4]$ as a methide abstracting reagent. Unfortunately, significant amounts (>80%) of what appears to be the methyl bridged dimeric cation, $\{[(\eta^5\text{-C}_5\text{H}_5)_2\text{Zr}(\text{CH}_2\text{SiMe}_2\text{CH}_2\text{CH}=\text{CH}_2)]_2(\mu_2\text{-CH}_3)\}^+$, are formed when stoichiometric amounts of $[\text{Ph}_3\text{C}][\text{B}(\text{C}_6\text{F}_5)_4]$ are used. Instead we compared the rates upon addition of a 3-molar equivalents of either $[n\text{-Bu}_4\text{N}]^+[\text{CH}_3\text{B}(\text{C}_6\text{F}_5)_3]^-$ or $[n\text{-Bu}_4\text{N}]^+[\text{B}(\text{C}_6\text{F}_5)_4]^-$ to CD_2Cl_2 solutions of **8** in order to hold the ionic strength constant. We found that the resulting variable temperature ^1H NMR spectra were indistinguishable from each other, though both were apparently accelerated from the NMR spectra without added anion. We conclude therefore, that excess $[\text{CH}_3\text{B}(\text{C}_6\text{F}_5)_3]^-$ does not significantly change the rate of olefin dissociation compared with the even less coordinating anion $[\text{B}(\text{C}_6\text{F}_5)_4]^-$. This leaves open the possibility of anion assistance occurring by similar coordination modes for both anions, through fluorine coordination for example. Solvent assistance has also been considered. The instability of **8** and its exceedingly high Lewis acidity restrict the choice of solvent. Whereas the rates of olefin dissociation in CD_2Cl_2 and $\text{C}_6\text{D}_5\text{Cl}$ are the same within experimental error, the close similarity of these two solvents leaves open the issue of solvent assistance in olefin dissociation.

In order to determine if olefin insertion was occurring reversibly, we isotopically labeled complex **1** with deuterium at the γ -carbon. Since the synthesis utilizes a 1:1 mixture of $\text{CD}_2\text{CHCH}_2\text{MgBr}$ and $\text{CH}_2\text{CHCD}_2\text{MgBr}$, the incorporation of deuterium was 50% at the γ -carbon and 50% at the terminal olefin carbon.

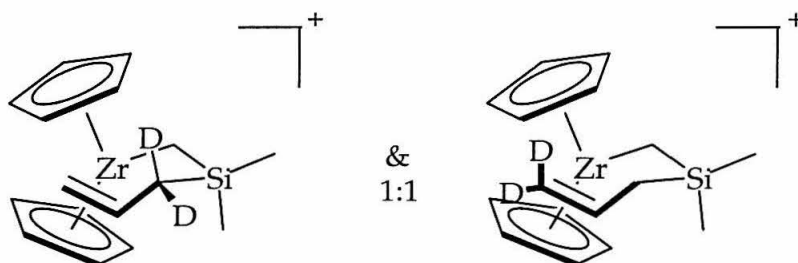


Figure 13. **8-d₂** is a 1:1 mixture of 3,3-d₂-2-sila-4-pentene and 5,5-d₂-2-sila-4-pentene.

Upon activation with $\text{B}(\text{C}_6\text{F}_5)_3$, there was no observed change in the peak intensities of the protons at the α -carbon or at the γ -carbon, which would be expected for reversible insertion and ring opening of the resulting cyclobutylmethylzirconocenium cation (Figure 14), indicating that no insertion is occurring. This was examined up to $-30\text{ }^\circ\text{C}$, above this temperature complex **8-d₂** begins to decompose irreversibly.

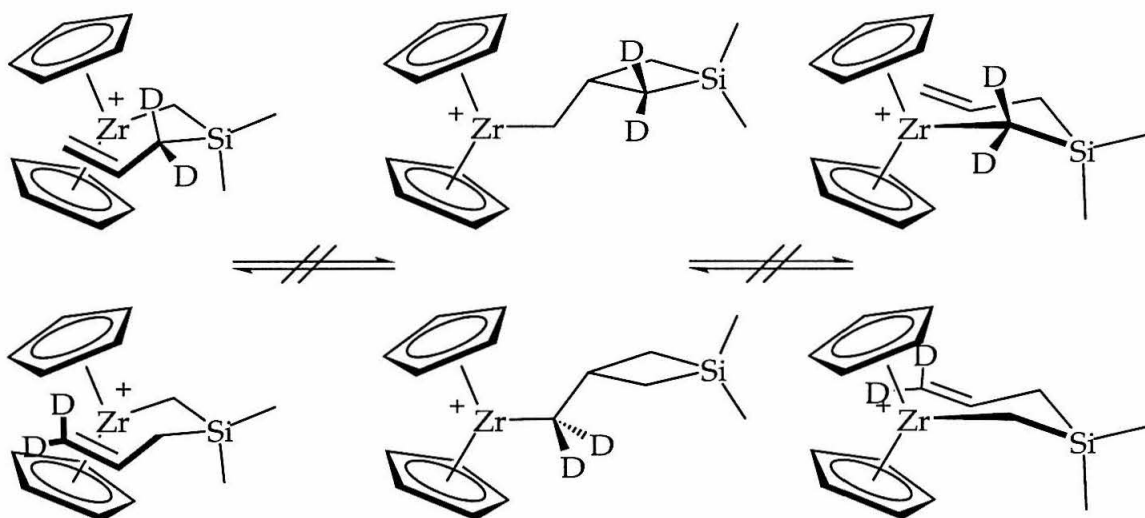


Figure 14. No alkyl-olefin insertion is observed in the ^1H NMR of **8-d₂**.

We were initially surprised by the lack of observed insertion, and thus undertook a DFT calculation. A comparison of the sila-substituted cyclization to the all carbon analog indicated that 1,1,3-trimethyl-1-sila-cyclobutane is 3 kcal.mol⁻¹ higher in energy than 4,4-dimethyl-4-sila-1-pentene, as compared to only 0.2 kcal.mol⁻¹ for the 4,4-dimethyl-1-pentene to 1,1,3-trimethylcyclobutane conversion.¹⁹ The calculated difference of only 2.7 kcal.mol⁻¹ would not seem to account for the very slow insertion **8-d**₂, considering the relatively facile insertion ($\Delta G^\ddagger(248\text{ K}) = 8.2\text{ kcal.mol}^{-1}$) reported by Casey and co-workers for ($\eta^5\text{-C}_5\text{Me}_5$)₂YCD₂CMe₂CH₂CH=CH₂.^{11b}

Olefin Substituent Effects.

In order to address the effects of methyl substitution on olefin binding to *d*⁰ metals, we sought to prepare olefins with a single methyl group at each vinylic position. The *cis*-hexenyl complex **6** was activated with B(C₆F₅)₃ in CD₂Cl₂ at -78 °C. However, the major species in solution is the anion bound complex, but a small fraction was identified as the complex **13** with a coordinated olefin. This assignment is consistent with the proton spectra, although not all of the peaks could be assigned, the fluorine NMR which shows C₆F₅ resonances corresponding to both coordinated and free MeB(C₆F₅)₃. The activation free energy for olefin exchange measured by NMR simulation was 11.4 kcal.mol⁻¹ at 223 K, which is much lower than that of the parent complex **8**. The *trans*-hexenyl complex **5** was similarly activated and did, in fact, yield complex **12** with a coordinated olefin and solvent-separated [H₃CB(C₆F₅)₃] anion. NMR simulation of the peak coalescence revealed that the free energy of activation was 13.3 kcal.mol⁻¹ for olefin dissociation, curiously essentially unchanged from the parent pentenyl complex **8**.²⁰ Examining simple models of the *cis*- and *trans*-hexenyl systems leads one to predict greater steric repulsion with olefin coordination for **13** *vs.* **12**. Perhaps most interesting is the relatively strong olefin binding for **14** that follows activation of complex **7**. The activation free energy for olefin dissociation is measured to be 14.4 kcal.mol⁻¹ at 248 K, 1.3 kcal.mol⁻¹ greater than for un-methyl-substituted **8**.²¹ Based on sterics alone, we would expect the olefin dissociation barrier to be less than for the parent complex **8**. Clearly this result is consistent with the notion that positive charge builds up at the internal olefin carbon: the electron-donating methyl stabilizes the positive charge in resonance structure **14b** (Figure 15).

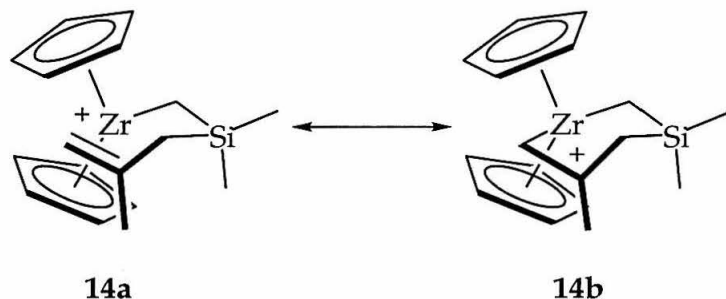


Figure 15. Methyl substituent stabilizes positive charge on olefinic carbon.

Ancillary Ligand Effects for Complexes Unlinked and Singly-Linked Zirconocenium Olefin Cations.

Cations **9** and **10** were activated in a similar fashion to **8**, and the dynamic behavior was examined by variable temperature NMR spectroscopy. The free energies of activation for these complexes were also very similar to that of **8**: ΔG^\ddagger (248 K) = 13.2 kcal·mol⁻¹ for **9**; ΔG^\ddagger (248 K) = 12.8 kcal·mol⁻¹ for **10**. Despite the presence an *ansa* [SiMe₂]-linker or a sterically rather demanding *t*-butyl cyclopentadienyl substituent, the olefin dissociation rates among the three metallocenium cations are essentially the same. Significantly, for both complexes **9** and **10**, line shape analysis reveals that site epimerization (inversion at Zr, Figure 16) occurs simultaneously with olefin dissociation.²²

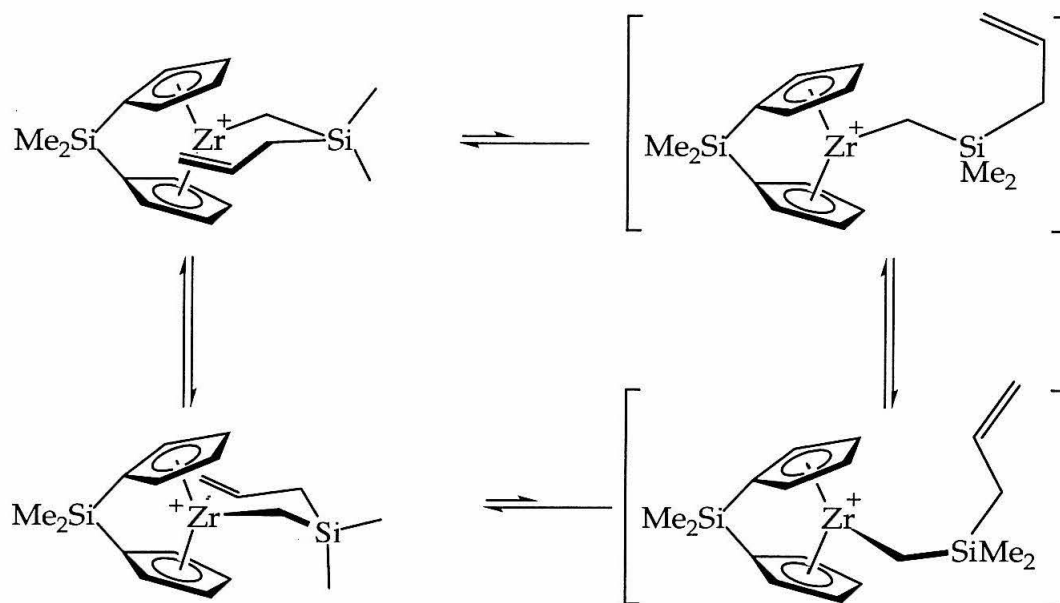


Figure 16. Site epimerization occurs simultaneously with olefin dissociation.

Doubly Bridged Ansa-Metallocenium Cation Olefin Complex.

Despite the similarity of olefin dissociation barriers for complexes **8**, **9**, and **10**, the dynamic behavior of the doubly [SiMe₂]-bridged complex **11** is distinct. For complex **11**, peak coalescence due to olefin dissociation in CD₂Cl₂ is not apparent until 0 °C as opposed to -55 °C for **8**. The free energy of activation for **11** (in C₆D₅Br, ΔG^\ddagger (283 K) = 15.6 kcal·mol⁻¹) is more than 2 kcal·mol⁻¹ greater than for **8**. In contrast to complexes **8**, **9**, and **10**, complex **11** could be activated cleanly by either B(C₆F₅)₃ or [Ph₃C][B(C₆F₅)₄] at -40 °C. Since the barriers for olefin dissociation are not measurably different with [CH₃B(C₆F₅)₃]⁻ or [B(C₆F₅)₄]⁻ as counter ion, it appears that anion does not assist in olefin dissociation. Additionally, at this temperature and even up to 75 °C, olefin dissociation and recoordination is *not accompanied by site epimerization* (Figure 16). It has been observed for this type of doubly bridged zirconocene complexes that the mechanism for ligand exchange is dissociative, whereas unbridged zirconocenes exchange ligands via an associative mechanism.²³ In light of these differences, it may be argued that olefin dissociation for complexes **8**, **9**, and **10** involves an associative pathway, whereas olefin facial exchange for complex **11** is

dissociative. Exactly how these differences influence the relative barriers for site epimerization are not clear.^{11b}

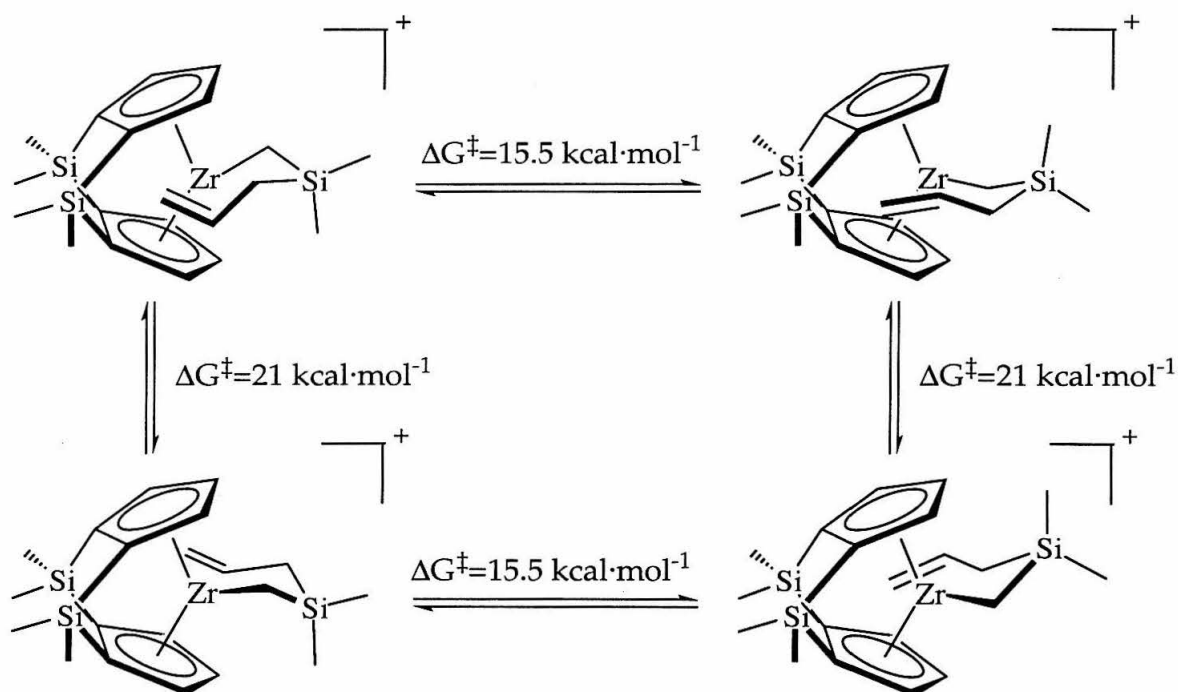


Figure 17. Olefin dissociation is faster than site epimerization for **11**.

Site epimerization for complex **11** cannot be observed until 85°C (ΔG^\ddagger (358 K) = 21.2 kcal·mol⁻¹) and then only when **4** is activated with the [Ph₃C][B(C₆F₅)₄] in C₆D₅Cl; all other combinations of solvent and activator result in decomposition at lower temperatures. The inversion at zirconium for **11** is not complicated by the presence of donor molecules, coordinating anions, or (potentially agostic) β -hydrogens,²⁴ and allows us to place a lower limit on the barrier for site epimerization of *ca.* 5.3 kcal·mol⁻¹ at 85 °C. The height of this barrier provides some of the strongest evidence to date of an inherent hindrance to site epimerization for cationic zirconocenium alkyls, as predicted by theoretical calculations.²⁵

For this ligand system we can observe competitive binding of the [CH₃B(C₆F₅)₃]⁻ to the metal center in C₆D₅Cl (Figure 18).

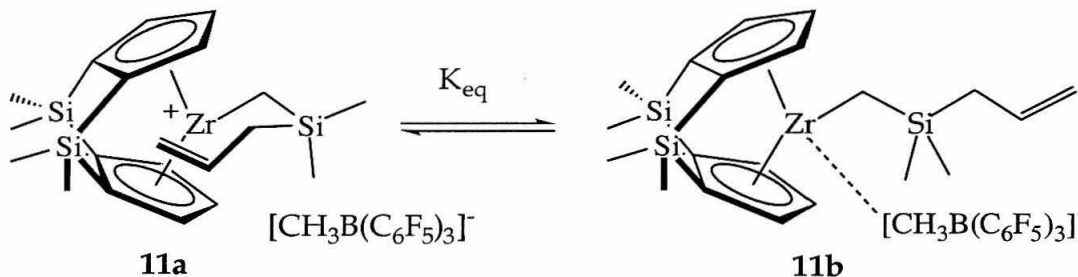


Figure 18. Equilibrium between olefin binding and anion binding.

The equilibrium was examined between 0 and 65 °C, revealing the following thermodynamic parameters in $\text{C}_6\text{D}_5\text{Cl}$: $\Delta H^0 = 7.2 \text{ kcal}\cdot\text{mol}^{-1}$ and $\Delta S^0 = 22 \text{ e.u.}$ Since the equilibrium favors the formation of the coordinated olefin complex at higher temperatures despite two species forming one, the separated ions must organize the solvent significantly. The same species appears in $\text{C}_6\text{D}_5\text{Br}$ and CD_2Cl_2 , but the equilibrium cannot be measured accurately because it does not appear until higher temperatures, just before decomposition sets in.²⁶

Attempts to Prepare a Doubly Bridged Ansa-Metallocenium Cation/Pendant All-Carbon Olefin Complex: β -Allyl Elimination.

We have also synthesized the neutral zirconocene methyl/2,2-dimethyl-4-pentenyl complexes **16** (Figure 19). In view of the reluctance of the pendant sila-substituted pentenes to undergo reversible olefin insertion, we prepared this complex as a precursor to a cation that could serve as a model for olefin insertion into a Zr-C bond. To our surprise, upon the addition of either $\text{B}(\text{C}_6\text{F}_5)_3$ or $[\text{Ph}_3\text{C}][\text{B}(\text{C}_6\text{F}_5)_4]$ at -40 °C in $\text{C}_6\text{D}_5\text{Cl}$ or $\text{C}_6\text{D}_5\text{Br}$ only allyl cation **16**, resulting from rapid and clean β -allyl elimination and loss of isobutene, was observed (Figure 19).²⁷ There was no evidence of β -methyl elimination occurring. So far as we are aware, this process represents the first example of β -allyl elimination.

The resulting cationic η^3 -allyl complex is fluxional, and its dynamics has been examined by magnetization transfer ($\Delta G^\ddagger = 12.4 \text{ kcal}\cdot\text{mol}^{-1}$). The fluxional process can be described as an $\eta^3 \rightleftharpoons \eta^1$ isomerization, consistent with the interconversion of the *syn* and *anti* methylene protons.

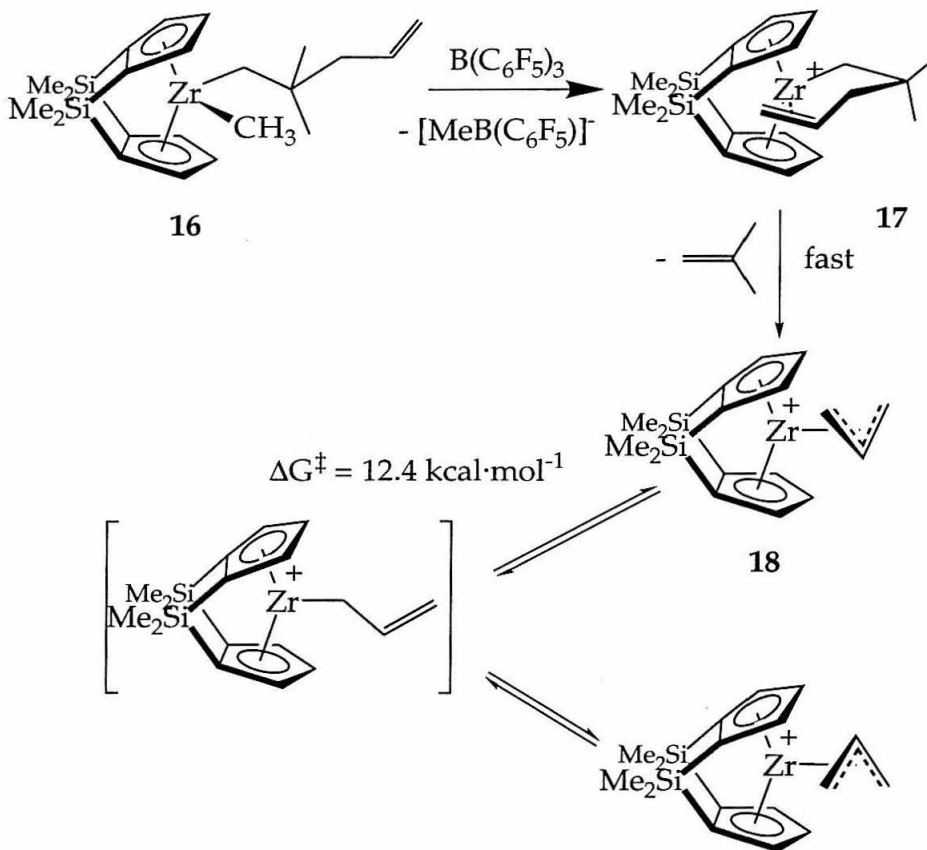


Figure 19. Preparation of allyl complex and resulting fluxional behavior.

If complex **16** is activated with $[\text{Ph}_3\text{C}][\text{B}(\text{C}_6\text{F}_5)_4]$ at $-78\text{ }^\circ\text{C}$, the presence of complex **17** was detected, though not all of the ^1H NMR spectrum could be assigned. Upon warming above $-40\text{ }^\circ\text{C}$, the peaks corresponding to **17** disappeared as the allyl complex **17** was formed. Interestingly, when **16-1,1-d₂** is activated under these conditions, in the ^1H NMR two doublets corresponding to protons on the α -carbon are present in equal intensity to the peaks which are assigned for the γ -carbon. This result implies that upon activation, insertion followed by ring opening occurs very quickly. More careful analysis was prevented due to poorly characterized complexes. Analogous olefin complexes are not observed when this reaction is carried out with other ligand combinations or if $\text{B}(\text{C}_6\text{F}_5)_3$ is used.

Conclusions

We have prepared a series of zirconocene alkyl cations with pendant olefins. In all cases the olefin binds to the metal and we can observe dynamic behavior by NMR spectroscopy that is consistent with olefin dissociation and fast recoordination. The binding of olefins with methyl substitution on the terminal vinyl carbon appears to be influenced primarily by steric considerations, whereas methyl substitution of the internal vinyl carbon appears to stabilize a positive charge buildup, stabilizing the olefin complex.

Ligand substitution has no discernible effect on olefin dissociation except for doubly bridged ligands. In these double [SiMe₂]-linked complexes, olefin dissociation is much faster than site epimerization of the alkyl group. However, site epimerization occurs at the same rate as olefin dissociation for complexes with all other ligands studied. This behavior is not consistent with any electronic properties of such ligands; however, it is consistent with known steric properties of these ligands. This change strongly implies that olefin dissociation in doubly linked metallocenes occurs by a dissociative mechanism while olefin dissociation from the unlinked and singly linked *ansa*-zirconocenes is assisted by either solvent or anion. While unlinked and singly [SiMe₂]-linked zirconocenes exhibit equal rates of olefin dissociation in the presence of either [MeB(C₆F₅)₃]⁻ or [B(C₆F₅)₄]⁻ counterions, it is conceivable that these anions are associating in a similar fashion, leading to a negligible difference in rate.

Cationic complexes with an all-carbon pendant olefin could not be isolated. Upon activation of neutral complexes with an all-carbon pendant olefin, isobutene was eliminated and the zirconocene allyl complex was observed in solution. This exhibits dynamic behavior, which we ascribe to $\eta^3 \rightleftharpoons \eta^1$ interconversion. This β -allyl elimination is novel and entirely selective despite the presence of 2 methyl groups.

Concerning the nature of the d^0 olefin complex, the results of this study are consistent with a buildup of positive charge on the internal olefin carbon only. This is based on the chemical shifts in the ¹H and ¹³C NMR spectra as well as the strengthened olefin binding upon methyl substitution of the internal vinyl carbon. Therefore, these studies favor a polarized olefin bonding model.

Experimental:

General Considerations. All reactions were carried out using standard Schlenk techniques or in an inert atmosphere glovebox. ^1H , ^{13}C , ^{19}F NMR spectra were obtained using a Varian Inova500 spectrometer. All NMR solvents were distilled from CaH_2 . $\text{Cp}_2\text{ZrMe}(\text{Cl})$ ²⁸, $\text{Me}_2\text{SiCp}_2\text{ZrMe}(\text{Cl})$ ²⁹, $\text{B}(\text{C}_6\text{F}_5)_3$ ³⁰, $[\text{Ph}_3\text{C}][\text{B}(\text{C}_6\text{F}_5)_4]$ ³¹, RpZrMeCl ³², *trans*- $\text{Cl}_3\text{SiCH}_2\text{CHCHCH}_3$ ³, *cis*- $\text{Cl}_3\text{SiCH}_2\text{CHCHCH}_3$ ³, and $\text{CH}_2\text{CHCD}_2\text{MgBr}$ ³³, 4,4-dimethyl-5-Iodo-1-pentene³⁴ were all prepared according to literature procedures. All solvents were dried on columns of anhydrous alumina and molecular sieves (4 Å). Reagents were purchased from Aldrich Chemical and were used as received.

Magnetization Transfer Experiments. Magnetization transfer experiments were carried out on a Varian Unity+ 500 MHz spectrometer. Reaction temperatures were determined by measuring the peak separation of an ethylene glycol or methanol standard before and after the experiments. Relaxation times (T_1) for the resonances of interest were measured at each temperature before the magnetization transfer experiment using the inversion recovery method. Magnetization transfer spectra were obtained by using a DANTE pulse sequence.³⁵ The data were fitted using the program CIFIT.³⁶

Simplified One Pot Preparation of $(\text{C}_5\text{H}_4)_2(\text{Si}(\text{CH}_3)_2)_2$. A 1 L Schlenk flask was purged with Ar and 400 mL THF was added via cannula transfer. Cyclopentadiene (20 g, 303 mmol) was added. This was cooled to 0 °C and butyl lithium (189 mL, 303 mmol) was added by syringe eventually forming white precipitate. This mixture was allowed to stir for 1 hour at room temperature. SiCl_2Me_2 (18.38 mL, 151 mmol) was added dropwise by syringe to the solution at 0 °C over 10 minutes. This was allowed to warm to room temperature and stir for 1 hour. The butyl lithium and SiCl_2Me_2 additions were repeated one time. After the SiCl_2Me_2 addition, the solution was allowed to warm to room temperature and stir overnight. The solvent was then removed *in vacuo* and 400 mL of petroleum ether was added and the resulting slurry was stirred and filtered at room temperature, this was quickly attached to an inert atmosphere filter frit and filtered. The remaining solid was rinsed with an additional 150 mL of petroleum ether. The solution was concentrated to ~100 mL and cooled to 0 °C for 1 hour. The solid precipitate was filtered and rinsed twice with cold petroleum ether. 15.3 g of colorless powder was obtained for an overall yield of

42%. The filtrate was collected and placed in a freezer at -30 °C and more pure product was later recovered. ¹H NMR (C₆D₆, 300 MHz) isomer 1: δ -0.44 (s, 6H, Si(CH₃), 0.37 (s, 6H, Si(CH₃), 3.44 (s, 2H, SiCH), 6.64 (m, 6H, CpH), 6.94 (m, 2H, CpH). isomer 2: δ -1.23 (s, 3H, Si(CH₃), 0.21 (s, 3H, Si(CH₃), 0.32 (s, 3H, Si(CH₃), 0.44 (s, 3H, Si(CH₃), 3.54 (s, 2H, SiCH), 6.64 (m, 6H, CpH), 6.82 (m, 2H, CpH).

4,4-dimethyl-5-Iodo-4-sila-1-pentene. Allylmagnesiumbromide (67.5 mL, 2 M in THF) was added dropwise to a 500 mL ether solution of chloro(chloromethyl)dimethylsilane (19.2 g, 135 mmol) at 0 °C over 1 hour. This was allowed to warm to room temperature and stir overnight. This was carefully quenched with 100 mL H₂O. The Organic layer was rinsed 3 times with 100 mL H₂O and once with 100 mL Brine. The crude oil was dissolved in 125 mL dry acetone and NaI (40 g, 266 mmol) was added and the mixture was stirred for 18 hours. This mixture was taken up in 100 mL of pentane and 100 mL H₂O. The organic layer was washed with an additional 100 mL of H₂O. The solvent was removed by rotary evaporation and the oil was distilled at 68-74 °C/10 mm Hg. 15.6 g of a colorless oil was collected for a 48% yield. ¹H NMR (CDCl₃, 300 MHz) δ 0.16 (s, 6H, Si(CH₃)₂), 1.66 (d, 2H SiCH₂CH, J_{HH}=7.2 Hz), 2.01 (s, 2H, ICH₂Si), 4.9 (m, 2H, SiCH₂CHCH₂), 5.78 (m, 1H, SiCH₂CH). Anal. Calcd for C₆H₁₁SiI: C, 30.01; H, 5.46; I, 52.84; Si, 11.69. Found: C, 30.21; H, 5.45.

2,4,4-trimethyl-5-Iodo-4-sila-1-pentene. This compound was prepared analogously to 4,4-dimethyl-5-Iodo-4-sila-1-pentene using CH₂C(CH₃)CH₂MgCl in place of Allylmagnesiumbromide. The final product was distilled at 95 °C/25 mm Hg and was isolated in 32% overall yield. ¹H NMR (CDCl₃, 300 MHz) δ 0.19(s, 6H, Si(CH₃)₂), 1.62 (s, 2H, SiCH₂CCH₃), 1.70 (s, 3H, CCH₃), 2.05 (s, 2H, ICH₂Si), 4.55 (s, 1H, CHHCCH₃(CH₂Si)), 4.65 (s, 1H, CHHCCH₃(CH₂Si)). Anal. Calcd for C₇H₁₃SiI: C, 33.08; H, 5.95; I, 49.93; Si, 11.05. Found: C, 33.21; H, 5.91.

5,5-dimethyl-6-Iodo-5-sila-cis-2-hexene. A solution of *cis*-Cl₃SiCH₂CHCHCH₃ (27.15 g, 143.3 mmol), prepared according to literature procedure, in 1 L of diethyl ether was cooled to 0 °C. Methylmagnesiumchloride (95.5 mL, 3 M, 286.6 mmol) was added over the course of 1 hour. The volatiles were removed by distillation under Ar and three fractions were obtained with varying amounts of methylated products. The first two fractions were collected from 95-107 °C. Over the course of 15 minutes, Buli (26.6 mL, 1.6 M, 42.5 mmol) was added *along the walls of the flask*, which were cooled to -78, to a 100 mL THF solution of

CH_2Br_2 (2.97 mL, 42.5 mmol) and the mixture of *cis*-butenylsilylchloride. This was allowed to stir at $-78\text{ }^\circ\text{C}$ for an additional 15 minutes. It was then allowed to warm and stir at room temperature for 20 minutes. 20 mL of pentane was added and the organic solution was rinsed repeatedly with H_2O and the volatiles were dried over MgSO_4 . The product was purified by column chromatography with a pentane eluant. The oil was distilled at $75\text{-}80\text{ }^\circ\text{C}/18\text{ mm Hg}$ for further purification. The oil and NaI (3 g, 20 mmol) were added to 25 mL of dry acetone and stirred for 24 hours. The mixture was added to 100 mL of pentane and was rinsed 4 times with 50 mL of H_2O and then dried over MgSO_4 . The volatiles were removed by rotary evaporation and the resulting oil was obtained in 9.1% yield. $^1\text{H NMR}$ (CDCl_3 , 300 MHz) δ 0.17 (s, 6H, $\text{Si}(\text{CH}_3)_2$), 1.58 (d, 3H, CHCH_3), 1.63 (d, 2H, CH_2CH), 2.02 (s, 2H, ICH_2Si), 5.4 (m, 2H, $\text{CH}_2\text{CHCHCH}_3$). Anal. Calcd for $\text{C}_7\text{H}_{13}\text{SiI}$: C, 33.08; H, 5.95; I, 49.93; Si, 11.05. Found: C, 33.60; H, 6.0.

5,5-dimethyl-6-Iodo-5-sila-*trans*-2-hexene. Starting with *trans*- $\text{Cl}_3\text{SiCH}_2\text{CHCHCH}_3$, which is prepared according to literature procedure, the preparation of this compound is identical to that of 5,5-dimethyl-6-Iodo-5-sila-*cis*-2-hexene. $^1\text{H NMR}$ (CDCl_3 , 300 MHz) δ 0.14 (s, 6H, $\text{Si}(\text{CH}_3)_2$), 1.56 (d, 2H, CH_2CH), 1.63 (d, 3H, CHCH_3), 2.0 (s, 2H, ICH_2Si), 5.35 (m, 2H, $\text{CH}_2\text{CHCHCH}_3$). Anal. Calcd for $\text{C}_7\text{H}_{13}\text{SiI}$: C, 33.08; H, 5.95; I, 49.93; Si, 11.05. Found: C, 34.07; H, 6.09.

3,3-dideutero-4,4-dimethyl-5-Iodo-4-sila-1-pentene. This was prepared analogously to 4,4-dimethyl-5-Iodo-4-sila-1-pentene using $\text{CH}_2\text{CHCD}_2\text{MgBr}$, which is prepared according to literature procedure. $^1\text{H NMR}$ (CDCl_3 , 300 MHz) δ 0.19(s, 6H, $\text{Si}(\text{CH}_3)_2$), 1.62 (d, 1H, SiCH_2CH), 2.0 (s, 2H, ICH_2Si), 4.85 (m, 1H, $\text{CH}_2\text{CH}(\text{CH}_2\text{Si})$), 5.7 (m, 1H, $\text{CH}_2\text{CH}(\text{CH}_2\text{Si})$). Anal. Calcd for $\text{C}_6\text{H}_9\text{D}_2\text{SiI}$: C, 29.76; H, 5.45; I, 52.40; Si, 11.60. Found: C, 29.82; H 5.51.

5,5-dideutero-4,4-dimethyl-5-Iodo-1-pentene. This was prepared according to literature procedures for the undeuterated iodopentene, but replaced the lithium aluminum hydride reduction with lithium aluminum deuteride reduction. $^1\text{H NMR}$ (300 MHz, CDCl_3) δ 1.10 (s, 6H, $\text{C}(\text{CH}_3)_2$), 2.15 (d, 2H, CH_2CH), 5.20 (m, 2H, $\text{CH}=\text{CH}_2$), 5.82 (m, 1H, $\text{CH}=\text{CH}_2$).

General procedure for preparation of zirconocene methyl,pentenyl (1, 2, 4-7, 16). A 25 mL schlenk flask with a rubber septum was purged with N_2 for 10

minutes. 10 mL of a degassed 3:2 mixture of petroleum ether and diethyl ether was added by syringe. To this was added 4,4-dimethyl-5-Iodo-4-sila-1-pentene (240 mg, 1.0 mmol) by syringe. This was cooled to -78 °C and *t*-Buli (1.18 mL, 2.0 mmol) was added dropwise by syringe over 7 minutes. This was stirred for 20 minutes at -78 °C. A toluene solution containing Cp₂ZrMe(Cl) (300 mg, 1.1 mmol) was added by syringe in <1 minute. This was stirred for 5 minutes at -78 °C then allowed to warm slowly to 0 °C over the course of 2 hours. The solvent was removed *in vacuo*. The flask was filled with argon and this flask was quickly attached to a swivel frit assembly and this was evacuated. 10 mL of Petroleum ether was vacuum transferred on to the solid. This was stirred at room temperature and then filtered. The remaining solid was rinsed once and the petroleum ether was removed *in vacuo* leaving behind a yellow, which was left under vacuum for 30 minutes to remove residual solvent.

($\eta^5\text{-C}_5\text{H}_5$)₂Zr(CH₃)(CH₂SiMe₂CH₂CH=CH₂) (1). ¹H NMR (C₆D₆, 499.85 MHz) δ -0.17 (s, 3H, ZrCH₃), 0.04 (s, 6H, Si(CH₃)₂), 0.05 (s, 2H, ZrCH₂Si), 1.50 (d of t, 2H, SiCH₂CHCH₂, J_{HH}=8.2, 1.1 Hz), 4.90 (m, 2H, SiCH₂CHCH₂), 5.71 (s, 10H, CpH), 5.73 (s, 1H, SiCH₂CHCH₂). ¹³C (C₆D₆, 125.70 MHz) δ 1.0, 28.5, 28.6, 44.8, 110.2, 112.1, 136.6.

($\eta^5\text{-C}_5\text{H}_5$)₂Zr(CH₃)(CH₂SiMe₂CD₂CH=CH₂)/($\eta^5\text{-C}_5\text{H}_5$)₂Zr(CH₃)(CH₂SiMe₂CH₂CH=CD₂) (1-d₂) ¹H NMR (C₆D₆, 499.85 MHz) δ -0.17 (s, 3H, ZrCH₃), 0.04 (s, 6H, Si(CH₃)₂), 0.05 (s, 2H, ZrCH₂Si), 1.50 (d, 1H, SiCH₂CHCD₂, J_{HH}=8.2 Hz), 4.90 (m, 1H, SiCD₂CHCH₂), 5.71 (s, 10H, CpH), 5.73 (s, 1H, SiCH₂CHCH₂). ¹³C (C₆D₆, 125.70 MHz) δ 1.0, 28.5, 28.6, 44.8, 110.2, 112.1, 136.6.

($\eta^5\text{-C}_5\text{H}_4\text{CMe}_3$)₂Zr(CH₃)(CH₂SiMe₂CH₂CH=CH₂) (2). ¹H NMR (C₆D₆, 499.85 MHz) δ -0.01 (s, 3H, ZrCH₃), 0.13 (s, 6H, ZrCH₂Si(CH₃)₂), 0.11 (s, 2H, ZrCH₂Si), 1.13 (s, 18H, C(CH₃)₃), 1.58 (d, 2H, SiCH₂CH, J_{HH}=8.2 Hz), 5.0 (m, 2H, SiCH₂CHCH₂), 5.50 (q, 2H, CpH, J_{HH}=2.4 Hz), 5.60 (q, 2H, CpH, J_{HH}=2.4 Hz), 5.92 (q, 2H, CpH, J_{HH}=2.4 Hz), 5.95 (m, 1H, SiCH₂CH), 6.16 (q, 2H, CpH, J_{HH}=2.4 Hz). ¹³C (C₆D₆, 125.70 MHz) δ 0.8, 28.6, 30.9, 31.7, 32.9, 41.1, 106.7, 107.7, 108.2, 109.3, 111.1, 112.0, 138.9.

(SiMe₂)₂($\eta^5\text{-C}_5\text{H}_3$)₂Zr(CH₃)(CH₂SiMe₂CH₂CH=CH₂) (4). ¹H NMR (C₆D₆, 499.85 MHz) δ -0.19 (s, 3H, ZrCH₃), -0.05 (s, 3H, Cp₂Si(CH₃)(CH₃)), 0.07 (s, 5H, Cp₂Si(CH₃)(CH₃), ZrCH₂), 0.14 (s, 6H, ZrCH₂Si(CH₃)₂), 0.44 (s, 6H,

(Si(CH₃)(CH₃))₂, 1.57 (d, 2H, SiCH₂CHCH₂, J_{HH}=8.1 Hz), 5.0 (m, 2H, SiCH₂CHCH₂), 5.95 (m, 1H, SiCH₂CH), 6.31 (t, 2H, CpH, J_{HH}=2.7), 6.59 (m, 4H, CpH). ¹³C (C₆D₆, 125.70 MHz) δ -4.8, -3.9, 0.4, 2.4, 2.5, 28.3, 29.9, 33.2, 110.2, 112.1, 113.0, 113.1, 134.2, 136.7.

(η⁵-C₅H₅)₂Zr(CH₃)(*trans*-CH₂SiMe₂CH₂CH=CHCH₃) (5). ¹H NMR (C₆D₆, 499.85 MHz) δ -0.17 (s, 3H, ZrCH₃), 0.06 (s, 6H, Si(CH₃)₂), 0.09 (s, 2H, ZrCH₂Si), 1.46 (d. of qt., 2H, SiCH₂CHCH, J_{HH}=7.8, 1.3 Hz), 1.70 (d. of q., 3H, CHCHCH₃, J_{HH}=6.3, 1.4 Hz), 5.36 (m, 1H, CHCHCH₃), 5.54 (s, 1H, CHCHCH₃), 5.72 (s, 10H, CpH). ¹³C (C₆D₆, 125.70 MHz) δ 1.2, 18.3, 26.4, 28.4, 45.6, 110.2, 122.6, 128.8.

(η⁵-C₅H₅)₂Zr(CH₃)(*cis*-CH₂SiMe₂CH₂CH=CHCH₃) (6). ¹H NMR (C₆D₆, 499.85 MHz) δ -0.19 (s, 3H, ZrCH₃), 0.05 (s, 6H, Si(CH₃)₂), 0.09 (s, 2H, ZrCH₂Si), 1.50 (d, 2H, SiCH₂CHCH), 1.62 (d, 3H, CHCHCH₃), 5.47 (m, 1H, CHCHCH₃), 5.63 (s, 1H, CHCHCH₃), 5.75 (s, 10H, CpH). ¹³C (CD₂Cl₂, 125.70 MHz) δ 2.8, 14.6, 23.4, 29.5, 47.9, 112.2, 122.3, 129.8. ¹³C NMR spectra was taken in CD₂Cl₂ in order to identify a resonance which was obscured in C₆D₆.

(η⁵-C₅H₅)₂Zr(CH₃)(CH₂SiMe₂CH₂C(CH₃)=CH₂) (7). ¹H NMR (C₆D₆, 499.85 MHz) δ -0.11 (s, 3H, ZrCH₃), 0.19 (s, 6H, Si(CH₃)₂), 0.2 (s, 2H, ZrCH₂Si), 1.62 (s, 2H, SiCH₂CCH₃), 1.80 (s, 3H, CCH₃), 4.70 (s, 1H, SiCH₂C(CH₃)CHH), 4.80 (s, 1H, SiCH₂C(CH₃)CHH), 5.75 (s, 10H, CpH). ¹³C (C₆D₆, 125.70 MHz) δ 1.7, 25.6, 28.6, 32.4, 45.3, 107.9, 110.2, 144.7.

(SiMe₂)₂(η⁵-C₅H₃)₂Zr(CH₃)(CH₂CMe₂CH₂CH=CH₂) (16). ¹H NMR (C₆D₆, 300 MHz) δ -0.61 (s, 3H, ZrCH₃), 0.10 (s, 3H, Si(CH₃)), 0.12 (s, 3H, Si(CH₃)), 0.45 (s, 6H, (Si(CH₃)(CH₃))₂), 0.62 (s, 2H, ZrCH₂Si(CH₃)₂), 0.97 (s, 6H, ZrCH₂C(CH₃)₂), 2.00 (d, 2H, C(CH₃)₂CH₂CHCH₂, J_{HH}=7.5 Hz), 5.07 (m, 2H, C(CH₃)₂CH₂CHCH₂), 5.90 (m, 1H, C(CH₃)₂CH₂CH), 6.32 (t, 2H, CpH, J_{HH}=2.1), 6.59 (s, 2H, CpH), 6.67 (s, 2H, CpH). ¹³C (C₆D₆, 75.4 MHz) δ -4.5, -3.6, 2.6, 2.8, 28.6, 31.8, 37.5, 52.5, 69.2, 110.2, 112.6, 113.3, 116.1, 137.3.

(SiMe₂)₂(η⁵-C₅H₃)₂Zr(CH₃)(CH₂CMe₂CH₂CH=CH₂) (16-d₂). ¹H NMR (C₆D₆, 300 MHz) δ -0.61 (s, 3H, ZrCH₃), 0.10 (s, 3H, Si(CH₃)), 0.12 (s, 3H, Si(CH₃)), 0.45 (s, 6H, (Si(CH₃)(CH₃))₂), 0.62 (s, 2H, ZrCH₂Si(CH₃)₂), 0.97 (s, 6H, ZrCH₂C(CH₃)₂), 2.00 (d, 2H, C(CH₃)₂CH₂CHCH₂, J_{HH}=7.5 Hz), 5.07 (m, 2H,

$C(CH_3)_2CH_2CHCH_2$), 5.90 (m, 1H, $C(CH_3)_2CH_2CH$), 6.32 (t, 2H, CpH, $J_{HH}=2.1$), 6.59 (s, 2H, CpH), 6.67 (s, 2H, CpH).

Me₂Si(η⁵-C₅H₄)₂Zr(CH₃)(CH₂SiMe₂CH₂CH=CH₂) (3). A solution of 4-sila-1-pentenylmagnesiumiodide in THF (3.94 mL, 2.87 mmol) was added against an Ar counterflow to a 120 mL methylene chloride solution of Me₂SiCp₂ZrCl₂ (1.0 g, 2.87 mmol) in a 250 mL Schlenk flask at 0 °C. This was allowed to warm to room temperature and stir overnight. The Solvent was removed and benzene was condensed onto the solvent and warmed to room temperature. This was filtered and the solvent was removed the resulting solid, which included 5-10% of the [Zr]R₂ and 5-10% of the [Zr]Cl₂ complexes, was rinsed 2 times with petroleum ether. This solid (0.67 g, 1.56 mmol) was dissolved in diethyl ether and at -78 °C a diethyl ether solution of MeLi (1.55 mL, 2.34 mmol) was added dropwise. This stirred at -78 °C for 1 hour and then was warmed to RT for 1 hour. The volatiles were removed and petroleum ether was condensed onto the solid. This solution was filtered and the solvent was removed *in vacuo* leaving a yellow oil behind. ¹H NMR (C₆D₆, 499.85 MHz) δ -0.06 (s, 3H, ZrCH₃), 0.07 (s, 3H, Cp₂Si(CH₃)(CH₃)), 0.10 (s, 6H, ZrCH₂Si(CH₃)₂), 0.11 (s, 2H, ZrCH₂Si), 0.13 (s, 3H, Cp₂Si(CH₃)(CH₃)), 1.55 (d of t, 2H, SiCH₂CHCH₂), 5.00 (s, 2H, SiCH₂CHCH₂), 5.41 (q, 2H, CpH), 5.53 (q, 2H, CpH), 6.53 (q, 2H, CpH), 6.89 (q, 2H, CpH). ¹³C (C₆D₆, 125.70 MHz) δ -5.9, -5.3, 0.8, 28.5, 29.0, 44.8, 102.4, 110.4, 112.1, 114.0, 120.0, 120.6, 136.65.

General procedure for activation of zirconocene methyl, alkenyl. Because the alkenyl complexes are typically an oil, calibrated solutions in either CD₂Cl₂ or C₆D₅Cl were prepared. In an inert atmosphere glove box, B(C₆F₅)₃ (20 mg, 39.1 μmol) was weighed out in a screw capped NMR tube with a teflon septum. 0.7 mL of NMR solvent was added and the septum cap was screwed on. The zirconocene solution (60 μL, 0.5 M, 30 μmol) was measured in a syringe. Outside of the glovebox, the walls of the NMR tube were cooled to -78 °C and then the zirconocene solution was added by syringe to the sealed NMR tube and the contents were carefully shaken, keeping the solution cold. The NMR solution immediately became bright yellow.

[(η⁵-C₅H₅)₂Zr(CH₂SiMe₂CH₂CH=CH₂)[MeB(C₆F₅)₃] (8). ¹H NMR (CD₂Cl₂, 499.85 MHz, -80 °C) δ 0.06 (s, 3H, ZrCH₂Si(CH₃)(CH₃)), 0.38 (d, 1H, ZrCHH, $J_{HH}=12.5$ Hz), 0.42 (s, 3H, BCH₃), 0.46 (s, 3H, ZrCH₂Si(CH₃)(CH₃)), 2.01 (d of d,

1H, SiCHHCH, $J_{\text{HH}}=11$ Hz, 11 Hz), 2.12 (m, 1H, SiCHHCH), 2.34 (m, 1H, SiCH₂CHCHH), 2.57 (d, 1H, ZrCHH, $J_{\text{HH}}=12.5$ Hz), 5.92 (d, 1H, SiCH₂CHCHH, $J_{\text{HH}}=17$ Hz), 6.62 (s, 5H, CpH), 6.65 (s, 5H, CpH), 8.65 (m, 1H, SiCH₂CH). ¹³C NMR (CD₂Cl₂, 125.70 MHz, -80 °C) δ 0.4 (q, Si(CH₃)₂, $J_{\text{C-H}}=119$), 1.7 (q, Si(CH₃)₂, $J_{\text{C-H}}=121$), 9.8 (q, B-CH₃, $J_{\text{C-H}} = 124.3$ Hz), 32.9 (t, ZrCH₂, $J_{\text{C-H}} = 128.7$ Hz), 53.5 (t, SiCH₂CHCH₂, $J_{\text{C-H}} = 113.6$ Hz), 99.5 ppm (t, SiCH₂CHCH₂, $J_{\text{C-H}} = 153$ Hz), 113.9 (d of qt, C₅H₅, $J_{\text{C-H}} = 167$ Hz), 115.3 (d of qt, C₅H₅, $J_{\text{C-H}} = 167$ Hz), 128.1 (s, B-C), 136.0 (d, C-F, $J_{\text{CF}}=247$ Hz), 137.0 (d, C-F, $J_{\text{CF}}=244$ Hz), 147.7 (d, C-F, $J_{\text{CF}}=246$), 175.1 (d, SiCH₂CHCH₂, $J_{\text{C-H}} = 155$ Hz) ¹⁹F NMR (CD₂Cl₂, 470.25 MHz, -80 °C) δ -167.0 (s, 6F), -164.3 (s, 3F, $J_{\text{FF}}=21$ Hz), -134.0 (s, 6F).

[(η^5 -C₅H₅)₂Zr(CH₂SiMe₂CD₂CH=CH₂)[MeB(C₆F₅)₃]/[(η^5 -C₅H₅)₂Zr(CH₂SiMe₂CH₂CH=CD₂)[MeB(C₆F₅)₃] (8-d₂). ¹H NMR (CD₂Cl₂, 499.85 MHz, -80 °C) δ 0.02 (s, 3H, Si(CH₃)(CH₃)), 0.25 (d, 1H, ZrCHHSiCH₂, $J_{\text{HH}}=13$ Hz), 0.30 (d, 1H, ZrCHHSiCD₂, $J_{\text{HH}}=13$ Hz), 0.36 (s, 3H, BCH₃), 0.41 (s, 3H, Si(CH₃)(CH₃)), 2.01 (d of d, 0.5H, SiCHHCH, $J_{\text{HH}}=11$ Hz, 11 Hz), 2.12 (m, 0.5H, SiCHHCH), 2.34 (m, 0.5H, SiCH₂CHCHH), 2.51 (d, 1H, ZrCHH, $J_{\text{HH}}=13$ Hz), 5.92 (d, 0.5H, SiCH₂CHCHH, $J_{\text{HH}}=17$ Hz), 6.57 (s, 5H, CpH), 6.59 (s, 5H, CpH), 8.62 (m, 1H, SiCH₂CH).

[(η^5 -C₅H₄CMe₃)₂Zr(CH₂SiMe₂CH₂CH=CH₂)[MeB(C₆F₅)₃] (9). ¹H NMR (CD₂Cl₂, 499.85 MHz, -80 °C) δ -0.31 (d, 1H, ZrCHH, $J_{\text{HH}}=12.5$ Hz), 0.04 (s, 3H, Si(CH₃)₂), 0.42 (s, 3H, BCH₃), 0.52 (s, 3H, Si(CH₃)₂), 1.09 (s, 18H, CCH₃), 2.04 (m, 2H, SiCH₂CHCH₂), 2.19 (t, 1H, Si 5.67CH₂CHCH₂), 2.60 (d, 1H, ZrCHH, $J_{\text{HH}}=12.5$ Hz), 5.96 (s, 1H, CpH), 6.31 (s, 1H, CpH), 6.55 (s, 2H, CpH), 6.71 (s, 1H, CpH), 6.99 (s, 1H, CpH), 7.11 (s, 2H, CpH), 8.81 (m, 1H, SiCH₂CHCH₂) ¹³C NMR (CD₂Cl₂, 125.70 MHz, -80 °C) δ 1.0, 3.2, 10.0, 31.3, 31.3, 33.3, 33.8, 34.3, 52.0, 99.0, 108.0, 110.5, 110.6, 111.8, 112.5, 115.9, 118.9, 119.7, 128.61, 135.6 (d, $J_{\text{CF}}=242$ Hz), 137.5 (d, $J_{\text{CF}}=236$ Hz), 145.0, 148.6(d, $J_{\text{CF}}=234$ Hz), 179.7. ¹⁹F NMR (CD₂Cl₂, 470.25 MHz, -80 °C) δ -168.3 (t, 6F, $J_{\text{FF}}=21$ Hz), -165.6 (t, 3F, $J_{\text{FF}}=21$ Hz), -135.2 (d, 6F, $J_{\text{FF}}=22$ Hz)

[Me₂Si(η^5 -C₅H₄)₂Zr(CH₂SiMe₂CH₂CH=CH₂)[MeB(C₆F₅)₃] (10). ¹H NMR (CD₂Cl₂, 499.85 MHz, -80 °C) δ 0.06 (s, 3H, ZrCH₂Si(CH₃)(CH₃)), 0.36 (s, 3H, ZrCH₂Si(CH₃)(CH₃)), 0.41 (s, 3H, BCH₃), 0.66 (s, 3H, Cp₂Si(CH₃)(CH₃)), 0.71 (s, 3H, Cp₂Si(CH₃)(CH₃)), 0.88 (s, 1H, ZrCHHSi, $J_{\text{HH}}=13$ Hz), 2.01 (d of d, 1H, SiCHHCHCH₂, $J_{\text{HH}}=12.2$ Hz), 2.18 (m, 1H, SiCHHCHCH₂), 2.34 (d, 1H,

ZrCHHSi, $J_{\text{HH}}=13$ Hz), 2.74 (d, 1H, SiCH₂CHCHH, $J_{\text{HH}}=6.5$), 5.78 (s, 2H, CpH), 5.80 (s, 1H, CpH), 5.82 (s, 1H, CpH), 5.99 (d, 1H, SiCH₂CHCHH, $J_{\text{HH}}=17$ Hz), 7.27 (s, 1H, CpH), 7.35 (s, 1H, CpH), 7.44 (s, 1H, CpH), 7.52 (s, 1H, CpH). ¹³C NMR (CD₂Cl₂, 125.70 MHz, -80 °C) δ -5.5, -5.4, 1.2, 1.4, 10.0, 32.6, 52.0, 100.1, 104.5, 107.6, 113.4, 114.1, 118.3, 118.8, 121.1, 123.6, 125.0, 128.4, 136.5 (d, $J_{\text{CF}}=240$ Hz), 137.9 (d, $J_{\text{CF}}=242$ Hz), 142.3 (d, $J_{\text{CF}}=238$ Hz), 168.1 ¹⁹F NMR (CD₂Cl₂, 470.25 MHz, -80 °C) δ -168.4 (t, 6F, $J_{\text{FF}}=20$ Hz), -162.2 (t, 3F, $J_{\text{FF}}=21$ Hz), -135.1 (d, 6F, $J_{\text{FF}}=21$ Hz).

[(SiMe₂)₂(η^5 -C₅H₃)₂Zr(CH₂SiMe₂CH₂CH=CH₂)] [MeB(C₆F₅)₃] (11-MeBArF).

¹H NMR (C₆D₅Cl, 499.85 MHz, -40 °C) δ -0.09 (d, 1H, ZrCHH, $J_{\text{HH}}=13.5$ Hz), -0.05 (s, 3H, Cp₂Si(CH₃)(CH₃)), 0.02 (s, 3H, ZrCH₂Si(CH₃)(CH₃)), 0.05 (s, 3H, Cp₂Si(CH₃)(CH₃)), 0.31 (s, 3H, ZrCH₂Si(CH₃)(CH₃)), 0.66 (s, 6H, Cp₂(Si(CH₃)(CH₃))₂), 1.44 (s, 3H, BCH₃), 1.74 (1H, d of d, SiCHHCHCH₂, $J_{\text{HH}}=8.4, 12.3$ Hz), 1.88 (m, 1H, SiHHCHCH₂), 1.96 (d, 1H, ZrCHH, $J_{\text{HH}}=13.5$ Hz), 1.97 (m, 1H, SiCH₂CHCHH), 5.49 (d of d, 1H, SiCH₂CHCHH, $J_{\text{HH}}=2.9, 17$ Hz), 6.10 (s, 1H, CpH), 6.15 (s, 1H, CpH), 6.57 (s, 1H, CpH), 6.64 (s, 1H, CpH), 6.92 (s, 1H, CpH), 6.97 (s, 1H, CpH), 8.08 (m, 1H, SiCH₂CHCH₂). ¹³C NMR (C₆D₅Cl, 125.70 MHz, -40 °C) δ -5.0, 4.2, 0.1, 1.2, 1.9, 2.1, 33.4, 46.9, 98.9, 115.1, 117.4, 117.5, 117.9, 118.0, 136.0, 137.1 (d, $J_{\text{CF}}=233$ Hz), 137.8 (d, $J_{\text{CF}}=241$ Hz), 148.9 (d, $J_{\text{CF}}=253$ Hz), 170.1. ¹⁹F NMR (CD₂Cl₂, 470.25 MHz, -40 °C) δ -167.7 (t, 6F, $J_{\text{FF}}=23$ Hz), -165.1 (t, 3F, $J_{\text{FF}}=21$ Hz), -135.0 (d, 6F, $J_{\text{FF}}=21$ Hz).

[(SiMe₂)₂(η^5 -C₅H₃)₂Zr(CH₂SiMe₂CH₂CH=CH₂)] [B(C₆F₅)₄] (11-BArF₄).

¹H NMR (C₆D₅Cl, 499.85 MHz, -40 °C) δ -0.08 (d, 1H, ZrCHH, $J_{\text{HH}}=13.5$ Hz), -0.04 (s, 3H, Cp₂Si(CH₃)(CH₃)), 0.03 (s, 3H, ZrCH₂Si(CH₃)(CH₃)), 0.08 (s, 3H, Cp₂Si(CH₃)(CH₃)), 0.33 (s, 3H, ZrCH₂Si(CH₃)(CH₃)), 0.67 (s, 6H, Cp₂(Si(CH₃)(CH₃))₂), 1.75 (1H, d of d, SiCHHCHCH₂, $J_{\text{HH}}=8.4, 12.3$ Hz), 1.92 (m, 1H, SiHHCHCH₂), 1.97 (d, 1H, ZrCHH, $J_{\text{HH}}=13.5$ Hz), 1.99 (m, 1H, SiCH₂CHCHH), 2.15 (s, 3H, Ph₃CCH₃), 5.49 (d of d, 1H, SiCH₂CHCHH, $J_{\text{HH}}=2.9, 17$ Hz), 6.09 (s, 1H, CpH), 6.16 (s, 1H, CpH), 6.59 (s, 1H, CpH), 6.67 (s, 1H, CpH), 6.92 (s, 1H, CpH), 6.98 (s, 1H, CpH), 8.10 (m, 1H, SiCH₂CHCH₂). ¹³C NMR (C₆D₅Cl, 125.70 MHz, -40 °C) δ -5.0, 4.3, 0.1, 1.2, 1.9, 2.1, 30.6, 33.4, 46.9, 52.7, 98.8, 115.1, 117.5, 117.7, 117.9, 118.1, 170.2. ¹⁹F NMR (CD₂Cl₂, 470.25 MHz, -40 °C) δ -169.2 (s, 8F), -165.3 (t, 4F, $J_{\text{FF}}=21$ Hz), -136.0 (s, 8F).

$[(\eta^5\text{-C}_5\text{H}_5)_2\text{Zr}(\text{trans-CH}_2\text{SiMe}_2\text{CH}_2\text{CH}=\text{CHCH}_3)[\text{MeB}(\text{C}_6\text{F}_5)_3]$ (12).

Coordinated Olefin: ^1H NMR (CD_2Cl_2 , 499.85 MHz, $-80\text{ }^\circ\text{C}$) -0.32 (d, 1H, ZrCHH , $J_{\text{HH}}=13.5$ Hz), 0.03 (s, 3H, $\text{Si}(\text{CH}_3)(\text{CH}_3)$), 0.25 (d, 3H, CHCHCH_3 , $J_{\text{HH}}=5.5$ Hz), 0.42 (s, 3H, BCH_3), 0.47 (s, 3H, $\text{Si}(\text{CH}_3)(\text{CH}_3)$), 1.76 (d of d, 1H, SiCHHCHCH_2 , $J_{\text{HH}}=12$ Hz, $J_{\text{HH}}=12$ Hz), 1.85 (m, 1H, SiCHHCHCH), 2.09 (d, 1H, ZrCHH , $J_{\text{HH}}=13.5$ Hz), 5.68 (m, 1H, CHCHCH_3), 7.55 (m, 1H, SiCH_2CHCH). ^{13}C NMR (CD_2Cl_2 , 125.70 MHz, $-80\text{ }^\circ\text{C}$) δ 0.7, 5.0, 9.5, 9.8 (BCH_3), 30.0, 45.9, 99.8, 112.0, 113.7, 128.3, 136.8, 137.7, 148.1, 167.4. ^{19}F NMR (CD_2Cl_2 , 470.25 MHz, $-80\text{ }^\circ\text{C}$) δ -135.3 (d, $J_{\text{FF}}=20$ Hz), -165.5 (t, $J_{\text{FF}}=19$ Hz), -168.3 (t, $J_{\text{FF}}=19$ Hz). Coordinated anion: ^{19}F NMR (CD_2Cl_2 , 470.25, $-80\text{ }^\circ\text{C}$) δ -166.4 (t, 6F, $J_{\text{FF}}=19$ Hz), -161.6 (t, 3F, $J_{\text{FF}}=20$ Hz), -136.2 (d, 6F, $J_{\text{FF}}=20$ Hz).

$[(\eta^5\text{-C}_5\text{H}_5)_2\text{Zr}(\text{cis-CH}_2\text{SiMe}_2\text{CH}_2\text{CH}=\text{CHCH}_3)[\text{MeB}(\text{C}_6\text{F}_5)_3]$ (13). ^1H NMR (CD_2Cl_2 , 499.85 MHz, $-80\text{ }^\circ\text{C}$) coordinated anion: δ -0.05 (s, 6H, $\text{Si}(\text{CH}_3)_2$), 0.33 (s, 3H, BCH_3), 1.37 (d, 2H, SiCH_2CHCH), 1.42 (d, 3H, CHCHCH_3), 1.53 (s, 2H, ZrCH_2), 5.37 (m, 2H, $\text{SiCH}_2\text{CHCHCH}_3$), 6.25 (s, 10H, CpH). ^{19}F NMR (CD_2Cl_2 , 282.15 MHz, $-80\text{ }^\circ\text{C}$) δ -166.3 (t, $J_{\text{FF}}=23$ Hz), -161.5 (t, $J_{\text{FF}}=23$ Hz), -136.2 (d, $J_{\text{FF}}=23$ Hz). coordinated olefin: δ -0.04 (s, shoulder on larger peak from coordinated anion, SiCH_3), 0.29 (s, 3H, SiCH_3), 1.16 (d, 1H, ZrCHH , $J_{\text{HH}}=12.9$ Hz), 1.90 (d, 3H, CHCH_3 , $J_{\text{HH}}=6.3$ Hz), 2.93 (d, 1H, ZrCHH , $J_{\text{HH}}=12.9$ Hz), 4.68 (m, 1H, CHCH_3), 6.34 (s, 5H, CpH), 6.56 (s, 5H, CpH), 7.10 (m, 1H, CH_2CH).

$[(\eta^5\text{-C}_5\text{H}_5)_2\text{Zr}(\text{CH}_2\text{SiMe}_2\text{CH}_2\text{C}(\text{CH}_3)=\text{CH}_2)[\text{MeB}(\text{C}_6\text{F}_5)_3]$ (14). ^1H NMR (CD_2Cl_2 , 499.85 MHz, $-80\text{ }^\circ\text{C}$) 0.11 (s, 3H, $\text{Si}(\text{CH}_3)(\text{CH}_3)$), 0.26 (d, 3H, CHCHCH_3 , $J_{\text{HH}}=5.5$ Hz), 0.39 (s, 3H, BCH_3), 0.41 (s, 3H, $\text{Si}(\text{CH}_3)(\text{CH}_3)$), 0.64 (d, 1H, ZrCHH , $J_{\text{HH}}=13.5$ Hz), 2.05 (d, 1H, ZrCHH , $J_{\text{HH}}=13$ Hz), 2.12 (d of d, 1H, SiCHHCHCH , $J_{\text{HH}}=9$ Hz, $J_{\text{HH}}=4$ Hz), 2.24 (d, 1H, $\text{SiCHHC}(\text{CH}_3)\text{CH}_2$, $J_{\text{HH}}=10$ Hz), 2.52 (overlapping, 1H, $\text{SiCH}_2\text{C}(\text{CH}_3)\text{CHH}$, $J_{\text{HH}}=6.5$), 2.52 (s, 1H, $\text{SiCH}_2\text{C}(\text{CH}_3)\text{CHH}$, $J_{\text{HH}}=6.5$ Hz), 5.46 (d, 1H, CHCHCH_3 , $J_{\text{HH}}=5.5$ Hz), 6.49 (s, 5H, CpH), 6.61 (s, 5H, CpH) ^{13}C NMR (CD_2Cl_2 , 125.70 MHz, $-80\text{ }^\circ\text{C}$) δ 1.8, 3.0, 10.1, 31.7, 39.2, 52.5, 90.9, 115.6, 116.1, 129.1, 136.3 (d, $J_{\text{CF}}=242$ Hz), 137.9 (d, $J_{\text{CF}}=239$ Hz), 148.0 (d, $J_{\text{CF}}=236$ Hz). ^{19}F NMR (CD_2Cl_2 , 470.25 MHz, $-80\text{ }^\circ\text{C}$) δ -168.3 (t, $J_{\text{FF}}=19$ Hz), -165.5 (t, $J_{\text{FF}}=19$ Hz), -135.3 (d, $J_{\text{FF}}=20$ Hz).

$[(\text{SiMe}_2)_2(\eta^5\text{-C}_5\text{H}_3)_2\text{Zr}(\text{CH}_2\text{SiMe}_2\text{CH}_2\text{CH}=\text{CH}_2)][\text{B}(\text{C}_6\text{F}_5)_4]$ (17-BArF₄).

Complete ^1H NMR spectrum could not be reported because not all of the peaks could be identified, but a partial list is included here and the spectrum is included

in Appendix Y. ^1H NMR (500 MHz, CD_2Cl_2) δ -0.38 (d, 0.5H, ZrCHH, $J_{\text{HH}}=12.5$ Hz), 0.06 (s, 3H, Si(CH_3)), 0.18 (s, 3H, Si(CH_3)), 0.96 (s, 6H, (Si(CH_3)(CH_3)) $_2$ (?)), 1.35 (s, 3H, CCH $_3$), 2.18 (s, >3H, Ph $_3$ CCH $_3$), 2.80 (d, 0.5H, ZrCHH, $J_{\text{HH}}=12.5$ Hz), 2.91 (m, 0.5H, CHH-CH=), 5.03 (m, 1H, CH=CHH), 8.42 (m, 1H, CH=CH $_2$).

[(SiMe $_2$) $_2$ (η^5 -C $_5$ H $_3$) $_2$ Zr(CH $_2$ CHCH $_2$)] [B(C $_6$ F $_5$) $_4$] (18-MeBArF $_3$). ^1H NMR ($\text{C}_6\text{D}_5\text{Cl}$, 499.85 MHz, -50 $^\circ\text{C}$) δ -0.05 (s, 6H, SiCH $_3$), 0.05 (s, 6H, SiCH $_3$), 1.44 (s, 3H, BCH $_3$), 2.71 (2H, d, CHH, $J_{\text{HH}}=7.5$ Hz), 3.07 (2H, d, CHH, $J_{\text{HH}}=15.0$ Hz), 5.83 (s, 1H, CpH), 5.88 (s, 1H, CpH), 5.97 (m, 1H, CH $_2$ CHCH $_2$), 6.05 (s, 2H, CpH), 6.38 (s, 2H, CpH). ^{13}C NMR (CD_2Cl_2 , 125.70 MHz, -80 $^\circ\text{C}$) δ -4.6, 3.0, 10.9, 24.6, 69.3, 107.2, 107.8, 108.0, 108.2, 111.6, 132.8, 142.4, 135.5, 137.0 (d, $J_{\text{CF}}=240$ Hz), 138.2 (d, $J_{\text{CF}}=241$ Hz), 149.1 (d, $J_{\text{FF}}=231$ Hz).

1. Brintzinger, H.-H.; Fischer, D.; Müllhaupt, R.; Rieger, B.; Waymouth, R. M. *Angew. Chem. Int. Ed. Engl.* **1995**, *34*, 1143.
2. (a) Cossee, P.; Arlman, E. J. *J. Catal.* **1964**, *3*, 89.
(b) Laverty, D. T.; Rooney, J. J. *J. Chem. Soc. Faraday. Trans. 1* **1983**, *79*, 869.
(c) Brookhart, M.; Green, M. L. H. *J. Organomet. Chem.* **1983**, *250*, 395.
3. Crabtree, R. H. *The Organometallic Chemistry of the Transition Metals*, 2nd ed.; John Wiley & Sons: New York, 1994; Chapter 5.
4. Mingos, D. M. P. Bonding of Unsaturated Organic Molecules to Transition Metals. In *Comprehensive Organometallic Chemistry*, 1st ed.; Wilkinson, G.; Stone, F. G. A.; Abel, E. A.; Pergamon Press: Oxford, 1982; Vol. 3, pp 47-54.
5. Kress, J.; Osborn, J. A. *Angew. Chem. Int. Ed. Engl.* **1992**, *31*, 1585.
6. Lowry, T. H.; Richardson, K. S. *Mechanism and Theory in Organic Chemistry*, 3rd ed.; HarperCollins: New York, 1987; Chapter 5, p 448.
7. Shriver, D. F.; Atkins, P. W. *Inorganic Chemistry*, 3rd ed.; W. H. Freeman and Company: New York, 1999; Chapter 1, pp 13-15.
8. (a) McGeary, M. J.; Tonker, T. L.; Templeton, J. L. *Organometallics* **1985**, *4*, 2102.

-
- (b) Casey, C. P.; Hornung, N. L.; Kosar, W. P. *J. Am. Chem. Soc.* **1987**, *109*, 4908.
9. Wu, Z.; Jordan, R. F.; Petersen, J. L. *J. Am. Chem. Soc.* **1995**, *117*, 5867.
10. (a) Carpentier, J.-F.; Wu, Z.; Lee, C. W.; Strömberg, S.; Christopher, J. N.; Jordan, R. F. *J. Am. Chem. Soc.* **2000**, *122*, 7750.
- (b) Carpentier, J.-F.; Maryin V. P.; Luci, J.; Jordan, R. F. *J. Am. Chem. Soc.* **2001**, *123*, 898.
11. (a) Casey, C. P.; Hallenbeck, S. L.; Pollock, D. W.; Landis, C. R. *J. Am. Chem. Soc.* **1995**, *117*, 9770.
- (b) Casey, C. P.; Hallenbeck, S. L.; Wright, J. M.; Landis, C. R. *J. Am. Chem. Soc.* **1997**, *119*, 9681.
- (c) Casey, C. P.; Fagan, M. A.; Hallenbeck, S. L. *Organometallics* **1998**, *17*, 287.
12. Galakhov, M. V.; Heinz, G.; Royo, P. *J. Chem. Soc., Chem. Commun.* **1998**, 17.
13. (a) Casey, C. P.; Carpenetti, D. W.; Sakuri, H. *J. Am. Chem. Soc.* **1999**, *121*, 9483.
- (b) Casey, C. P.; Carpenetti, D. W. *Organometallics* **2000**, *19*, 3970.
14. Fleming, I.; Patel, S. K.; Urdi, C. J. *J. Chem. Soc. Perkin Trans I* **1989**, 115.
15. Iseki, K.; Kuroki, Y.; Takahashi, M.; Satoshi, K.; Kobayashi, Y. *Tetrahedron*, **1997**, 3513.
16. Michnick, T. J.; Matteson, D. S. *Synlett* **1991**, 631.
17. Cunico, R. F.; Gill, H. S. *Organometallics* **1982**, *1*, 1.
18. GNMR, v. 3.6; Cherwell Scientific Publishing: Oxford, 1996.
19. Jaguar 3.5, Schrodinger, Inc., Portland, Oregon, 1998.

-
20. This product was produced concomitantly with what appears to be a metallocene with a coordinated anion. The ratio of these two species does not change over a wide variety of temperatures and they do not appear to exchange with each other at temperatures up to -30 °C.
21. This value for ΔG^\ddagger is extrapolated from activation parameters which were determined from an Eyring plot determined over a 30 °C range; the free energy at 273 K is 14.8 kcal.mol⁻¹.
22. Although the symmetry for **8** does not allow measurement of the site epimerization rate, we assume that inversion at zirconium also accompanies olefin dissociation for this cation.
23. (a) Wendt O., Bercaw, J. E. *Manuscript in Preparation*
(b) Beck, S.; Lieber, S.; Schaper, F.; Geyer, A.; Brintzinger, H.-H. *J. Am. Chem. Soc.* **2001**, *123*, 1483.
24. a) Deck, P. A.; Marks, T. J. *J. Am. Chem. Soc.* **1995**, *117*, 6128.
(b) Casey, C. P.; Fagan, M. A.; Hallenbeck, S. L. *Organometallics* **1998**, *17*, 287.
25. a) Bierwagen, E. P.; Bercaw, J. E.; Goddard, W. A. *J. Am. Chem. Soc.* **1994**, *116*, 1481.

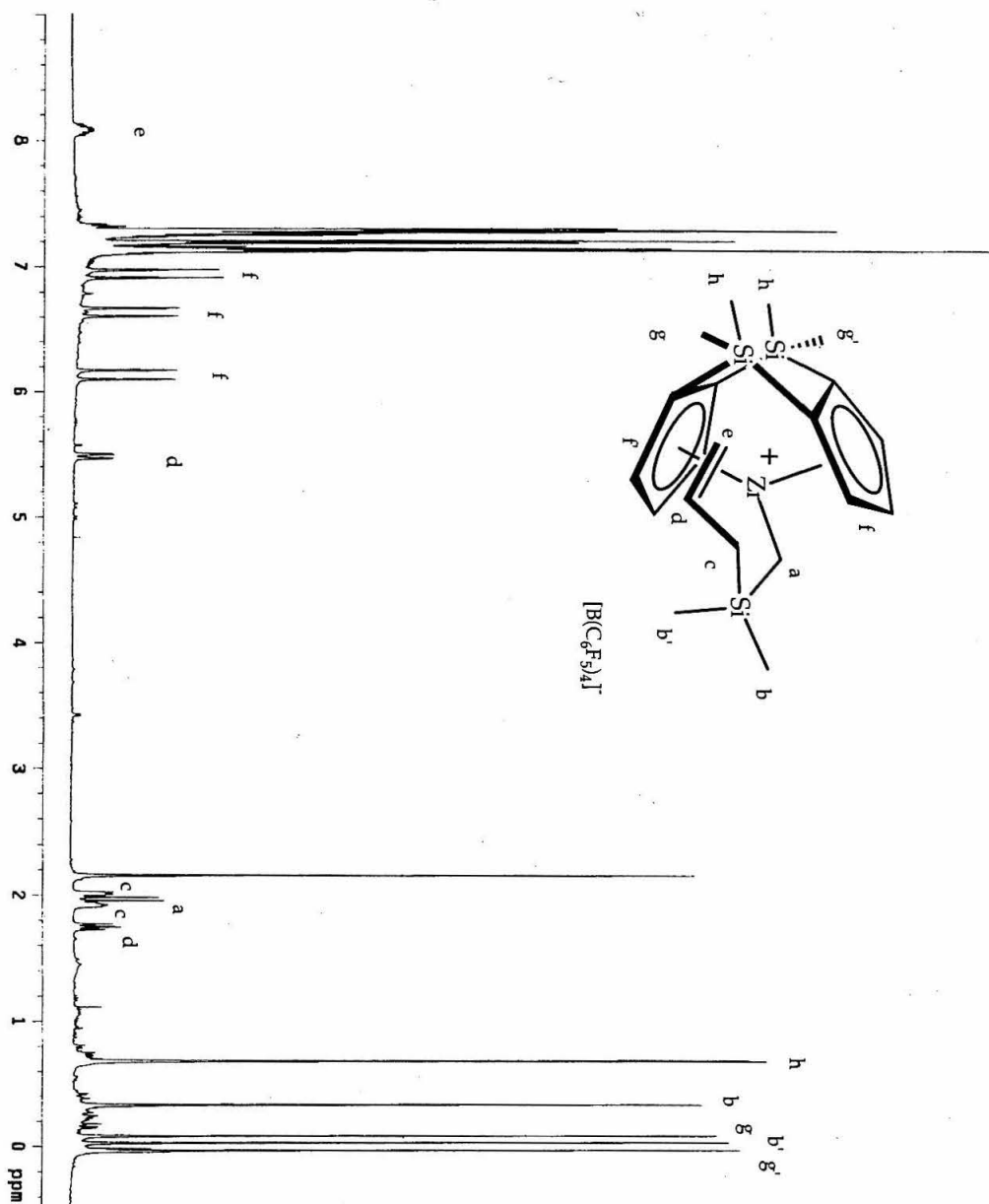
b) Additional DFT calculations show that the inversion barrier for the model complex [1,2-(SiMe₂)₂(η^5 -C₅H₃)₂ZrCH₃]⁺ is 6.9 kcal·mol⁻¹, which is greater than the lower limit given by this experimental study. We used DFT-GGAII as found in Jaguar[®].
26. Compound **11**, when heated to higher temperatures, decomposes to give a paramagnetic species that shows no peaks in the proton or fluorine NMR. After sitting overnight in an NMR tube, crystals of this species grew. We determined the structure of this species using X-ray crystallography, revealing it to be a Zr(III) bromide bridged dimer [(1,2-(SiMe₂)₂(η^5 -C₅H₃)₂Zr]₂(μ_2 -Br)₂ (**15**). Based on analogous iodide and chloride bridged Zr(III) dimers, we expect that this complex is

diamagnetic, but upon cooling the NMR tube, there is no discernible species present. Unfortunately, the amount of **15** that was isolated precluded further study. The mechanism of the reaction forming **15** is unknown at this time.

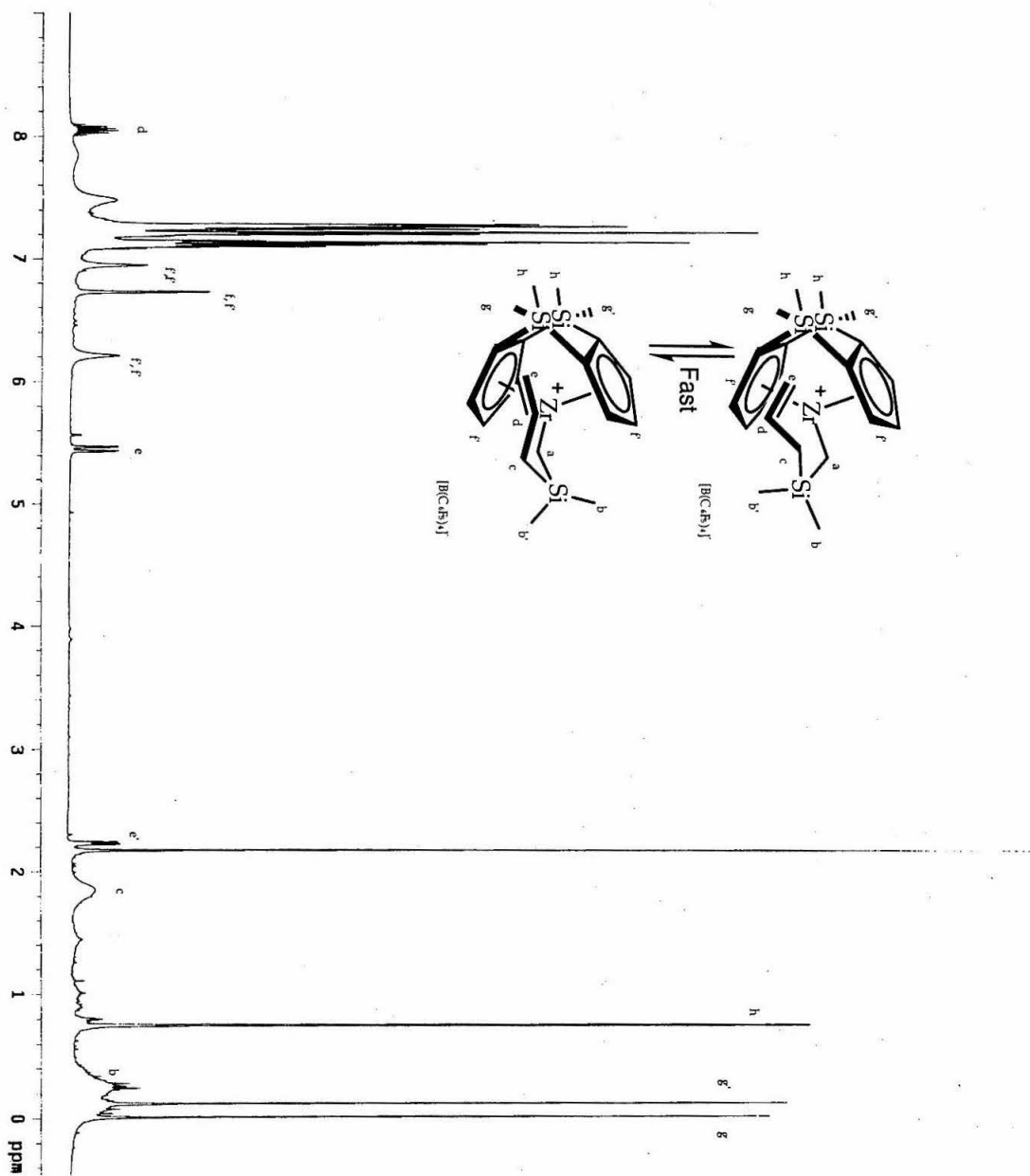
27. The pentenyl complex, **17**, can only be observed when **16** is activated at $-78\text{ }^{\circ}\text{C}$ with $[\text{Ph}_3\text{C}][\text{B}(\text{C}_6\text{F}_5)_4]$ in CD_2Cl_2 . Although it is not entirely pure, the diagnostic peaks in the ^1H NMR spectrum of the olefin complex can be observed: a multiplet at 8.4 ppm and a matching set of doublets at -0.4 ppm and 2.8 ppm. Upon warming to $-50\text{ }^{\circ}\text{C}$ all peaks corresponding **17** disappear, but the course of the decomposition of the proposed olefin complex is not easily followed.
28. Couturier, S.; Gautheron, B. *J. Organomet. Chem.* **1978**, *157*, C61.
29. Bajgur, C. S.; Tikkanen, W. R.; Peterson, J. L. *Inorg. Chem.* **1985**, *24*, 2539.
30. Massey, A. G.; Park, A. J. *J. Organomet. Chem.* **1964**, *2*, 245.
31. Chien, J. C. W.; Tsai, W.-M.; Rausch, M. D. *J. Am. Chem. Soc.* **1991**, *113*, 8570.
32. Cano, A.; Cuenca, T.; Gómez-Sal, P.; Manzanero, A.; Royo, P. J. *Organomet. Chem.* **1996**, *526*, 227.
33. Hill E. A.; Boyd, W. A.; Desai, H.; Darki, A.; Bivens, L. *J. Organomet. Chem.* **1996**, *514*, 1.
34. Pattenden, G.; Teaque, S. J. *Tetrahedron* **1987**, 5637.
35. Morris, G.A.; Freeman, R. *J. Magn. Reson.* **1978**, *29*, 433-462.
36. Bain, A.D.; Cramer, J.A. *J. Magn. Reson.* **1996**, *118A*, 21-27.

Complex	Temperature	ΔG^\ddagger (kcal.mol ⁻¹)
8	250 K	13.1
9	248 K	13.3
10	248 K	12.8
11	283 K	15.5
12	248 K	13.2
13	223 K	11.4
14	248 K, 283 K	14.4 ^a , 14.9

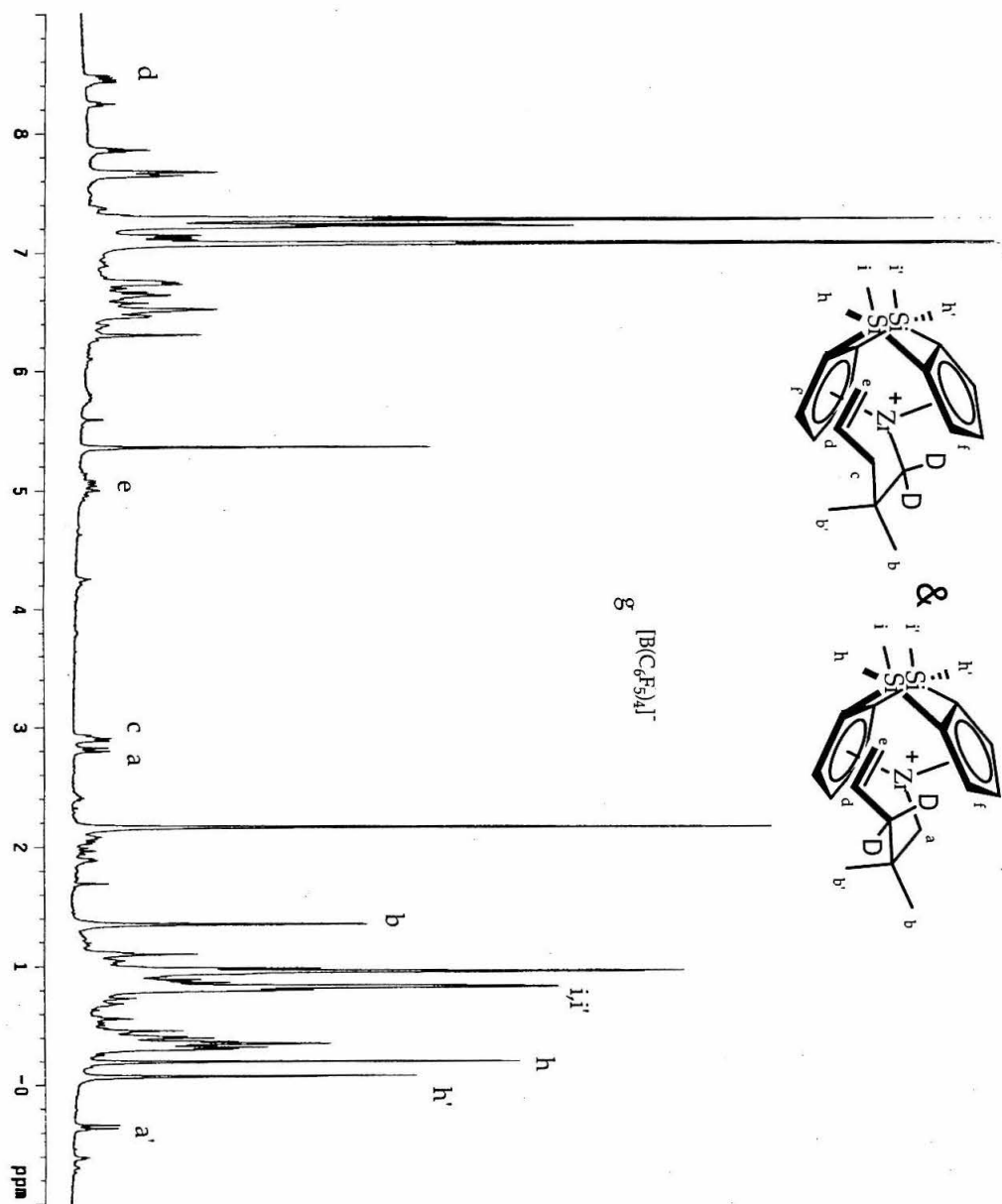
Table 1. Free energies of activation for zirconocene complexes. a) value was extrapolated from Eyring plot spanning 30 °.

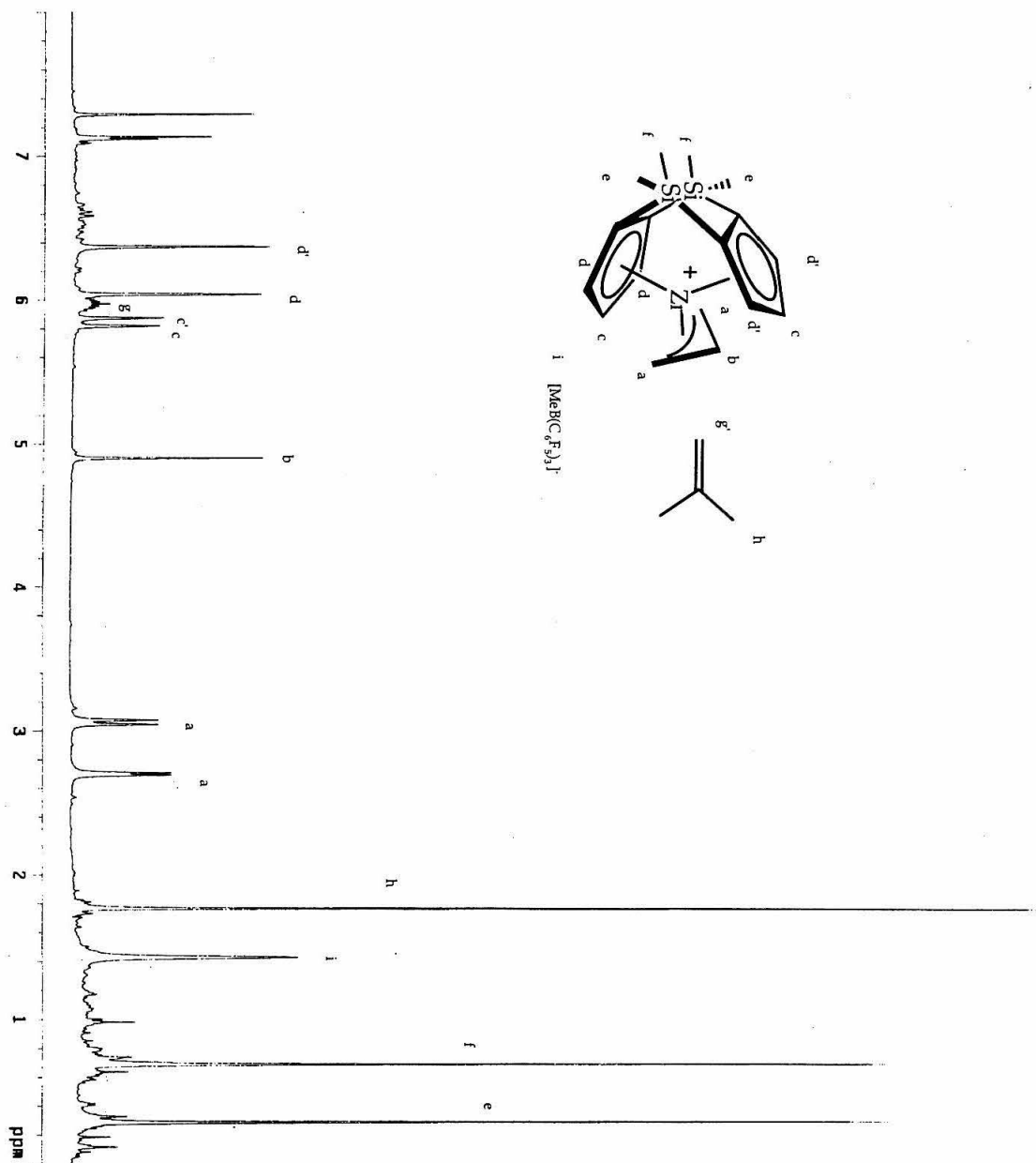
Appendix D. Selected ^1H NMR SpectraStatic ^1H NMR of **11** at -30 in $\text{C}_6\text{D}_5\text{Cl}$ 

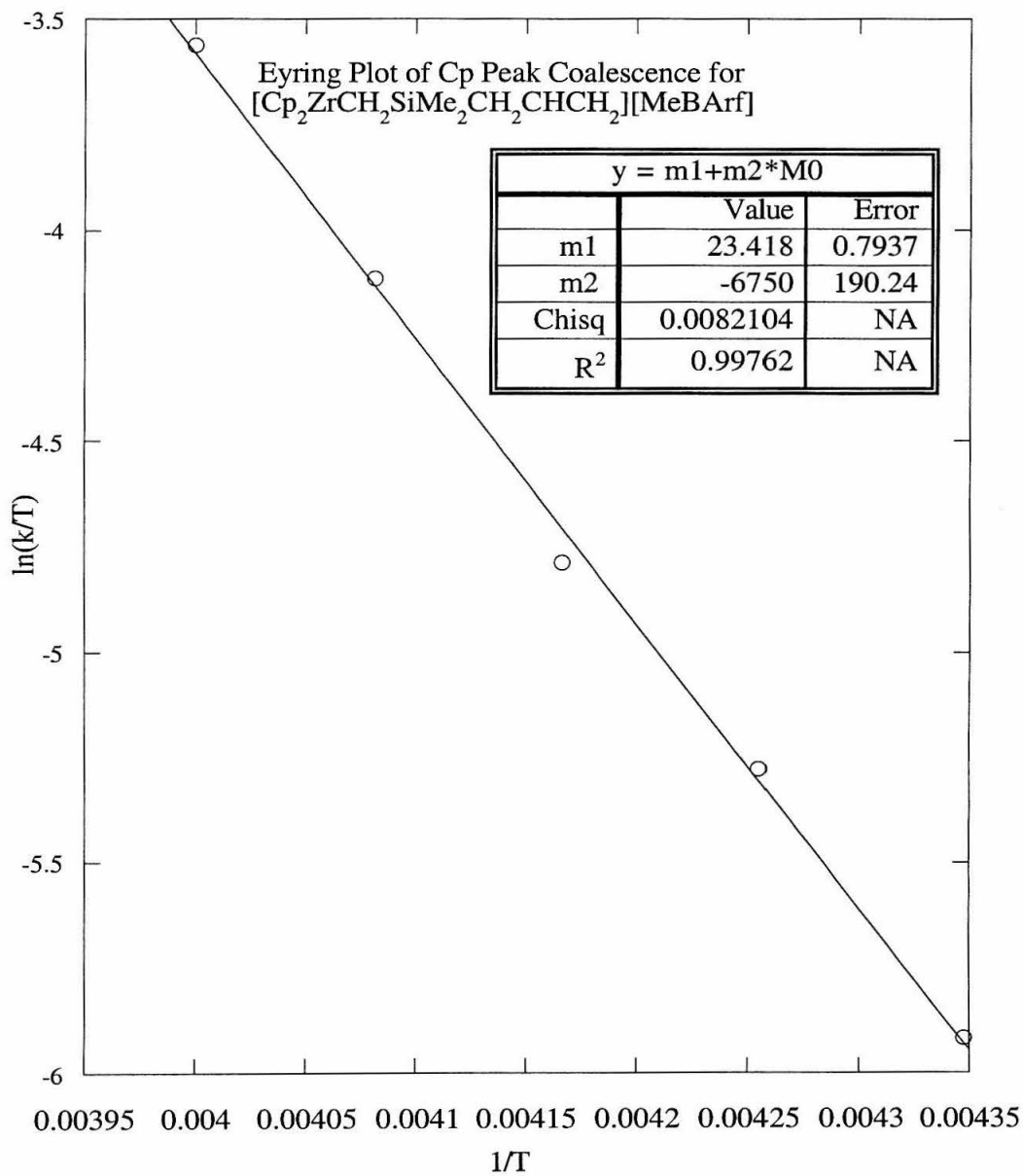
Dynamic ^1H NMR of **11** at 65 °C in $\text{C}_6\text{D}_5\text{Cl}$ showing coalesced resonances for cyclopentadienyl and silapentenyl $[\text{SiMe}_2]$ protons but interannulated $[\text{SiMe}_2]$ protons remain static.



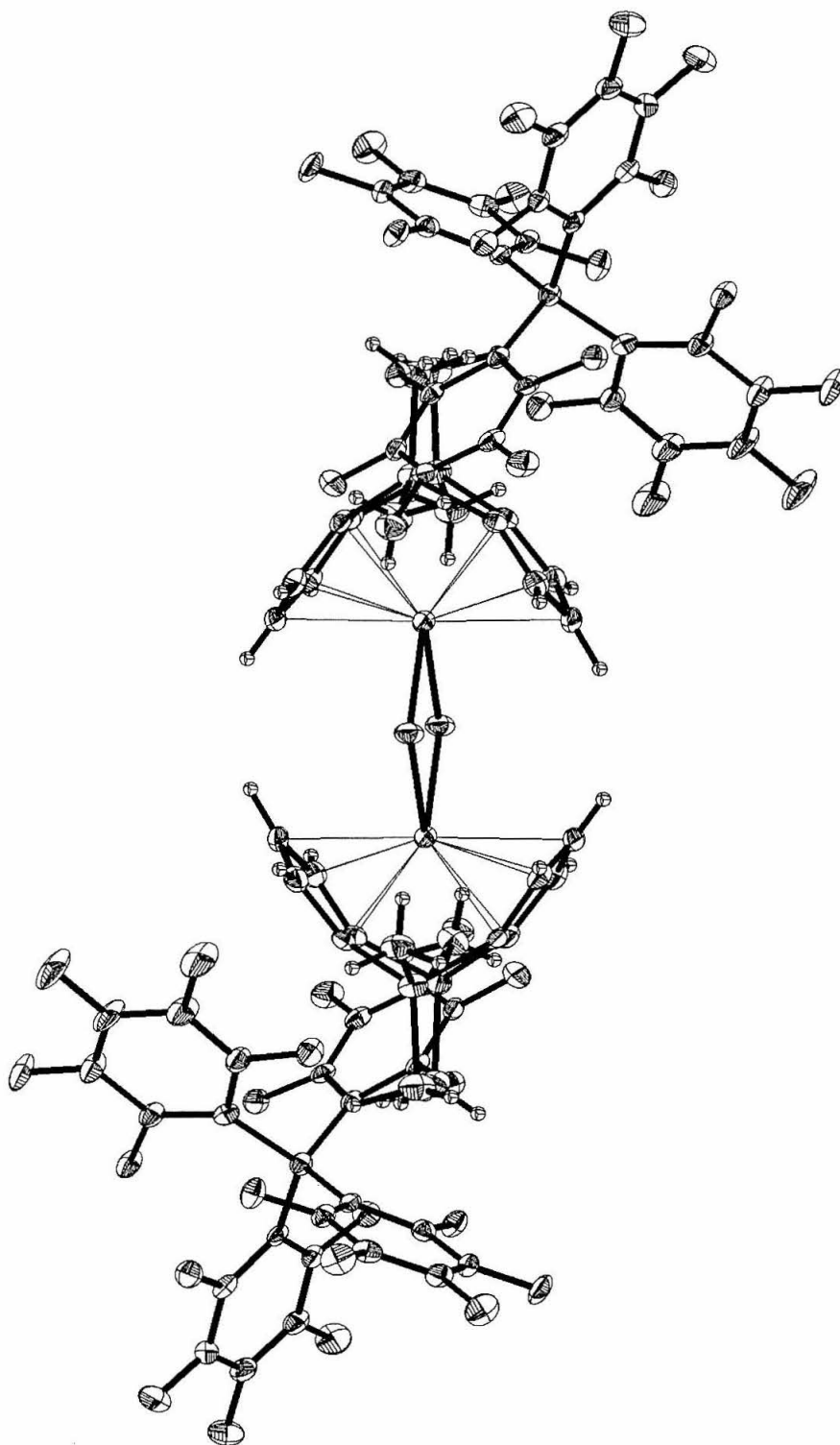
Static ^1H NMR of 17-d₂ at -30 in $\text{C}_6\text{D}_5\text{Cl}$



Static ^1H NMR of **18** at -30 in $\text{C}_6\text{D}_5\text{Cl}$ 

Appendix E. Representative Eyring Plot from ^1H NMR lineshape analysis

Appendix F. Crystal Structure of 15



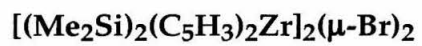
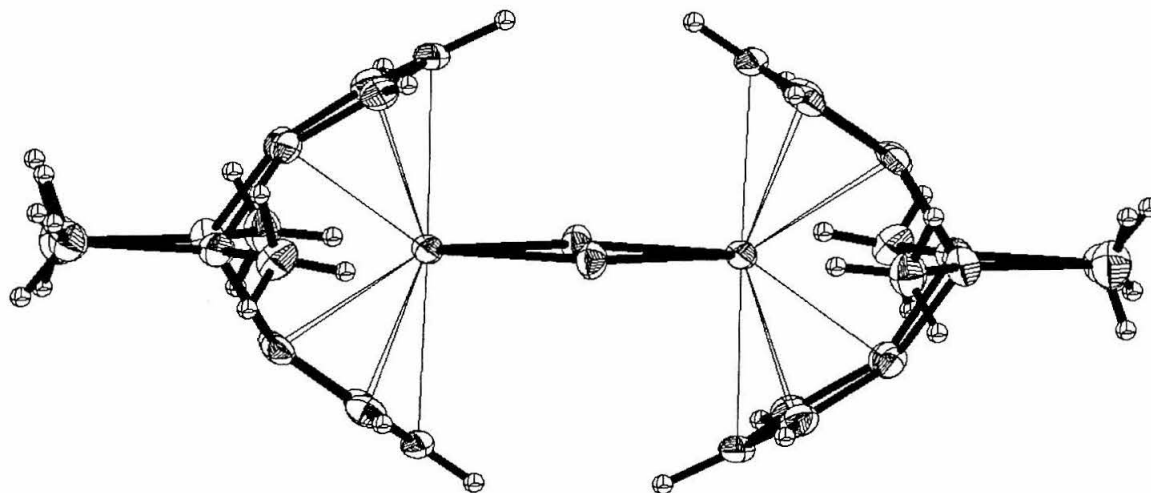
Crystal Structure data for 15

Crystal Structure Analysis of:

(shown below)

Contents

Table 1.	Crystal data
Table 2.	Atomic Coordinates
Table 3.	Selected bond distances and angles
Table 4.	Full bond distances and angles (for deposit)
Table 5.	Anisotropic displacement parameters
Table 6.	Hydrogen atomic coordinates
Table 7.	Observed and calculated structure factors (for deposit)



Note: The crystallographic data has been deposited in the Cambridge Database (CCDC). The deposition number is 151303.

Table 1. Crystal data and structure refinement for CGB3.

Empirical formula	$C_{14}H_{18}BrSi_2Zr \cdot BC_{24}F_{20} \cdot 2C_6H_5Br$
Formula weight	1406.66
Crystallization Solvent	Unknown
Crystal Habit	Blade
Crystal size	0.33 x 0.30 x 0.17 mm ³
Crystal color	Red/yellow dichroic

Data Collection

Preliminary Photos	Rotation
Type of diffractometer	CCD area detector
Wavelength	0.71073 Å MoKa
Data Collection Temperature	98(2) K
q range for 12039 reflections used	
in lattice determination	2.27 to 28.20°
Unit cell dimensions	a = 12.4209(7) Å a = 111.6510(10)° b = 15.0413(9) Å b = 99.1430(10)° c = 15.8523(9) Å g = 107.3110(10)°
Volume	2504.6(3) Å ³
Z	2
Crystal system	Triclinic
Space group	P-1

Density (calculated)	1.865 Mg/m ³
F(000)	1372
Data collection program	Bruker SMART
q range for data collection	1.58 to 28.44°
Completeness to q = 28.44°	90.9 %
Index ranges	-15 = h = 15, -19 = k = 19, -21 = l = 20
Data collection scan type	ω scans at 5 ϕ settings
Data reduction program	Bruker SAINT v6.2
Reflections collected	37315
Independent reflections	11472 [R _{int} = 0.0812]
Absorption coefficient	2.772 mm ⁻¹
Absorption correction	None
Max. and min. transmission (calculated)	0.6441 and 0.4587

Structure solution and Refinement

Structure solution program	SHELXS-97 (Sheldrick, 1990)
Primary solution method	Direct methods
Secondary solution method	Difference Fourier map
Hydrogen placement	Difference Fourier map
Structure refinement program	SHELXL-97 (Sheldrick, 1997)
Refinement method	Full matrix least-squares on F ²
Data / restraints / parameters	11472 / 0 / 806
Treatment of hydrogen atoms	Unrestrained

Goodness-of-fit on F^2	1.292
Final R indices [$I > 2s(I)$, 8069 reflections]	$R1 = 0.0453$, $wR2 = 0.0872$
R indices (all data)	$R1 = 0.0686$, $wR2 = 0.0903$
Type of weighting scheme used	Sigma
Weighting scheme used	$w = 1/\sigma^2(Fo^2)$
Max shift/error	0.003
Average shift/error	0.000
Largest diff. peak and hole	1.584 and -1.566 e.Å ⁻³

Special Refinement Details

Refinement of F^2 against ALL reflections. The weighted R-factor (wR) and goodness of fit (S) are based on F^2 , conventional R-factors (R) are based on F , with F set to zero for negative F^2 . The threshold expression of $F^2 > 2s(F^2)$ is used only for calculating R-factors(gt) etc. and is not relevant to the choice of reflections for refinement. R-factors based on F^2 are statistically about twice as large as those based on F , and R-factors based on ALL data will be even larger.

All esds (except the esd in the dihedral angle between two l.s. planes) are estimated using the full covariance matrix. The cell esds are taken into account individually in the estimation of esds in distances, angles and torsion angles; correlations between esds in cell parameters are only used when they are defined by crystal symmetry. An approximate (isotropic) treatment of cell esds is used for estimating esds involving l.s. planes.

Table 2. Atomic coordinates ($\times 10^4$) and equivalent isotropic displacement parameters ($\text{\AA}^2 \times 10^3$) for CGB3. $U(\text{eq})$ is defined as the trace of the orthogonalized U^{ij} tensor.

	x	y	z	U_{eq}
Zr(1)	8697(1)	8700(1)	4079(1)	16(1)
Br(1)	10070(1)	10491(1)	4042(1)	23(1)
Br(2)	7465(1)	4227(1)	832(1)	59(1)
Br(3)	1439(1)	9790(1)	2175(1)	86(1)
Si(1)	6991(1)	7407(1)	1933(1)	24(1)
Si(2)	6856(1)	6449(1)	3654(1)	22(1)
F(22)	5957(2)	630(2)	1632(1)	25(1)
F(23)	4842(2)	-1414(2)	935(2)	36(1)
F(24)	3759(2)	-2258(2)	1985(2)	38(1)
F(25)	3821(2)	-977(2)	3748(2)	34(1)
F(26)	4953(2)	1047(2)	4476(1)	23(1)
F(28)	5584(2)	4127(1)	4449(1)	21(1)
F(29)	6261(2)	5284(2)	6294(1)	25(1)
F(30)	7435(2)	4769(2)	7524(1)	29(1)
F(31)	8023(2)	3093(2)	6825(1)	27(1)

F(32)	7440(2)	1952(2)	4951(1)	21(1)
F(34)	7376(2)	4250(2)	3559(2)	27(1)
F(35)	9581(2)	5096(2)	3543(2)	48(1)
F(36)	10976(2)	3979(2)	3310(2)	52(1)
F(37)	10109(2)	2012(2)	3109(2)	35(1)
F(38)	7939(2)	1149(2)	3125(2)	24(1)
F(40)	6242(2)	2593(2)	1660(1)	25(1)
F(41)	4532(2)	2770(2)	602(1)	31(1)
F(42)	2477(2)	2639(2)	1031(1)	34(1)
F(43)	2185(2)	2341(2)	2583(1)	28(1)
F(44)	3887(2)	2131(2)	3657(1)	22(1)
B(1)	6175(3)	2229(3)	3438(3)	16(1)
C(1)	8269(3)	7238(3)	2589(2)	20(1)
C(2)	8242(3)	6874(3)	3311(2)	20(1)
C(3)	9414(3)	7279(3)	3901(3)	24(1)
C(4)	10175(3)	7894(3)	3580(3)	23(1)
C(5)	9483(3)	7862(3)	2772(3)	23(1)
C(6)	6720(3)	8096(3)	3098(2)	19(1)
C(7)	6665(3)	7699(3)	3804(2)	19(1)
C(8)	6935(3)	8549(3)	4682(3)	21(1)
C(9)	7160(3)	9450(3)	4557(3)	22(1)
C(10)	7025(3)	9181(3)	3591(3)	20(1)

C(11)	7576(4)	8337(4)	1454(3)	29(1)
C(12)	5738(5)	6238(4)	1032(3)	35(1)
C(13)	7233(4)	6459(3)	4829(3)	26(1)
C(14)	5678(4)	5226(3)	2727(3)	27(1)
C(21)	5561(3)	959(3)	3105(2)	16(1)
C(22)	5469(3)	266(3)	2204(2)	19(1)
C(23)	4880(3)	-801(3)	1817(3)	24(1)
C(24)	4329(3)	-1217(3)	2347(3)	25(1)
C(25)	4374(3)	-582(3)	3232(3)	21(1)
C(26)	4977(3)	486(3)	3594(2)	17(1)
C(27)	6434(3)	2945(3)	4589(2)	16(1)
C(28)	6185(3)	3816(3)	4994(2)	17(1)
C(29)	6503(3)	4424(3)	5956(3)	18(1)
C(30)	7108(3)	4181(3)	6586(2)	20(1)
C(31)	7404(3)	3332(3)	6223(2)	20(1)
C(32)	7088(3)	2755(3)	5254(2)	18(1)
C(33)	7515(3)	2644(3)	3328(2)	18(1)
C(34)	8026(3)	3655(3)	3434(3)	22(1)
C(35)	9156(3)	4110(3)	3435(3)	30(1)
C(36)	9865(3)	3556(3)	3317(3)	34(1)
C(37)	9428(3)	2560(3)	3220(3)	27(1)
C(38)	8275(3)	2137(3)	3230(2)	20(1)

C(39)	5177(3)	2383(3)	2736(2)	16(1)
C(40)	5255(3)	2515(3)	1927(2)	19(1)
C(41)	4359(3)	2600(3)	1356(2)	21(1)
C(42)	3341(3)	2553(3)	1572(2)	22(1)
C(43)	3194(3)	2398(3)	2358(2)	20(1)
C(44)	4094(3)	2306(3)	2903(2)	18(1)
C(51)	8591(4)	5260(3)	658(3)	34(1)
C(52)	9750(4)	5658(3)	1223(3)	32(1)
C(53)	10598(4)	6415(3)	1084(3)	37(1)
C(54)	10246(5)	6738(4)	404(3)	41(1)
C(55)	9069(6)	6316(5)	-99(4)	48(2)
C(56)	8257(5)	5621(5)	-11(3)	45(1)
C(61)	1540(4)	9558(3)	941(3)	37(1)
C(62)	525(4)	9076(4)	183(3)	41(1)
C(63)	630(5)	8962(4)	-698(4)	57(2)
C(64)	1727(6)	9320(5)	-799(4)	75(2)
C(65)	2717(5)	9757(5)	-47(4)	78(2)
C(66)	2639(4)	9884(4)	832(4)	47(1)

Table 3. Selected bond lengths [Å] and angles [°] for CGB3.

Zr(1)-Cent(1)	2.156	Cent(1)-Zr(1)-Cen(2)	122.6
Zr(1)-Cent(2)	2.159	Pln(1)-Zr(1)-Pln(2)	111.8
Zr(1)-Pln(1)	2.148	Br(1)#1-Zr(1)-Br(1)	88.901(15)
Zr(1)-Pln(2)	2.148	Zr(1)#1-Br(1)-Zr(1)	91.099(15)
Zr(1)-C(6)	2.386(3)		
Zr(1)-C(7)	2.394(3)		
Zr(1)-C(2)	2.394(3)		
Zr(1)-C(1)	2.402(3)		
Zr(1)-C(3)	2.490(4)		
Zr(1)-C(10)	2.497(4)		
Zr(1)-C(8)	2.507(4)		
Zr(1)-C(5)	2.507(4)		
Zr(1)-C(4)	2.557(4)		
Zr(1)-C(9)	2.570(4)		
Zr(1)-Br(1)#1	2.7314(5)		
Zr(1)-Br(1)	2.7545(5)		

Symmetry transformations used to generate equivalent atoms:

#1 $-x+2,-y+2,-z+1$

Table 4. Bond lengths [Å] and angles [°] for CGB3.

Zr(1)-Cent(1)	2.156	Si(1)-C(12)	1.835(5)
Zr(1)-Cent(2)	2.159	Si(1)-C(11)	1.848(4)
Zr(1)-Pln(1)	2.148	Si(1)-C(1)	1.892(4)
Zr(1)-Pln(2)	2.148	Si(1)-C(6)	1.894(4)
Zr(1)-C(6)	2.386(3)	Si(2)-C(13)	1.840(4)
Zr(1)-C(7)	2.394(3)	Si(2)-C(14)	1.845(4)
Zr(1)-C(2)	2.394(3)	Si(2)-C(2)	1.888(4)
Zr(1)-C(1)	2.402(3)	Si(2)-C(7)	1.898(4)
Zr(1)-C(3)	2.490(4)	F(22)-C(22)	1.354(4)
Zr(1)-C(10)	2.497(4)	F(23)-C(23)	1.344(4)
Zr(1)-C(8)	2.507(4)	F(24)-C(24)	1.353(4)
Zr(1)-C(5)	2.507(4)	F(25)-C(25)	1.337(4)
Zr(1)-C(4)	2.557(4)	F(26)-C(26)	1.350(4)
Zr(1)-C(9)	2.570(4)	F(28)-C(28)	1.350(4)
Zr(1)-Br(1)#1	2.7314(5)	F(29)-C(29)	1.350(4)
Zr(1)-Br(1)	2.7545(5)	F(30)-C(30)	1.334(4)
Br(1)-Zr(1)#1	2.7314(5)	F(31)-C(31)	1.348(4)
Br(2)-C(51)	1.896(4)	F(32)-C(32)	1.353(4)
Br(3)-C(61)	1.889(4)	F(34)-C(34)	1.356(4)

F(35)-C(35)	1.351(4)	C(6)-C(10)	1.419(5)
F(36)-C(36)	1.341(4)	C(6)-C(7)	1.453(5)
F(37)-C(37)	1.335(4)	C(7)-C(8)	1.402(5)
F(38)-C(38)	1.356(4)	C(8)-C(9)	1.395(5)
F(40)-C(40)	1.346(4)	C(8)-H(8)	0.88(3)
F(41)-C(41)	1.348(4)	C(9)-C(10)	1.399(5)
F(42)-C(42)	1.333(4)	C(9)-H(9)	0.87(4)
F(43)-C(43)	1.344(4)	C(10)-H(10)	0.94(3)
F(44)-C(44)	1.361(4)	C(11)-H(11A)	0.99(4)
B(1)-C(33)	1.656(5)	C(11)-H(11B)	0.88(4)
B(1)-C(27)	1.658(5)	C(11)-H(11C)	0.93(4)
B(1)-C(39)	1.659(5)	C(12)-H(12A)	0.75(7)
B(1)-C(21)	1.663(5)	C(12)-H(12B)	0.81(5)
C(1)-C(5)	1.434(5)	C(12)-H(12C)	1.20(6)
C(1)-C(2)	1.440(5)	C(13)-H(13A)	1.02(4)
C(2)-C(3)	1.408(5)	C(13)-H(13B)	0.89(4)
C(3)-C(4)	1.409(5)	C(13)-H(13C)	0.86(4)
C(3)-H(3)	0.99(4)	C(14)-H(14A)	0.86(4)
C(4)-C(5)	1.400(5)	C(14)-H(14B)	1.01(5)
C(4)-H(4)	1.03(4)	C(14)-H(14C)	1.06(4)
C(5)-H(5)	0.95(4)	C(21)-C(26)	1.384(5)

C(21)-C(22)	1.384(5)	C(42)-C(43)	1.378(5)
C(22)-C(23)	1.386(5)	C(43)-C(44)	1.374(5)
C(23)-C(24)	1.372(5)	C(51)-C(52)	1.384(6)
C(24)-C(25)	1.357(5)	C(51)-C(56)	1.418(7)
C(25)-C(26)	1.392(5)	C(52)-C(53)	1.414(6)
C(27)-C(28)	1.381(5)	C(52)-H(52)	1.14(4)
C(27)-C(32)	1.394(5)	C(53)-C(54)	1.398(6)
C(28)-C(29)	1.372(5)	C(53)-H(53)	1.09(4)
C(29)-C(30)	1.374(5)	C(54)-C(55)	1.370(7)
C(30)-C(31)	1.379(5)	C(54)-H(54)	1.09(4)
C(31)-C(32)	1.374(5)	C(55)-C(56)	1.286(7)
C(33)-C(38)	1.373(5)	C(55)-H(55)	0.68(3)
C(33)-C(34)	1.395(5)	C(56)-H(56)	0.75(4)
C(34)-C(35)	1.366(5)	C(61)-C(66)	1.369(6)
C(35)-C(36)	1.371(6)	C(61)-C(62)	1.375(6)
C(36)-C(37)	1.372(5)	C(62)-C(63)	1.376(6)
C(37)-C(38)	1.388(5)	C(62)-H(62)	1.02(4)
C(39)-C(40)	1.382(5)	C(63)-C(64)	1.366(7)
C(39)-C(44)	1.392(5)	C(63)-H(63)	0.94(4)
C(40)-C(41)	1.387(5)	C(64)-C(65)	1.356(8)
C(41)-C(42)	1.350(5)	C(64)-H(64)	0.92(4)

C(65)-C(66)	1.358(7)	C(6)-Zr(1)-C(8)	55.84(12)
C(65)-H(65)	0.82(4)	C(7)-Zr(1)-C(8)	33.16(12)
C(66)-H(66)	0.94(4)	C(2)-Zr(1)-C(8)	95.74(12)
		C(1)-Zr(1)-C(8)	111.71(12)
Cent(1)-Zr(1)-Cen(2)	122.6	C(3)-Zr(1)-C(8)	114.30(13)
Pln(1)-Zr(1)-Pln(2)	111.8	C(10)-Zr(1)-C(8)	53.78(12)
C(6)-Zr(1)-C(7)	35.40(11)	C(6)-Zr(1)-C(5)	96.45(12)
C(6)-Zr(1)-C(2)	79.74(12)	C(7)-Zr(1)-C(5)	112.44(12)
C(7)-Zr(1)-C(2)	68.16(12)	C(2)-Zr(1)-C(5)	56.03(12)
C(6)-Zr(1)-C(1)	68.30(12)	C(1)-Zr(1)-C(5)	33.89(12)
C(7)-Zr(1)-C(1)	78.55(12)	C(3)-Zr(1)-C(5)	53.96(13)
C(2)-Zr(1)-C(1)	34.95(12)	C(10)-Zr(1)-C(5)	115.50(13)
C(6)-Zr(1)-C(3)	113.19(12)	C(8)-Zr(1)-C(5)	145.59(13)
C(7)-Zr(1)-C(3)	96.40(12)	C(6)-Zr(1)-C(4)	123.66(12)
C(2)-Zr(1)-C(3)	33.45(12)	C(7)-Zr(1)-C(4)	123.45(12)
C(1)-Zr(1)-C(3)	55.88(13)	C(2)-Zr(1)-C(4)	55.30(12)
C(6)-Zr(1)-C(10)	33.70(11)	C(1)-Zr(1)-C(4)	55.36(12)
C(7)-Zr(1)-C(10)	56.11(12)	C(3)-Zr(1)-C(4)	32.39(12)
C(2)-Zr(1)-C(10)	113.43(12)	C(10)-Zr(1)-C(4)	147.59(13)
C(1)-Zr(1)-C(10)	97.15(12)	C(8)-Zr(1)-C(4)	146.67(12)
C(3)-Zr(1)-C(10)	146.87(12)	C(5)-Zr(1)-C(4)	32.09(12)

C(6)-Zr(1)-C(9)	54.97(12)	C(2)-Zr(1)-Br(1)	138.92(9)
C(7)-Zr(1)-C(9)	54.72(12)	C(1)-Zr(1)-Br(1)	109.56(9)
C(2)-Zr(1)-C(9)	122.87(12)	C(3)-Zr(1)-Br(1)	121.01(9)
C(1)-Zr(1)-C(9)	123.23(13)	C(10)-Zr(1)-Br(1)	83.89(9)
C(3)-Zr(1)-C(9)	146.18(13)	C(8)-Zr(1)-Br(1)	123.01(9)
C(10)-Zr(1)-C(9)	32.02(12)	C(5)-Zr(1)-Br(1)	82.93(9)
C(8)-Zr(1)-C(9)	31.87(11)	C(4)-Zr(1)-Br(1)	89.64(9)
C(5)-Zr(1)-C(9)	147.46(13)	C(9)-Zr(1)-Br(1)	92.01(9)
C(4)-Zr(1)-C(9)	178.17(12)	Br(1)#1-Zr(1)-Br(1)	88.901(15)
C(6)-Zr(1)-Br(1)#1	139.56(9)	Zr(1)#1-Br(1)-Zr(1)	91.099(15)
C(7)-Zr(1)-Br(1)#1	110.08(8)	C(12)-Si(1)-C(11)	111.7(2)
C(2)-Zr(1)-Br(1)#1	110.13(9)	C(12)-Si(1)-C(1)	118.1(2)
C(1)-Zr(1)-Br(1)#1	140.00(9)	C(11)-Si(1)-C(1)	108.94(19)
C(3)-Zr(1)-Br(1)#1	84.14(9)	C(12)-Si(1)-C(6)	115.7(2)
C(10)-Zr(1)-Br(1)#1	120.48(9)	C(11)-Si(1)-C(6)	110.01(19)
C(8)-Zr(1)-Br(1)#1	83.83(9)	C(1)-Si(1)-C(6)	90.47(15)
C(5)-Zr(1)-Br(1)#1	122.02(9)	C(12)-Si(1)-Zr(1)	148.71(18)
C(4)-Zr(1)-Br(1)#1	90.99(9)	C(11)-Si(1)-Zr(1)	99.52(14)
C(9)-Zr(1)-Br(1)#1	89.84(9)	C(1)-Si(1)-Zr(1)	48.43(10)
C(6)-Zr(1)-Br(1)	109.42(9)	C(6)-Si(1)-Zr(1)	47.92(10)
C(7)-Zr(1)-Br(1)	140.00(9)	C(13)-Si(2)-C(14)	113.9(2)

C(13)-Si(2)-C(2)	110.2(2)	C(3)-C(2)-C(1)	107.2(3)
C(14)-Si(2)-C(2)	114.10(18)	C(3)-C(2)-Si(2)	126.2(3)
C(13)-Si(2)-C(7)	109.06(18)	C(1)-C(2)-Si(2)	122.0(3)
C(14)-Si(2)-C(7)	117.00(19)	C(3)-C(2)-Zr(1)	77.0(2)
C(2)-Si(2)-C(7)	90.25(15)	C(1)-C(2)-Zr(1)	72.85(19)
C(13)-Si(2)-Zr(1)	101.32(15)	Si(2)-C(2)-Zr(1)	96.80(15)
C(14)-Si(2)-Zr(1)	144.78(15)	C(2)-C(3)-C(4)	109.6(3)
C(2)-Si(2)-Zr(1)	47.59(11)	C(2)-C(3)-Zr(1)	69.5(2)
C(7)-Si(2)-Zr(1)	47.62(10)	C(4)-C(3)-Zr(1)	76.4(2)
C(33)-B(1)-C(27)	101.0(3)	C(2)-C(3)-H(3)	127(2)
C(33)-B(1)-C(39)	113.1(3)	C(4)-C(3)-H(3)	123(2)
C(27)-B(1)-C(39)	113.6(3)	Zr(1)-C(3)-H(3)	119(2)
C(33)-B(1)-C(21)	115.0(3)	C(5)-C(4)-C(3)	107.6(3)
C(27)-B(1)-C(21)	113.5(3)	C(5)-C(4)-Zr(1)	72.0(2)
C(39)-B(1)-C(21)	101.3(3)	C(3)-C(4)-Zr(1)	71.2(2)
C(5)-C(1)-C(2)	106.6(3)	C(5)-C(4)-H(4)	129(2)
C(5)-C(1)-Si(1)	122.9(3)	C(3)-C(4)-H(4)	123(2)
C(2)-C(1)-Si(1)	125.0(3)	Zr(1)-C(4)-H(4)	118(2)
C(5)-C(1)-Zr(1)	77.1(2)	C(4)-C(5)-C(1)	109.0(3)
C(2)-C(1)-Zr(1)	72.20(19)	C(4)-C(5)-Zr(1)	75.9(2)
Si(1)-C(1)-Zr(1)	95.48(15)	C(1)-C(5)-Zr(1)	69.1(2)

C(4)-C(5)-H(5)	127(2)	C(8)-C(9)-C(10)	108.2(3)
C(1)-C(5)-H(5)	124(2)	C(8)-C(9)-Zr(1)	71.6(2)
Zr(1)-C(5)-H(5)	122(2)	C(10)-C(9)-Zr(1)	71.1(2)
C(10)-C(6)-C(7)	106.5(3)	C(8)-C(9)-H(9)	125(2)
C(10)-C(6)-Si(1)	125.8(3)	C(10)-C(9)-H(9)	127(2)
C(7)-C(6)-Si(1)	122.8(3)	Zr(1)-C(9)-H(9)	123(2)
C(10)-C(6)-Zr(1)	77.5(2)	C(9)-C(10)-C(6)	108.9(3)
C(7)-C(6)-Zr(1)	72.61(19)	C(9)-C(10)-Zr(1)	76.8(2)
Si(1)-C(6)-Zr(1)	95.97(14)	C(6)-C(10)-Zr(1)	68.8(2)
C(8)-C(7)-C(6)	106.8(3)	C(9)-C(10)-H(10)	131.5(19)
C(8)-C(7)-Si(2)	124.9(3)	C(6)-C(10)-H(10)	119.6(19)
C(6)-C(7)-Si(2)	123.6(3)	Zr(1)-C(10)-H(10)	118(2)
C(8)-C(7)-Zr(1)	77.9(2)	Si(1)-C(11)-H(11A)	110(2)
C(6)-C(7)-Zr(1)	71.99(19)	Si(1)-C(11)-H(11B)	108(2)
Si(2)-C(7)-Zr(1)	96.54(15)	H(11A)-C(11)-H(11B)	106(3)
C(9)-C(8)-C(7)	109.6(3)	Si(1)-C(11)-H(11C)	105(2)
C(9)-C(8)-Zr(1)	76.5(2)	H(11A)-C(11)-H(11C)	107(3)
C(7)-C(8)-Zr(1)	69.0(2)	H(11B)-C(11)-H(11C)	121(3)
C(9)-C(8)-H(8)	129(2)	Si(1)-C(12)-H(12A)	111(5)
C(7)-C(8)-H(8)	121(2)	Si(1)-C(12)-H(12B)	105(3)
Zr(1)-C(8)-H(8)	120(2)	H(12A)-C(12)-H(12B)	137(6)

Si(1)-C(12)-H(12C)	104(2)	F(23)-C(23)-C(24)	120.8(3)
H(12A)-C(12)-H(12C)	78(5)	F(23)-C(23)-C(22)	120.5(3)
H(12B)-C(12)-H(12C)	115(4)	C(24)-C(23)-C(22)	118.7(3)
Si(2)-C(13)-H(13A)	106(2)	F(24)-C(24)-C(25)	120.7(3)
Si(2)-C(13)-H(13B)	112(2)	F(24)-C(24)-C(23)	119.6(3)
H(13A)-C(13)-H(13B)	107(3)	C(25)-C(24)-C(23)	119.7(3)
Si(2)-C(13)-H(13C)	112(2)	F(25)-C(25)-C(24)	120.2(3)
H(13A)-C(13)-H(13C)	114(3)	F(25)-C(25)-C(26)	120.1(3)
H(13B)-C(13)-H(13C)	106(3)	C(24)-C(25)-C(26)	119.8(3)
Si(2)-C(14)-H(14A)	104(3)	F(26)-C(26)-C(21)	121.3(3)
Si(2)-C(14)-H(14B)	121(2)	F(26)-C(26)-C(25)	114.9(3)
H(14A)-C(14)-H(14B)	114(4)	C(21)-C(26)-C(25)	123.8(3)
Si(2)-C(14)-H(14C)	109(2)	C(28)-C(27)-C(32)	113.4(3)
H(14A)-C(14)-H(14C)	99(3)	C(28)-C(27)-B(1)	127.0(3)
H(14B)-C(14)-H(14C)	107(3)	C(32)-C(27)-B(1)	119.2(3)
C(26)-C(21)-C(22)	113.4(3)	F(28)-C(28)-C(29)	114.7(3)
C(26)-C(21)-B(1)	126.5(3)	F(28)-C(28)-C(27)	121.0(3)
C(22)-C(21)-B(1)	119.6(3)	C(29)-C(28)-C(27)	124.2(3)
F(22)-C(22)-C(21)	119.5(3)	F(29)-C(29)-C(28)	120.5(3)
F(22)-C(22)-C(23)	115.8(3)	F(29)-C(29)-C(30)	119.3(3)
C(21)-C(22)-C(23)	124.7(3)	C(28)-C(29)-C(30)	120.2(3)

F(30)-C(30)-C(29)	121.0(3)	F(37)-C(37)-C(36)	119.8(3)
F(30)-C(30)-C(31)	120.7(3)	F(37)-C(37)-C(38)	121.2(3)
C(29)-C(30)-C(31)	118.2(3)	C(36)-C(37)-C(38)	119.0(4)
F(31)-C(31)-C(32)	120.9(3)	F(38)-C(38)-C(33)	121.4(3)
F(31)-C(31)-C(30)	119.4(3)	F(38)-C(38)-C(37)	113.8(3)
C(32)-C(31)-C(30)	119.8(3)	C(33)-C(38)-C(37)	124.8(3)
F(32)-C(32)-C(31)	116.3(3)	C(40)-C(39)-C(44)	113.3(3)
F(32)-C(32)-C(27)	119.6(3)	C(40)-C(39)-B(1)	126.9(3)
C(31)-C(32)-C(27)	124.1(3)	C(44)-C(39)-B(1)	119.6(3)
C(38)-C(33)-C(34)	112.8(3)	F(40)-C(40)-C(39)	120.8(3)
C(38)-C(33)-B(1)	127.3(3)	F(40)-C(40)-C(41)	115.8(3)
C(34)-C(33)-B(1)	119.5(3)	C(39)-C(40)-C(41)	123.3(3)
F(34)-C(34)-C(35)	116.4(3)	F(41)-C(41)-C(42)	120.1(3)
F(34)-C(34)-C(33)	118.8(3)	F(41)-C(41)-C(40)	119.2(3)
C(35)-C(34)-C(33)	124.8(4)	C(42)-C(41)-C(40)	120.6(3)
F(35)-C(35)-C(34)	120.9(4)	F(42)-C(42)-C(41)	121.0(3)
F(35)-C(35)-C(36)	119.6(4)	F(42)-C(42)-C(43)	119.9(3)
C(34)-C(35)-C(36)	119.5(4)	C(41)-C(42)-C(43)	119.1(3)
F(36)-C(36)-C(35)	121.0(4)	F(43)-C(43)-C(44)	120.9(3)
F(36)-C(36)-C(37)	120.0(4)	F(43)-C(43)-C(42)	120.1(3)
C(35)-C(36)-C(37)	119.0(4)	C(44)-C(43)-C(42)	119.0(3)

F(44)-C(44)-C(43)	116.3(3)	C(51)-C(56)-H(56)	117(3)
F(44)-C(44)-C(39)	119.1(3)	C(66)-C(61)-C(62)	121.9(4)
C(43)-C(44)-C(39)	124.7(3)	C(66)-C(61)-Br(3)	118.2(3)
C(52)-C(51)-C(56)	121.5(4)	C(62)-C(61)-Br(3)	119.9(4)
C(52)-C(51)-Br(2)	117.0(3)	C(61)-C(62)-C(63)	118.3(5)
C(56)-C(51)-Br(2)	121.5(3)	C(61)-C(62)-H(62)	120(2)
C(51)-C(52)-C(53)	117.3(4)	C(63)-C(62)-H(62)	122(2)
C(51)-C(52)-H(52)	106(2)	C(64)-C(63)-C(62)	119.7(5)
C(53)-C(52)-H(52)	136(2)	C(64)-C(63)-H(63)	119(3)
C(54)-C(53)-C(52)	119.9(4)	C(62)-C(63)-H(63)	122(3)
C(54)-C(53)-H(53)	120(2)	C(65)-C(64)-C(63)	120.9(6)
C(52)-C(53)-H(53)	120(2)	C(65)-C(64)-H(64)	113(3)
C(55)-C(54)-C(53)	118.1(5)	C(63)-C(64)-H(64)	126(3)
C(55)-C(54)-H(54)	119(2)	C(64)-C(65)-C(66)	120.7(6)
C(53)-C(54)-H(54)	123(2)	C(64)-C(65)-H(65)	123(3)
C(56)-C(55)-C(54)	125.0(5)	C(66)-C(65)-H(65)	116(3)
C(56)-C(55)-H(55)	124(3)	C(65)-C(66)-C(61)	118.5(5)
C(54)-C(55)-H(55)	110(3)	C(65)-C(66)-H(66)	126(3)
C(55)-C(56)-C(51)	118.2(5)	C(61)-C(66)-H(66)	116(3)
C(55)-C(56)-H(56)	124(3)		

Symmetry transformations used to generate equivalent atoms:

#1 $-x+2,-y+2,-z+1$

Table 5. Anisotropic displacement parameters ($\text{\AA}^2 \times 10^4$) for CGB3. The anisotropic displacement factor exponent takes the form: $-2p^2 [h^2 a^* U^{11} + \dots + 2 h k a^* b^* U^{12}]$

	U^{11}	U^{22}	U^{33}	U^{23}	U^{13}	U^{12}
Zr(1)	153(2)	145(2)	198(2)	87(2)	49(1)	57(2)
Br(1)	215(2)	183(2)	217(2)	57(2)	-13(2)	64(2)
Br(2)	410(3)	519(3)	683(4)	164(3)	241(3)	67(3)
Br(3)	996(5)	633(4)	417(3)	221(3)	117(3)	-335(4)
Si(1)	217(6)	231(6)	222(6)	106(5)	31(4)	49(5)
Si(2)	218(6)	167(5)	296(6)	121(5)	94(5)	64(5)
F(22)	242(12)	254(12)	250(12)	112(10)	116(9)	76(10)
F(23)	355(14)	243(12)	324(13)	4(11)	108(11)	69(11)
F(24)	349(14)	151(12)	502(15)	72(11)	114(11)	5(10)
F(25)	346(14)	254(13)	438(14)	208(11)	183(11)	41(11)
F(26)	245(12)	209(11)	243(12)	123(10)	105(9)	62(9)
F(28)	203(11)	202(11)	253(11)	117(9)	48(9)	105(9)
F(29)	276(12)	195(11)	260(12)	67(10)	77(9)	104(10)
F(30)	314(13)	290(13)	196(11)	55(10)	38(9)	108(10)
F(31)	250(12)	311(13)	228(12)	127(10)	-19(9)	108(10)

F(32)	191(11)	209(11)	246(11)	106(9)	21(9)	108(9)
F(34)	223(12)	190(11)	445(14)	173(10)	112(10)	100(10)
F(35)	287(14)	235(13)	990(20)	351(14)	233(14)	52(11)
F(36)	187(13)	433(16)	1070(20)	455(16)	293(14)	95(11)
F(37)	185(12)	372(14)	669(17)	323(13)	219(11)	170(11)
F(38)	157(11)	186(11)	465(14)	209(10)	122(10)	75(9)
F(40)	217(12)	359(13)	289(12)	204(10)	132(9)	145(10)
F(41)	340(13)	373(14)	238(12)	194(11)	65(10)	123(11)
F(42)	283(13)	447(15)	304(13)	188(11)	-16(10)	194(11)
F(43)	121(11)	402(14)	341(13)	160(11)	56(9)	131(10)
F(44)	159(11)	299(12)	230(11)	151(10)	82(9)	76(9)
B(1)	150(20)	170(20)	190(20)	96(18)	54(17)	70(17)
C(1)	210(20)	132(18)	185(19)	11(15)	63(15)	51(16)
C(2)	200(20)	110(18)	260(20)	65(16)	72(16)	50(15)
C(3)	250(20)	170(20)	310(20)	104(18)	73(18)	119(17)
C(4)	170(20)	180(20)	330(20)	71(18)	93(17)	93(17)
C(5)	250(20)	200(20)	250(20)	83(18)	134(17)	87(17)
C(6)	100(18)	178(19)	270(20)	98(17)	40(15)	42(15)
C(7)	119(18)	179(19)	280(20)	117(17)	81(15)	44(15)
C(8)	180(20)	260(20)	270(20)	176(19)	102(17)	105(17)
C(9)	170(20)	150(20)	310(20)	64(18)	73(17)	77(16)
C(10)	128(19)	210(20)	310(20)	163(18)	61(16)	71(16)

C(11)	280(20)	290(30)	210(20)	100(20)	30(20)	50(20)
C(12)	340(30)	280(30)	330(30)	120(20)	0(20)	70(20)
C(13)	360(30)	190(20)	270(20)	130(20)	140(20)	90(20)
C(14)	260(20)	200(20)	340(30)	140(20)	90(20)	53(19)
C(21)	93(17)	172(19)	230(20)	99(16)	18(14)	66(15)
C(22)	109(18)	240(20)	230(20)	130(17)	49(15)	53(16)
C(23)	180(20)	230(20)	240(20)	34(18)	44(16)	88(17)
C(24)	160(20)	160(20)	400(20)	96(19)	61(18)	44(16)
C(25)	147(19)	210(20)	300(20)	150(18)	68(16)	49(16)
C(26)	143(18)	180(19)	220(20)	106(16)	72(15)	66(15)
C(27)	118(18)	144(18)	221(19)	104(16)	55(15)	38(15)
C(28)	118(18)	167(19)	260(20)	137(17)	41(15)	45(15)
C(29)	127(18)	145(19)	280(20)	87(17)	77(15)	56(15)
C(30)	149(19)	210(20)	162(19)	46(16)	26(15)	9(16)
C(31)	125(18)	220(20)	230(20)	119(17)	2(15)	49(16)
C(32)	109(18)	126(18)	270(20)	88(16)	15(15)	23(15)
C(33)	147(19)	200(20)	175(19)	87(16)	24(15)	45(16)
C(34)	162(19)	220(20)	300(20)	120(18)	55(16)	83(17)
C(35)	220(20)	200(20)	510(30)	210(20)	102(19)	52(17)
C(36)	140(20)	350(20)	580(30)	290(20)	155(19)	34(18)
C(37)	170(20)	310(20)	420(30)	220(20)	113(18)	123(18)
C(38)	150(19)	200(20)	280(20)	145(17)	78(16)	53(16)

C(39)	113(18)	139(18)	199(19)	66(15)	30(14)	44(15)
C(40)	153(19)	182(19)	240(20)	112(16)	69(16)	52(16)
C(41)	260(20)	200(20)	123(18)	77(16)	24(16)	59(17)
C(42)	200(20)	210(20)	200(20)	76(16)	-25(16)	99(17)
C(43)	141(19)	200(20)	230(20)	69(17)	45(15)	83(16)
C(44)	190(20)	145(19)	193(19)	66(16)	49(15)	56(16)
C(51)	290(20)	320(20)	330(20)	60(20)	125(19)	110(20)
C(52)	300(20)	310(20)	290(20)	90(20)	86(19)	130(20)
C(53)	370(30)	350(30)	290(20)	50(20)	40(20)	160(20)
C(54)	550(30)	310(30)	450(30)	170(20)	180(20)	240(20)
C(55)	660(40)	540(40)	360(30)	240(30)	50(30)	410(30)
C(56)	210(30)	680(40)	250(30)	20(30)	-30(20)	190(30)
C(61)	390(30)	300(20)	430(30)	210(20)	100(20)	120(20)
C(62)	230(20)	450(30)	420(30)	200(20)	40(20)	10(20)
C(63)	400(30)	750(40)	420(30)	250(30)	20(30)	80(30)
C(64)	660(40)	780(40)	440(40)	70(30)	270(30)	-30(30)
C(65)	340(30)	800(50)	550(40)	-180(30)	240(30)	-60(30)
C(66)	310(30)	420(30)	480(30)	20(20)	40(20)	160(20)

Table 6. Hydrogen coordinates ($\times 10^4$) and isotropic displacement parameters ($\text{\AA}^2 \times 10^3$) for CGB3.

	x	y	z	U_{iso}
H(3)	9690(30)	7190(30)	4480(30)	41(12)
H(4)	11060(40)	8320(30)	3940(30)	47(12)
H(5)	9750(30)	8180(30)	2390(20)	27(11)
H(8)	6950(30)	8470(20)	5210(20)	7(9)
H(9)	7350(30)	10070(30)	5010(20)	24(11)
H(10)	7130(30)	9590(20)	3260(20)	7(8)
H(11A)	6950(40)	8540(30)	1220(30)	40(12)
H(11B)	8110(30)	8910(30)	1930(30)	32(12)
H(11C)	7780(30)	7970(30)	930(20)	16(10)
H(12A)	5730(60)	5770(50)	1100(50)	120(30)
H(12B)	5260(40)	6450(30)	850(30)	48(16)
H(12C)	6160(50)	5840(40)	440(40)	84(17)
H(13A)	7560(30)	5900(30)	4750(20)	28(11)
H(13B)	6600(30)	6290(30)	5020(20)	22(11)
H(13C)	7700(30)	7070(30)	5270(30)	23(11)
H(14A)	5660(40)	4790(30)	2960(30)	42(14)

H(14B)	4870(40)	5200(30)	2450(30)	51(14)
H(14C)	5990(30)	4910(30)	2150(30)	30(11)
H(52)	9770(40)	5190(30)	1640(30)	47(12)
H(53)	11530(40)	6750(30)	1500(30)	48(13)
H(54)	10840(40)	7380(30)	330(30)	58(14)
H(55)	8990(30)	6450(30)	-460(20)	10(12)
H(56)	7620(40)	5400(30)	-280(30)	28(13)
H(62)	-280(40)	8780(30)	270(30)	34(11)
H(63)	-30(40)	8600(30)	-1250(30)	43(13)
H(64)	1880(40)	9310(30)	-1350(30)	40(13)
H(65)	3390(40)	9980(30)	-80(30)	44(14)
H(66)	3280(40)	10230(30)	1390(30)	47(13)
